ANALYSIS OF SELECTED CELL POPULATIONS IN TISSUES

BY MALDI MS

By

Hans Rudolf Aerni

Dissertation

Submitted to the Faculty of the

Graduate School of Vanderbilt University

in partial fulfillment of the requirements

for the degree of

DOCTOR OF PHILOSOPHY

in

Chemistry

August, 2011

Nashville, Tennessee

Approved

Professor Richard M. Caprioli

Professor David E. Cliffel

Professor David L. Hachey

Professor John A. McLean

Professor Kevin L. Schey

Dedicated to my parents, Hans and Gerda Aerni.

ACKNOWLEDGMENTS

The power of imagination makes us infinite.

—John Muir

It is a pleasure to thank the many people who made my dissertation work possible. First I would like to thank my research advisor, Dr. Richard Caprioli, for his support, guidance and superior mentorship. You have created an inventive and challenging environment where I was allowed to pursue my interests and learn and grow as an independent scientist. Thanks also to the other members of my Ph.D. committee, Drs. David Hachey, David Cliffel, John McLean and Kevin Schey for their support, invaluable input and advice to help see this project to its successful completion.

I am indebted to my colleagues and collaborators with whom I had the pleasure of working throughout my studies at Vanderbilt University. I would like to thank my collaborators at Vanderbilt University including Dr. Ariel Deutch, Dr. Paul Laibinis, and Zhou Xu. I am grateful for the opportunity to work with you on exciting projects. Your advice has provided me with insightful perspectives that I will always treasure. Special thanks go to Dr. Axel Wellmann who provided samples and to Dr. Kristina Schwamborn who provided pathological support for this work.

I wish to thank all current and former members of the Mass Spectrometry Research Center. You have been amazing colleagues and friends who have provided me with an exhilarating, fun, and encouraging work environment.

TABLE OF CONTENTS

APPENDIX

LIST OF TABLES

LIST OF FIGURES

Figure

LIST OF ABBREVIATIONS

CAN   Acetonitrile

AMBIC   Ammonium bicarbonate

AR   Antigen retrieval

ARM   Automated reagent multispotter

CASI   Continuous Accumulation of Selected Ions

ccRCC   Clear cell renal cell carcinoma

Cf-PD   Californium plasma desorption

CHCA   α-cyano-4-hydroxycinnamic acid

DAC   Diammonium citrate

DC   Direct current

DHA   2,5-Dihydroxyacetophenone

DHB   2,5-dihydroxbenzoic acid

DTE   Dithioerythritol

ESI   Electrospray ionization

eV   Electron volt

FAB   Fast atom bombardment

FD   Field desorption

FFPE   Formalin-fixed paraffin-embedded

FID   Free induction decay

FT   Fourier transform

FT-ICR   Fourier transform cyclotron resonance

FWHM   Full width at half maximum

GP   Globus pallidus

H&E   Hematoxylin and eosin

IAA	Iodoacetamide
ICAT	Isotope-coded affinity tags
ID	Inner diameter
IMS	Imaging mass spectrometry
ITO	Indium tin oxide
LC	Liquid chromatography
LCM	Laser capture microdissection
LDI	Laser desorption/ionization
LMD	Laser microdissection
LPC	Laser pressure catapulting
MALDI	Matrix-assisted laser desorption ionization
MRM	Multiple reaction monitoring
MSNs	Medium spiny neurons
MudPIT	Multidimensional protein identification technology
OD	Outer diameter
PCa	Prostate cancer
PCR	Polymeras chain reaction
PDMS	Polydimethylsiloxane
RF	Radio frequency
RNA	Ribonucleic acid
S/N	Signal-to-noise
SA	Sinapinic acid
SIMS	Secondary ion mass spectrometry
SN	Substantia nigra
TFA	Trifluoroacetic acid
TIC	Total Ion Count

TOF	Time of flight
TRIS	2-Amino-2-(hydroxymethyl)-1,3-propanediol

CHAPTER I

Background and Objectives

Molecular techniques for the study of biological systems are continuing to drive our understanding of cellular biology and are providing significant advances for prevention, diagnosis and treatment of disease. Genomics, transcriptomics and proteomics are among the chief technologies that enable the discovery and study of molecular events at the cell, tissue, organ and individual level while providing new insights into biological systems.[1, 2] Genomics, the study of genomes, reveals inherited variations of the genome such as mutations and polymorphisms as well as genomic alterations like chromosomal deletions and amplification or changes in DNA methylation status, all of which have important implications for the function of a cell. Transcriptomics reveals patterns of active gene expression measured by profiling of RNA's that may result in protein synthesis. The ability of genomics and transcriptomics to predict the abundance, location, functional state and interactions of proteins in cells or tissues is limiting. Knowing the genomic sequence is helpful but gene expression alone does only partially explain the active biological processes especially as many of the regulatory functions controlling gene expression remain unknown. It is now clear that it is the proteins that execute nearly all of the cells functions. Proteomics, the large-scale study of the proteome, is therefore an important discipline that contributes at a direct level to a full description of cellular processes.[3]

Analytical Challenges in Proteomics

The comprehensive analysis of proteins in a biological sample remains daunting analytical challenge. First, the number of protein forms expected in an organism can greatly exceed the number of genes. As an example, the number of known protein coding genes in humans is currently at 20,300. At this time, experimental evidence at the protein level for roughly 70 % of these genes has been found yet the total number of proteins and various protein forms remains unknown. Some estimations put the total number of human proteins at one million.[4] Many factors that contribute to the complexity of proteomic samples are already known including single nucleotide polymorphism, alternative splicing of primary transcripts, post-translational modifications and protein truncations. These can vary with time, location, physiological and pathological as well as pharmacological perturbations.[4] The dynamic nature of proteins, and the fact that protein expression levels can vary widely, make the analysis of proteins extremely challenging. Currently available proteomic workflows can detect several thousand proteins in one experiment. However, this requires time consuming fractionation of the samples as our ability to simultaneously detect low abundant proteins in the presence of higher abundant proteins remains rather limited due to limited dynamic range of current analytical platforms. As an example, in yeast cells, protein abundance can vary in the range between $50 - 10^6$ copies per cell[5] while the concentration range in blood can easily exceed more than 12 orders of magnitude.[6] However, the dynamic range of mass spectrometers for complex mixtures analysis is estimated to be less than 10^3 for complex mixtures[7] although fractionation and enrichment of proteins can extend this significantly and dynamic ranges in the order of 10^6 have been reported.[8]

Direct amplification strategies similar to PCR in genomic research are not available for proteins. Consequently, proteomic experiments depend on the availability of sufficient sample material for analysis. Moreover, extraction and processing of proteins, e.g. membrane proteins,[9] can be challenging and introduce bias into proteomic experiments. Therefore, development of improved technologies that can provide higher sensitivity, protein coverage, while eliminating bias, is highly desirable.

It is increasingly recognized that mapping of the complete proteome is a task that is not currently achievable by a single laboratory or technology. This has led to a global collaboration for the study of proteins that relies heavily on bioinformatics for data integration and analysis.[4] Protein mining, quantification,[10, 11] mapping of modifications,[10] protein-protein interaction[11] and functional studies are all critical parts of this collaboration. Over time, a comprehensive systems view of all proteins will be generated that alone, or integrated with other omics datasets will provide a detailed picture of molecular processes. In this regard, proteomics experiments are designed to answer specific questions which in turn can lead to a better understanding of the biological systems at hand.

Proteomic Technologies for Marker Discovery in Tissues

Mass spectrometry is a powerful tool for the study of proteins in tissues as it can provide high sensitivity and molecular specificity that enables the identification, characterization and quantitation of proteins. One increasingly important focus of tissue proteomics is the search for diagnostically useful protein markers that could improve the diagnosis and management of disease.

A generally accepted workflow for protein marker discovery consists of the following steps: candidate discovery, qualification, verification, research assay optimization, marker validation and commercialization.[12] Most of the early studies have focused on readily available body fluids such as blood and urine as they could be easily obtained in the clinic with minimal risk for the patient.[6] However, as discussed, these samples proved challenging due to their complexity and limited dynamic range of current proteomic technologies. It is now recognized that cells from the original site of the pathology, which is often located in a tissue, could be a better source for marker discovery due to the generally lower concentration range of proteins in tissue compared with bodyfluids.[13, 14] Shotgun proteomic strategies using bulk tissue remain common for marker discovery in tissue but these approaches require hundreds of μg up to mg quantities of protein, especially if multidimensional protein identification technology[15] (MudPIT) is used. This often limits the cellular specificity of these projects as enrichment of large quantities of specific cell populations from morphologically complex tissues is not practical.

A number of alternative proteomic strategies that are useful for marker discovery directly in the tissue have been developed that can provide improved cellular specificity

and higher throughput. Two of these strategies will be discussed, Matrix-assisted laser desorption ionization (MALDI) Imaging MS (IMS) and laser capture microdissection (LCM)-based proteomics combined with MALDI MS. It is important to stress that neither approach, direct imaging by MALDI IMS nor LCM-based proteomics is superior. However, both approaches have unique advantages that can provide insight into the molecular makeup of tissues with high sensitivity and cellular specificity.

Matrix-Assisted Laser Desorption Ionization

MALDI is a soft ionization technique that has emerged as an indispensable tool for the analysis of organic (macro)molecules including peptides and proteins. The discovery of MALDI MS originates back to work of Tanaka.[16] He used ultrafine cobalt powder as an inorganic matrix that was dispersed in glycerol for ionization of proteins as large as 34 kDa. Independent from Tanaka, Karas and Hillenkamp demonstrated that an organic matrix such as nicotinic acid can act as a matrix for MALDI ionization of proteins.[17] Subsequent improvements in instrumentation and discovery of new organic matrix molecules and sample preparation protocols[18] lead to widespread adoption of MALDI MS for biological research. Common analytes are drugs,[19] metabolites and lipids,[20, 21] carbohydrates,[22] nucleic acids,[23] polymers[24] and peptides and proteins.[25] Recently, MALDI has become an important tool for bacterial fingerprinting[26] and direct mapping of proteins and peptides in tissues and cells using imaging mass spectrometry (IMS).[27, 28] Today, MALDI has mostly replaced many of the earlier used desorption methods[29] for peptides and proteins including laser desorption/ionization (LDI), field desorption (FD), secondary ion mass spectrometry (SIMS), fast atom bombardment (FAB) and californium plasma desorption (^{252}Cf-PD). The importance of the new soft ionization

techniques Electrospray (ESI) and MALDI for biological mass spectrometry was underlined with the Nobel Prize in chemistry in 2002.

The MALDI MS Experiment

The general experimental protocol for MALDI MS of proteins and peptides requires extracting or mixing of the analytes with a solution containing the matrix compound and deposition of this solution onto a surface such as a stainless steel target. Good spectra are obtained if the molar matrix/analyte ratio is maintained between 200:1 and 10,000:1 for small molecules or large proteins respectively.[25] As the solvent evaporates, co-crystallization of matrix and analyte occur resulting in a layer of small crystals. Finally, the sample is introduced into a mass spectrometer and the co-crystals are irradiated with a pulsed laser for desorption/ionization of the sample.

Matrix selection in MALDI MS remains largely empirical.[30] Desirable features of a matrix compound are a high absorbance cross section for the laser, high tolerance towards contaminants, a high vacuum stability, the ability to form morphologically homogeneous evenly distributed crystals layers and most importantly, the ionization of the analyte providing high sensitivity detection.

Figure 1 shows examples of some of the most commonly used matrix molecules for MALDI: 2,5-Dihydroxbenzoic acid (DHB)[31] (1) and α-Cyano-4-hydroxycinnamic acid (CHCA)[32] (2) show good performance for the analysis of peptides. Sinapinic acid[33] (SA) (3) is typically used for protein analysis but DHB remains a good alternative if the proteins are glycosylated. Finally, 2,5-Dihydroxyacetophenone[34](DHA) (4) is an excellent choice for the ionization of many lipids.[35]

The exact mechanism of MALDI is still actively investigated and various models have been put forward to describe the ionization/desorption process.[36, 37, 38, 39] While many questions remain concerning the exact mechanism of ion formation, its experimental implementation and practical parameters enabling reliable and reproducible analysis have been well characterized.
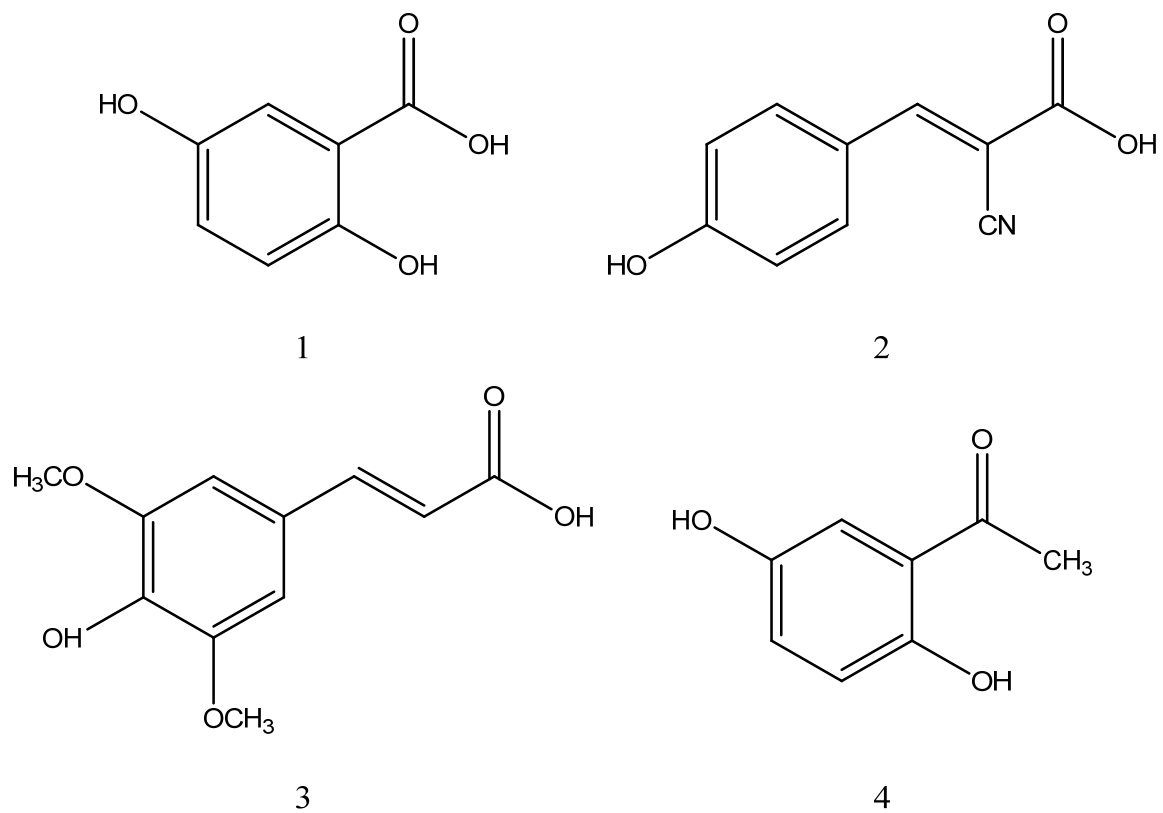
Figure 1: Structures for common MALDI matrix compounds. (1) 2,5-Dihydroxybenzoic acid (2) α-Cyano-4-hydroxycinnamic acid (3) Sinapinic acid (4) 2,5-Dihydroxy-acetophenone (DHA)

Advantages of MALDI MS

MALDI MS has several unique advantages that make this technique desirable for the analysis of proteins and peptides. First, MALDI is a soft ionization technique that can ionize small molecules, peptides and proteins with molecular weights up to the MDa mass range[40] with high speed and sensitivity.[41] Second, MALDI mostly produces singly charged ions which simplifies spectrum interpretation and provides high peak capacity for complex mixture analysis. Third, sample preparation and acquisition of samples in MALDI can be fast and automated allowing high-throughput analysis. Fourth, it can tolerate relatively high concentrations of common contaminants such as salts and detergents which are often present in protein samples.[42] This reduces the need for time consuming sample preparation. Lastly, samples can be archived for several months if retrospective analysis is required.

MALDI Imaging Mass Spectrometry for Spatial Mapping of Proteins in Tissues

An increasingly important application of MALDI MS is imaging mass spectrometry (IMS) a technology for spatial analysis of molecules in tissues. IMS was first described by Caprioli[43] who demonstrated that the spatial arrangement and relative abundance of proteins in tissues can be revealed by systematically analyzing a matrix coated tissue with the use of MALDI TOF MS. The technology is rapidly evolving and applications for mapping of a wide range of compounds in tissues including small molecules like drugs[44, 45, 46] and their metabolites,[47, 48] lipids[21, 49, 50, 51, 52, 53] proteins[54, 55, 56, 57, 58] and peptides[59, 60] have been demonstrated.

Figure 2 shows a typical workflow for MALDI Imaging MS. Tissue samples or whole animals are sectioned and placed onto target plate such as a conductive glass slide

or a gold coated MALDI target. Alternatively, cells of interest are deposited or grown on a MALDI target. The dried samples are coated with a layer of matrix and the sample is loaded in a mass spectrometer. A region of interest is selected and the laser is systematically rastered over the tissue to obtain a spectrum from each pixel. Finally, the resulting spectra are processed[61] and assembled into an ion image. The result of this experiment is a 4 dimensional dataset consisting of the x and y pixel coordinates and the *m/z* and intensity values. By extracting single ion species or selected mass regions of interest, hundreds of ion images can be plotted revealing the distribution of the analyte molecules in or across tissues. Several of these ion images can be acquired from co-registered serial sections enabling 3D imaging[62, 63] of a tissue or whole animals.[64]

IMS has a number of unique advantages compared with analysis of bulk tissue samples. First, it provides the relative abundance and distribution of molecules in a tissue creating an ion map that shows the distribution and relative abundance of molecules in a tissue. Second, it does not require molecule specific probes which enables discovery of *a priori* unknown protein forms including post-translational modified or truncated proteins. Lastly it requires minimal sample preparation, is easy to use and it can provide high-throughput approaching cellular specificity.
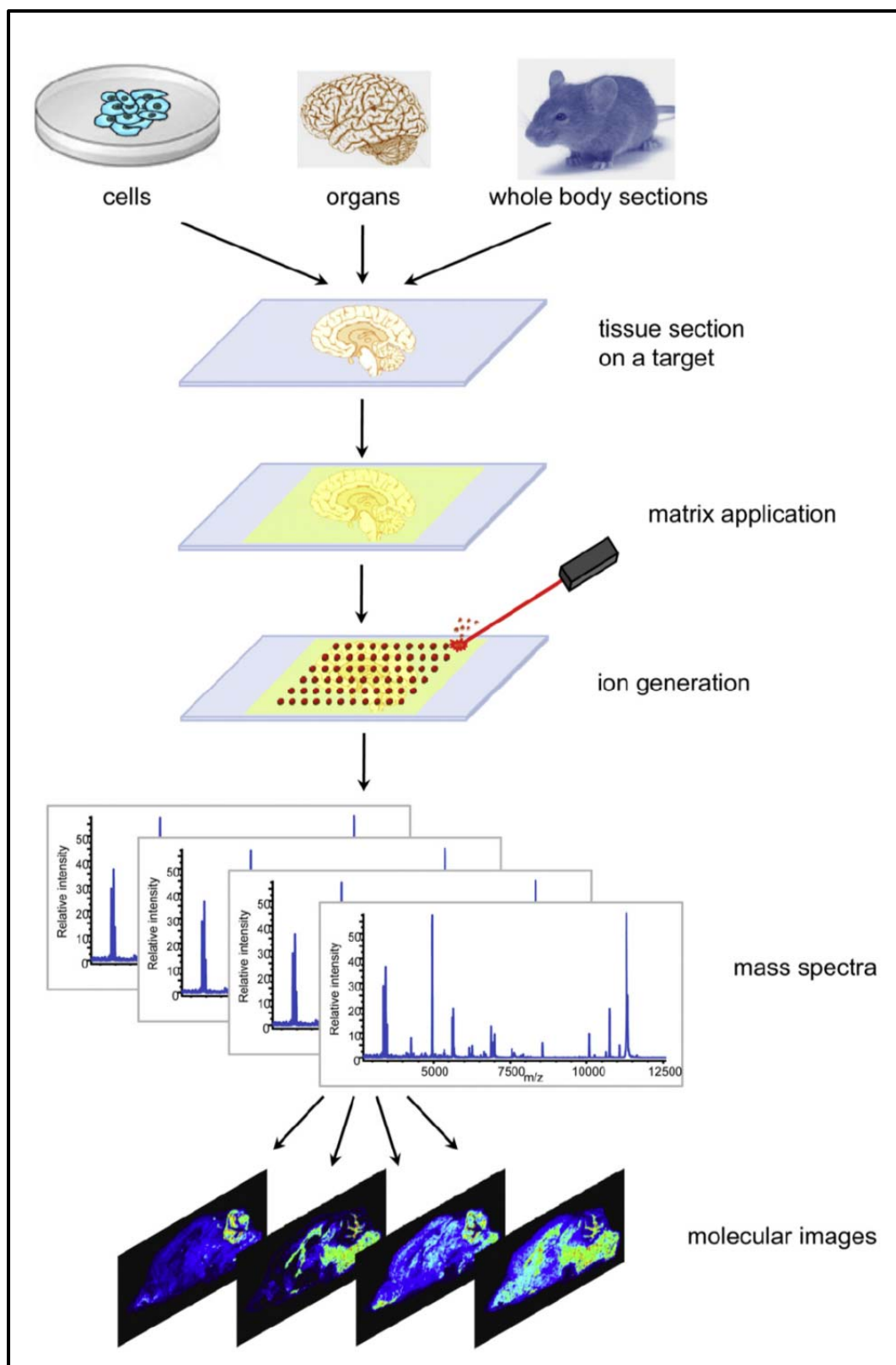
Figure 2: A general workflow for MALDI Imaging MS.[65]

Laser Capture Microdissection for Tissue Proteomics

Enrichment of well-defined pure cell populations from morphologically heterogeneous tissues is an important task in cell research, organ culture, tissue engineering and for the procurement of selected cell populations for molecular assays including DNA/RNA profiling and proteomics. In the past, mechanical isolation of pure cell populations has been accomplished by gross dissection of tissue prior to tissue extraction or the use of specialized tools such as tissue punches.[66] Alternatively a combination of sharp needles and wires have been used for dissection of selected cells from thin tissue sections.[67] Manual dissection with assistance of a microscope, especially if combined with micromanipulators, can achieve good precision but it is labor-intensive and requires a high degree of manual dexterity. The need to increase throughput and specificity of cell isolation led to the development of laser assisted dissection techniques; laser capture microdissection (LCM)[68] and laser microdissection (LMD).[69, 70] Both approaches are commonly referred to as laser microdissection but the underlying technology used for dissection is different.[71]

The first generation of LCM instruments used a heat-generating pulse from a mid-infrared laser to fuse cells of interest to a heat sensitive membrane attached to a cap placed in close proximity above the tissue (Figure 3A). Cells are removed from the section when the cap is lifted off the tissue. This approach has the advantage that the laser mainly interacts with the capture membrane thus enabling gentle cell isolation. The resolution of this technique is limited by the relatively large laser spot diameter although single cell dissection has been demonstrated.[68]
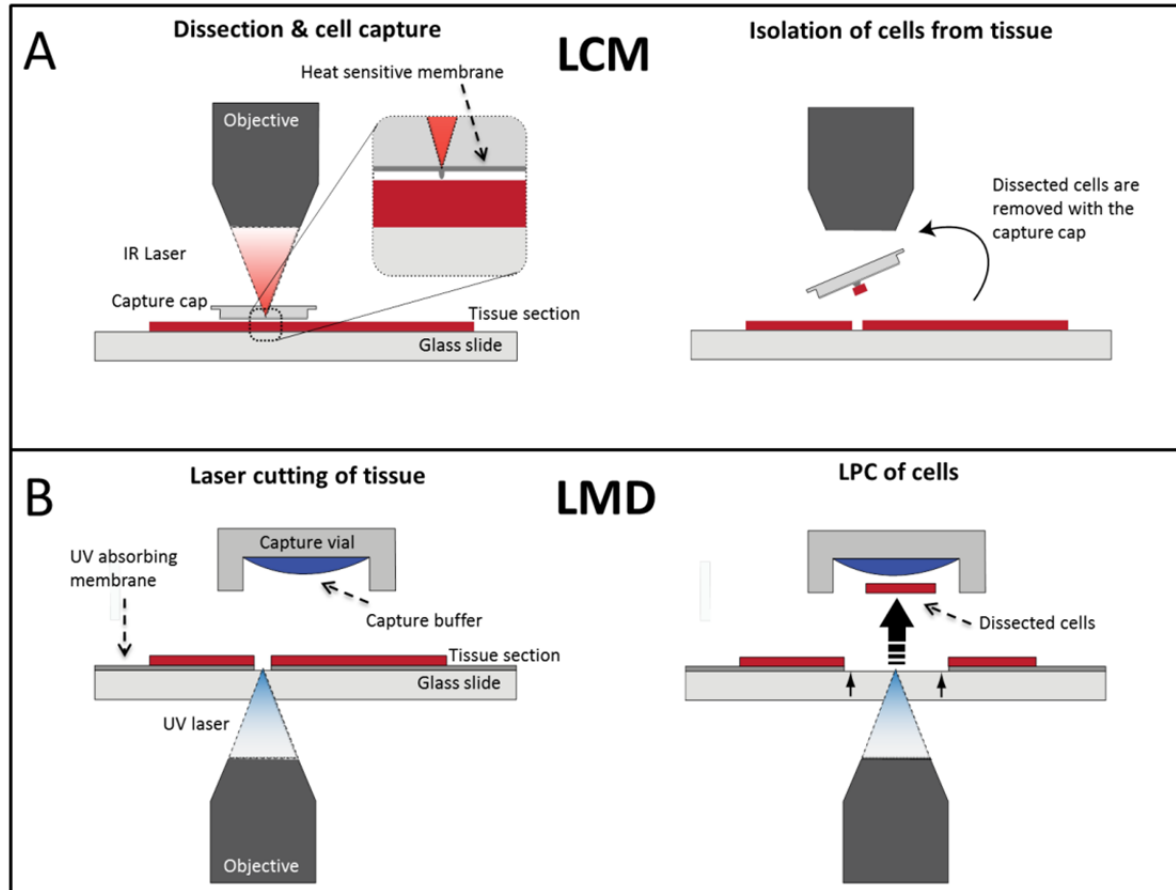
Figure 3: Laser assisted dissection of thin tissue sections. (A) LCM using a heat sensitive membrane activated with an IR laser. Cells underneath the activated membrane fuse with the membrane and are lifted off the tissue with the capture cap. (B) Laser microdissection of tissue. The tissue around the cells of interest is cut with a focused laser beam and cells of interest are laser catapulted into a capture vial above the sample.

The second generation of LCM instruments circumvents the use of capture caps which is advantageous for enrichment of cells from large tissue sections. LMD uses a three step process for dissection of tissue. Tissues are mounted onto a UV sensitive membrane or coating[72] attached to a glass slide. In the first step, the membrane and tissue is cut with a focused low-energy UV laser that isolates the desired tissue region from the bulk tissue by cutting through the membrane and tissue matrix. In the second step cells are removed from the tissue by laser-induced forward transport a process known as laser pressure catapulting (LPC).[73] Lastly, tissue is captured in a capture cap typically placed several millimeters away from the tissue. LMD has been commercialized on several instrument platforms. Leica uses an upright microscope allowing gravity assisted dissection.[74] One potential disadvantage of this setup is that tissue debris can be deposited into the collection vessel which may result in contamination of the isolated cells. A solution to this problem is an inverted microscope design which is available from Carl Zeiss. Cells are collected upward into a collection vessel which eliminates contamination issue but it requires capturing of the cells in a hanging droplet such as a buffer or mineral oil although sticky capture caps are also available. The spatial resolution of LMD is allows routine dissection of single cells. Using a research grade instrument dissection at subcellular resolution has been demonstrated[75] indicating the potential of this technique for subcellular enrichment of cell organelles. Frequency-tripled Nd:YAG lasers with 355 nm wavelength have replaced nitrogen lasers on the newest generation of LMD systems because they offer improved beam homogeneity and shorter pulse duration which improves spatial resolution and reduces optical breakdown of the tissue.[73] Tissue damage by the laser can be reduced by tightly focused beams. With this setup dissection of living

14

cells with cell progeny rates of 98 % could be demonstrated.[76] However, the use of a laser absorbing material such as a polymer membrane is critical for dissection of histological specimen as dissection directly from the glass slide can result in excessive sample degradation.[73] Mechanistic studies of LPC using membrane slides have shown that catapulting is driven by plasma formation for tightly focused beams or photothermal ablation for defocused laser beams with beam spot size sizes greater than 35 μm.[73] In general, tightly focused beams used for LPC reduce sample degradation and are therefore desired for LMD from membrane slides. In summary, LCM and LMD are laser assisted dissection technologies soft enough to enable dissection of biomolecules including DNA and proteins at the single cell level without the risk of excessive sample degradation.

Instrumentation for MALDI MS

MALDI has been interfaced with a wide variety of mass analyzers. Initially, most MALDI work was carried out with time of flight (TOF) analyzers but development of atmospheric and intermediate pressure ion sources has since resulted in broad adaption to a large number of analyzer geometries and hybrid instruments. A brief introduction into MALDI TOF MS and its ongoing adaption to alternative mass analyzers and hybrid instruments is provided.

MALDI TOF MS

MALDI is intrinsically a pulsed ionization method that creates discrete ion packets. Consequently it is an excellent match for TOF mass analyzers which are capable of recording the entire spectrum for each ionization event. The use of TOF analyzers for MALDI originates back to the work of Wiley and McLaren who introduced time-lag-focusing[77] for TOF analyzers. Advances in electronics and hardware design were required before the full potential of this technique could be realized. Some key milestones were the design of the reflector by Mamyrin[78] and the development of post source decay[79] which allowed peptide sequencing on reflector instruments. Further improvements in reliability and electronics such as lasers and ion gate technology led to the development of commercially available TOF/TOF instruments.[80, 81] The improved performance and availability of these instruments has resulted in widespread adoption of MALDI TOF and TOF/TOF MS for protein analysis and characterization.

A brief description of the principles of basic MALDI TOF instruments follows. Readers seeking a detailed discussion of the theory behind MALDI TOF instruments are

referred to the comprehensive overview by Vestal and Juhasz.[82] Figure 4 shows a schematic overview of a typical linear MALDI TOF instrument. First a sample target with the co-crystalized sample is loaded into the ion source operated at 10^{-7} to 10^{-8} Torr. High voltage, typically 20-25 kV, is applied to the sample target and the extraction plate. A single pulse of a focused UV laser is then directed at the sample crystals, causing desorption/ionization while triggering data acquisition using a transient recorder connected to the detector and amplifier. Some of the typical lasers used for MALDI include a nitrogen laser operated at 337 nm, and a frequency tripled Nd:YAG or Nd:YLF laser at 355 and 349 nm respectively. Alternative laser sources, including IR lasers, can also be employed. Typical pulse lengths for the UV lasers are in the low ns range. The lasers are focused to the desired spot size, which is typically between 10 and 100 μm although smaller laser spots have been reported.[59, 83, 84] Spatially structured and modulated laser beam profiles have also been explored to reduce sample consumption and to improve the performance of commercially available instruments.[85, 86] The laser pulse desorbs/ionizes the samples, propelling the ions into the field-free space between the sample target and the extraction plate. Depending on the polarity of the potential applied, positive or negative ions can be selected for analysis. After a short delay, either the extraction plate or the sample plate is pulsed and ions are accelerated toward the field-free drift tube where they undergo separation in space due to their differences in velocity. The pulsed acceleration of the ions, also known as time lag focusing or delayed extraction, corrects for differences in the position and kinetic energy of the ions thereby improving resolution.
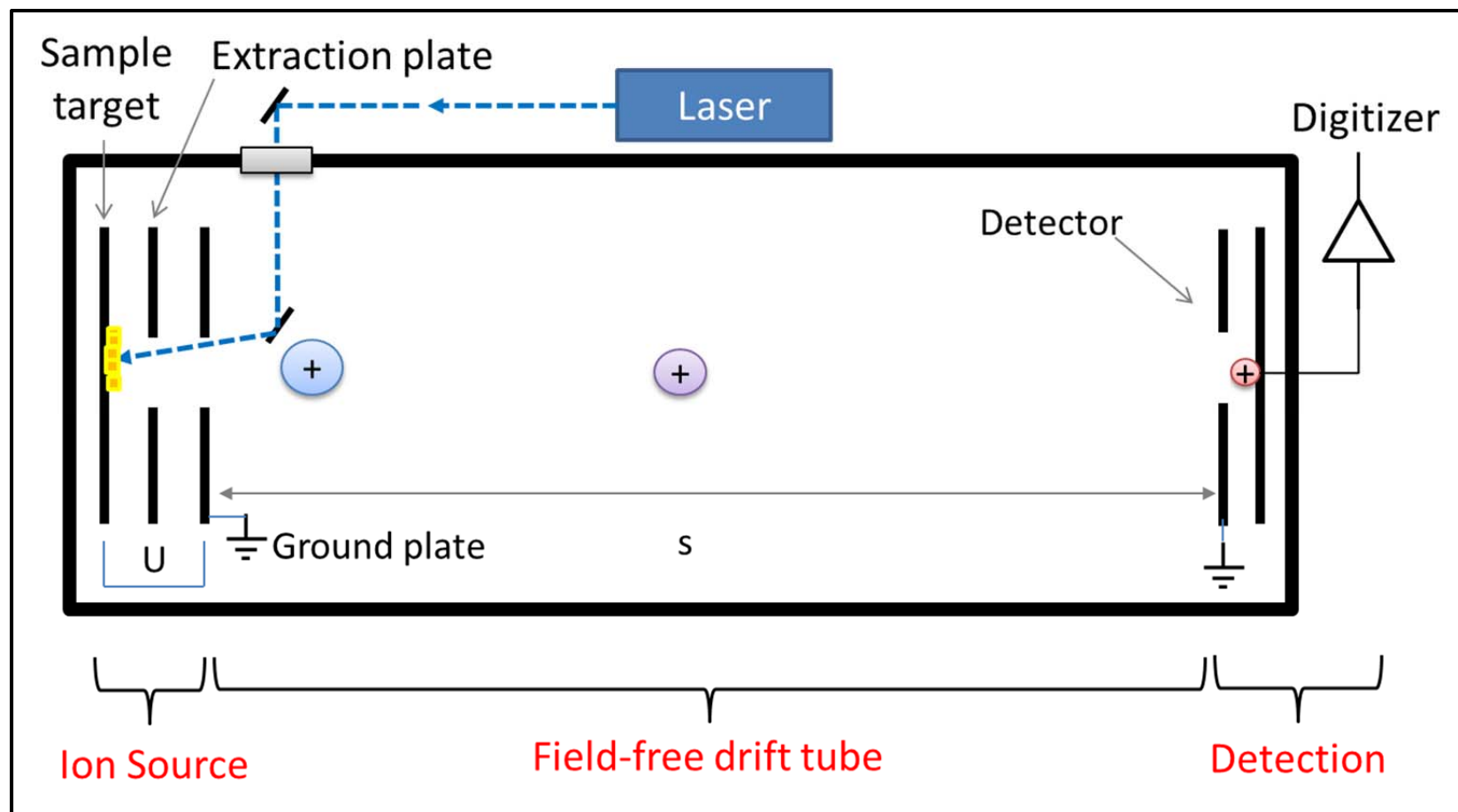
Figure 4: Scheme of a linear MALDI TOF instrument. Ionization takes place in the ion source by a short laser pulse. Ions are accelerated in an electric field towards the field-free drift tube. Ions of the same charge state have the same kinetic energy but differ in velocities according to their mass. As a result, ions with different *m/z* are separated in space resulting in a shorter TOF for smaller ions.

While the kinetic energy of all ions is constant after acceleration the velocity of the ions is inversely proportional to their *m/z* ratio. Therefore, ions with small *m/z* arrive earlier at the detector than heavier ions. This is illustrated in Equation 1 where the relationship between the drift time, t_d, and its *m/z* ratio is described. The drift time is proportional to the square root of the *m/z* ratio and depends on the length of the field-free drift tube (s), the acceleration voltage (U), and the electron charge (e), which are easily experimentally determined or are already known constants. The total time-of-flight (t_{total}) is the sum of the laser pulse duration (t_o), the time needed for acceleration (t_a), and the drift time.

$$t_d = \frac{s}{\sqrt{2eU}} \cdot \sqrt{\frac{m}{z}} \qquad (1)$$

$$t_{total} = t_0 + t_a + t_d \qquad (2)$$

Typical time-of-flight measurements for instruments with 20-25 kV acceleration voltage are in the low μs range for peptides and up to several 100 μs for proteins. The ability to detect a theoretically unlimited mass range from a single ionization event at high speeds combined with the high ion transmission of TOF analyzers renders MALDI TOF instruments a powerful tool for proteomic analysis. Challenges of the technique are the need for compound specific matrix materials, a drop off in sensitivity for high mass proteins and the need for careful optimization of the sample preparation protocols especially if high reproducibility is required. Overall, MALDI TOF MS is a powerful technology that continues to provide high performance for peptide sequencing and intact

protein mass determination. Recently, MALDI TOF MS has become an important tool for the direct spatial mapping of molecules such as drugs, lipids and proteins in tissues.

Additional Mass Analyzers for MALDI MS

The versatility and advantages of MALDI has led to its implementation with a number of mass analyzers and hybrid instruments. Here the operation principles and advantages of several of these instruments are briefly discussed, with a focus on mass analyzers like ion traps (3D-IT) and linear ion traps (LIT) and hybrid instruments such as QqTOF, Q-trap-TOF, and QqLIT. Moreover Fourier transform (FT) hybrid instruments including the LIT-Orbitrap and a QqFourier transform cyclotron resonance (FT-ICR) instrument will be described. Several advantages arise when these mass analyzers are combined with MALDI. First, the ion source is decoupled from the mass analysis which reduces the effect of the sample geometry on mass accuracy. Second, conductive sample targets which prevent sample charging and mass shift in axial TOF instruments are no longer needed. Hence, non-conductive targets can be analyzed, reducing the need for additional sample transfer and enabling the use of complex chip designs.[87] Historically, most of these instruments were developed for atmospheric pressure ionization techniques like ESI. As a result, the atmospheric pressure MALDI (AP MALDI) source is maintained at elevated pressure, ranging from tens of mTorr to atmospheric pressure.[88] The higher pressure in the ion source rapidly cools the ions thereby reducing in-source fragmentation. This has the advantage that higher laser power can be used for each laser pulse providing higher ion yields for each laser shot. Moreover, the relatively high pressure in the source reduces sublimation of the matrix, which can be a concern for some matrix compounds (e.g. 2,5-DHB) in axial TOF instruments. As a result, decoupled

ion sources combined with the unique advantages of the corresponding mass analyzers provide new opportunities especially for the analysis of small molecules and peptides.

Quadrupole Ion Trap and Linear Quadrupole Ion Traps

Quadrupole ion trap instruments are extremely common in proteomic research. The original analyzer design was described by Paul[89] in 1953. Its most widely used design consists of hyperbolic electrodes serving as end caps and a ring electrode. The operation of the quadrupole ion trap is based on the creation of stable trajectories for selected ions. Unwanted ions are removed from the trap by their collision with the wall or by resonant ejection. Essentially a potential well is created from which ions are ejected to a detector by applying a RF-voltage scan allowing sequential detection of the ions according to their *m/z* ratio.[90] Tandem MS can be performed after removing unwanted ions from the trap (Figure 5A). The precursor ions are activated by their collision with a gas such as helium. Numerous low-energy collisions provide sufficient energy for fragmentation and fragment ions are scanned out of the trap as described above. The ability to rapidly scan the trap and to perform multistage tandem MS make this analyzer a powerful tool for peptide sequencing. Resolving power of this analyzer is dependent on scan range and scan speed, but typically unit resolution is used with the ability to obtain higher resolving power for a narrow mass window operated at lower scan speed. Disadvantages of the 3D-IT are the small trapping volume and limited ion storage capacity. This has led to the development of LIT instruments which have the same capabilities of a 3D-IT but provide higher sensitivity and dynamic range.[91] Figure 5 shows a schematic of a linear ion trap. Ions are trapped in the center of a quadrupole device using RF potentials applied to the quadrupole rods and DC potentials applied to the front and back section of the trap. Ions

can be scanned out either axially (AB Sciex) or radially (e.g. Thermo Fisher LTQ) for detection. Both 3D-ITs and LITs have been applied for MALDI MS especially for the analysis of drugs and metabolites in tissues and peptide analysis.[92, 93] The ability to perform MS^n and the high sensitivity makes these instruments well-suited for structure elucidation of drugs and metabolites and for peptide sequencing.
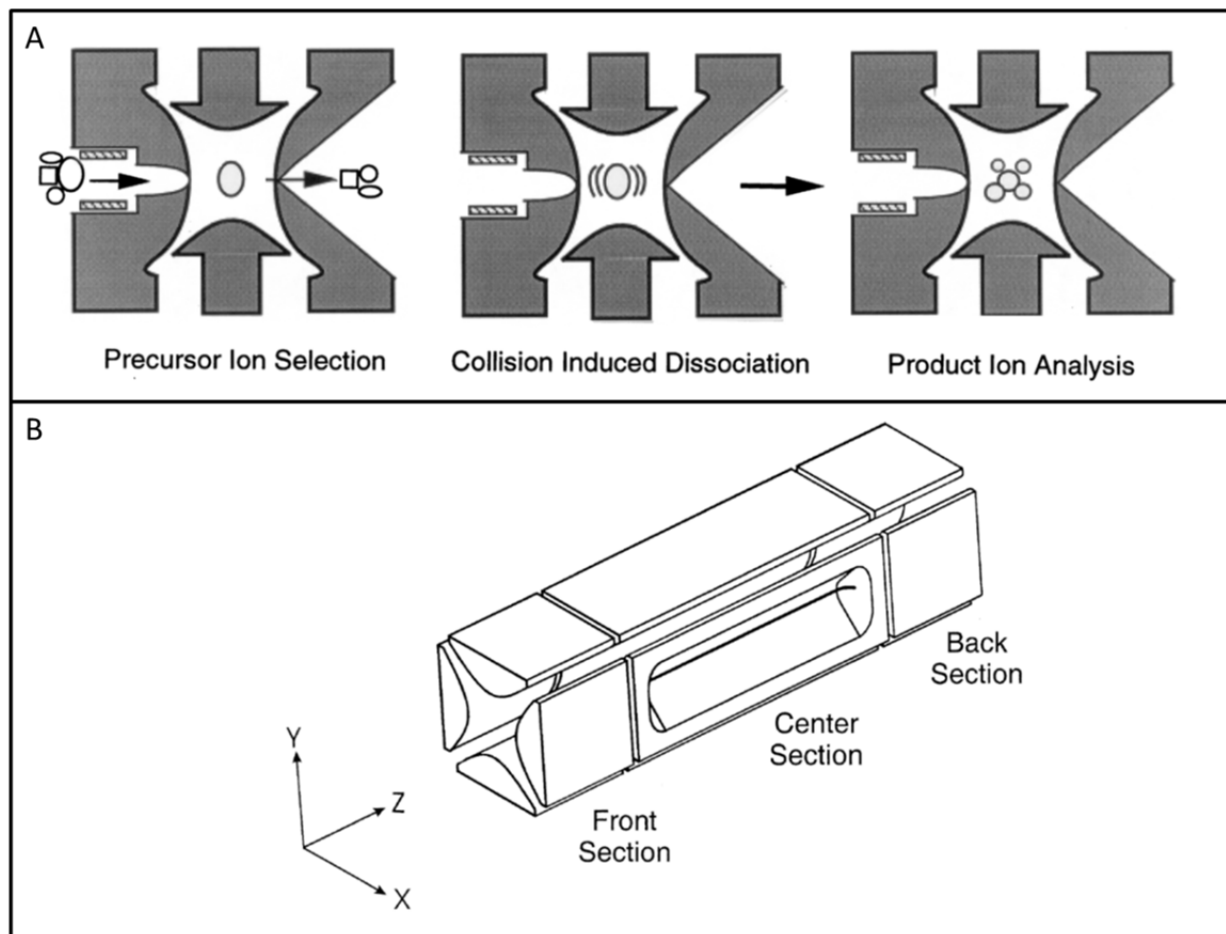
Figure 5: Ion trap designs. (A) Schematic of the fragmentation of ions in a 3D quadrupole ion trap[94] (B) Diagram of a linear quadrupole ion trap[91] as implemented in the Thermo Fisher LTQ which is one of the most widely used LITs in proteomics.

Hybrid Instruments for MALDI MS

A number of hybrid mass analyzers with MALDI MS ion sources have been developed, including QqTOF,[95, 96] Q-trap-TOF, QqLIT,[97] LIT-Orbitrap and Qq-FT-ICR. These advantages of two mass analyzers include improved performance and increased capabilities as compared to single mass analyzers. Specifically, ions formed by MALDI at a high laser repetition rate form a quasi-continuous ion beam that can be manipulated in the instrument similar to the ion beams in ESI instruments. As an example, ions can be mass selected with high resolution in the first quadrupole. Hence, QqTOF instruments and QqLIT combine the advantages of triple quadrupole instruments with the unique capabilities of the reflector TOF and the linear ion trap analyzer. The TOF analyzer allows simultaneous detection of fragment ions with high mass resolution and mass accuracy which can provide high scan speeds. As there is no low mass cut off, simultaneous detection of all fragment ions can be achieved with high speed, which is desirable for structure elucidation and peptide *de novo* sequencing. QqLITs have slower scan speed but they provide MS^n capability and are well-suited for quantitative analysis as they can provide the functionality and sensitivity of a triple quadrupole instruments while providing the versatility of a linear ion trap.

One increasingly important class of hybrid instruments incorporate Fourier transform analyzers such as the Orbitrap[98] and FT-ICR.[99] Typical hybrid instrument geometries for these analyzers are LIT-Orbitrap, and LIT-FT-ICR and Qq-FT-ICR. When combined with a linear ion trap or a quadrupole, they are versatile tools for MALDI that are well-suited for complex mixture analysis when high peak capacity and mass accuracy are required. The advantages of FT analyzers are high resolving power (up to 10^5 for the

orbitrap and 10^5-10^6 for FT-ICR) and high mass accuracy (in the low ppm range or better). The following discussion will focus on the function of FT-ICR analyzers. Readers interested in a detailed description of the Orbitrap and its application may refer to an excellent review by Perry.[100] The operation principle of FT-ICR analyzers is the measurement of the cyclotron frequency of initially coherent ion packets in a uniform magnetic field. Figure 6A shows a schematic of an ICR cell placed in the field of a superconducting magnet. Ions are injected into the trap where they are axially trapped by applying a DC potential to the front and back trapping plates of the cell. The confined ions undergo cyclotron motion in the center of the trap (Figure 6B) but the ion motion is non-coherent and radii of this motion is too small to induce a measurable image charge on the detector plates.[99] For detection the ions need to be brought into close proximity of the detection plates where they can induce a charge. Thus, excitation with an amplified radiofrequency chirp is carried out. When the excitation radiofrequency matches the cyclotron frequency of a ion, spatially coherent ion packets with large radii are generated which are suitable for detection. Useful measurement of all ions in the cell requires simultaneous excitation of all ions in the trap which is achieved with a frequency sweep or "chirp" (Figure 6C). The excited ion packets spiral outwards towards the detection plates where they induce an image charge that is amplified and recorded by a transient recorder. This recorded transient *free induction decay* (FID) represents the time domain signal which is then computed into the frequency domain using fast Fourier transformation. The measured frequency is inversely proportional to the *m/z* ratio of the ions and the amplitude of the signal is proportional to the number of ions in the trap.
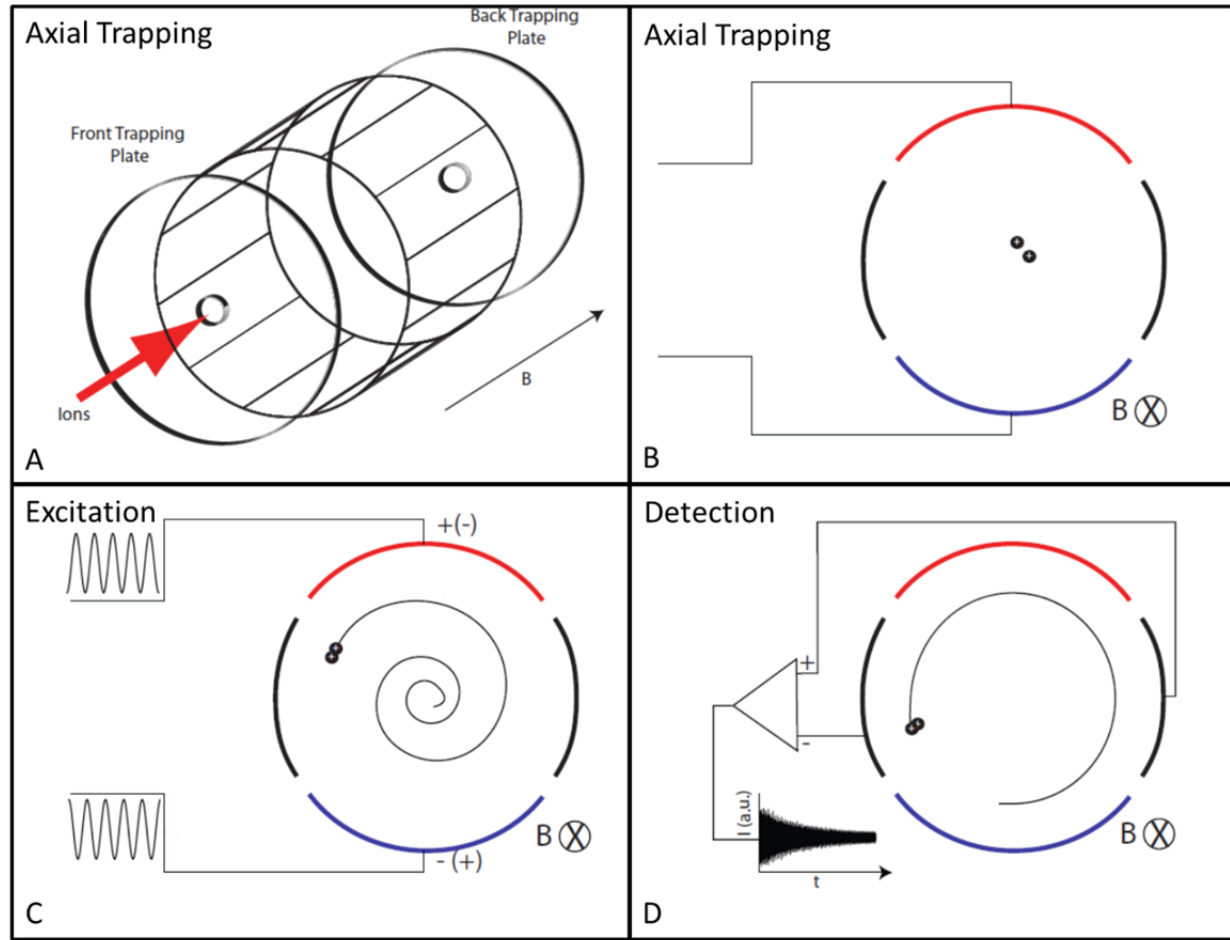
Figure 6: Operation principle of a FT-ICR analyzer (A) Injection of ions into a ion trap and axial trapping. (B) Ions in the center of the trap undergo non-coherent cyclotron motion with small radii. (C) Excitation of the ions with RF energy creates coherent ion packets that orbit close to the detection electrodes. (D) Induction of an image charge on the detection plates for detection.

Several parameters directly depend on the strength of the magnetic field.[90, 101] Resolving power and scan speed increase linearly with higher magnetic field strength while the upper mass limit, ion trapping time, ion energy and number of trapped ions increase quadratically. Typical magnets have field strengths of 7, 9.4 and 12 tesla while high field magnets for FT-ICR MS with field strengths up to 21 tesla are under development.

Summary of Research Objectives

Proteomic discovery in tissue samples with single cell specificity is challenging because the currently available technologies are limited by spatial resolution, sensitivity, or dynamic range. Single cell analysis is desirable because it can provide insight into the function of cells in their native tissue microenvironment. In addition, the complexity of the sample is reduced which is important for discovery of lower abundance proteins. Protein expression in cells is influenced by normal physiological and pathological stimuli in the tissue microenvironment, and mapping these changes is critical for biological research and for developing new diagnostic tools for disease. One emerging method for tissue analysis is MALDI IMS which is capable of directly mapping proteins in thin tissue sections with resolutions approaching single cells. IMS enables direct discovery and identification of proteins from a tissue. However, current sample preparation strategies, specifically the coating of the tissue with the matrix and reagents, limit the spatial resolution of IMS because the proteins tend to delocalize during this step. Therefore, improved methods for coating the tissue with the matrix solution are needed in order to provide higher spatial resolution and sensitivity.

Indirect approaches for the analysis of cells in tissues require isolation of these cells prior to analysis. Enrichment of large numbers of cells has the potential to increase the sensitivity and dynamic range of the experiment. In this approach, cellular specificity is limited only by the method used for cell isolation. LCM has shown promise for the isolation of single cells and it is increasingly used for proteomic discovery. Unfortunately, proteomic experiments require enrichment of large numbers of cells, typically several thousand, to overcome sample losses during cell isolation, protein

extraction and analysis. Enrichment of large numbers of cells can be tedious or impractical when analyzing morphologically complex tissues or samples containing cells of interest at low abundance.

Ideally, a method would be developed that combines the high spatial resolution and the speed of IMS with the ability to enrich cells prior to analysis. Not only would this increase the specificity of the molecular profiles but it would increase the throughput of LCM-based proteomics which is critical for development of the next generation of diagnostic tools. Importantly, by removing the cells from the tissue environment, new opportunities for protein processing and analysis can be explored. The goals of this work were to develop new analytical workflows that enable the analysis of proteins from a subset of cells in a heterogeneous tissue with single cell specificity and high sensitivity. These aims were accomplished through the following objectives:

Objective 1:   To optimize automated sample preparation platforms for direct analysis of proteins in tissues using MALDI IMS.

Objective 2:   To develop a workflow for the enrichment, processing and analysis of selected cell populations from tissues providing cell type specific protein analysis with high sensitivity.

CHAPTER II

Mapping Proteins in Tissue by MALDI Imaging MS[*]

Abstract

Direct mapping of proteins in tissue sections by MALDI Imaging MS is emerging for the discovery of clinically useful proteins in tissue samples, as was described in chapter 1. There are several challenges to overcome to make IMS of proteins routine including reproducible and automated matrix application and improved strategies for identification of the proteins from the tissue. This chapter describes the optimization of two automatic matrix deposition robots for matrix application. One approach uses a computer controlled vibrational matrix deposition robot that is optimized and applied for imaging of proteins in mouse brain. The second device is an automated reagent multispotter (ARM) that is optimized for printing matrix spot arrays. Applications of the ARM for the imaging of proteins in mouse epididymis and in human clear cell renal cell carcinoma (ccRCC) tissue are discussed. Lastly, a new workflow for the identification of proteins using multidimensional protein fractionation and top-down protein sequencing is introduced.

Introduction

Matrix Application for MALDI IMS of Proteins

Localization of proteins in tissues using MALDI Imaging MS relies on a workflow for tissue processing that preserves the location of the protein in the tissue. The critical sample processing steps for IMS are known and have been discussed extensively.[28, 102] Briefly, animal tissues are surgically removed and immediately snap frozen in liquid nitrogen or alternate freezing agents such as fluorocarbons[103] while taking care to preserve the original shape of the tissue. The frozen tissue is sectioned in a cryostat and thaw-mounted onto a conductive substrate such as an ITO-coated glass slide or a gold-coated MALDI target. At these section thicknesses (typically 12 μm for IMS), most of the cells are cut open during sectioning, providing access of the matrix solution to the cells for protein extraction. The sections are dried in a vacuum desiccator and washed in series of graded solvents washes to remove salts and lipids that could interfere with the MALDI experiment.[104, 105] If desired, staining with MALDI compatible stains can be performed, enabling simultaneous histology and MALDI IMS from the same tissue section.[106] Matrix is applied after drying the washed tissue in a vacuum desiccator. The matrix application step remains one of the most challenging parts of the experiment as it needs to be carefully balanced to promote protein extraction while limiting potential delocalization of the proteins which would reduce the spatial resolution of the technique. If the applied coating is coated too dry, poor protein extraction and poor MALDI spectra quality is observed. Wetter coatings tend to improve spectra quality but coatings that are too wet may cause protein delocalization.[107] Once the tissue is coated with the matrix it is systematically rastered by a focused laser. The resulting spectra are processed to remove

excessive background and assembled into an ion image that shows the distribution of the protein in the tissue.

Several strategies have been developed for matrix application for protein imaging. Spotting approaches using fine capillaries or pipette tips permit rapid analysis of cells in a tissue but placement accuracy is limited. Typical spot sizes obtained with this technique are between 1-2 mm for matrix deposition with a pipette and 0.3-1 mm for matrix deposition with a capillary. Spectrum quality from spotted tissue can be excellent but the spatial resolution of spotting techniques is limited by the size of the matrix spot. Therefore, the mass spectrum obtained from each spot represent a composite spectrum from all the cells covered by the matrix. This can be limiting especially if the tissue is morphologically complex. To increase spatial resolution, spray based matrix applications have been developed. Among the spray techniques described are electrospray[43] and pneumatically assisted sprayers such as airbrush[108] and the TM sprayer[61] and reagent sprayers for thin layer chromatography. Trained personnel can achieve uniform and reproducible coatings, but the process is difficult to standardize between users and laboratories. Recently, a new matrix application robot for vibrational matrix deposition has been developed enabling automated matrix coating of tissues while actively monitoring the matrix deposition process.[109] Here, optimization of the sprayer for matrix deposition on mouse brain is described.

Matrix application for MALDI IMS of proteins in tissues with spray-based approaches requires careful control of the matrix deposition process to balance protein extraction with delocalization of proteins over the tissue section. A solution to this problem would be to deposit the matrix as discrete micro spots that would limit protein

delocalization to the region wetted by the matrix solution. However, the problem with nozzle-based printers is that the high volatility of the solvents used for MALDI causes crystallization of the matrix in or around the nozzle resulting in clogging[110, 111, 112] and inconsistent matrix deposition especially if high concentration matrix solutions are being used. To overcome this problem, an automated matrix deposition robot was developed and optimized for protein imaging.[113] Here, the operation of this spotter and its use for matrix printing for protein imaging is discussed and applications that highlight the unique capabilities of this spotter are presented.

Protein Identification

Protein imaging can rapidly reveal the distribution of mass-to-charge ratios of proteins but identification of the detected peaks must be carried out separately. Direct approaches using MALDI TOF/TOF MS have been successful for this purpose especially if the molecular weight of the protein is below 12 kDa[114] and the peak intensity is high.[54] However, this approach often fails for lower intensity peaks, and fragmentation of larger proteins tends to result in spectra with poor sequence coverage. Therefore, indirect protein identification strategies are required. In many cases homogenization of whole organs is carried out followed by protein fractionation. Among the most commonly used protein identification strategies are combinations of reversed phase separation and gel electrophoresis followed by in-gel digestion and protein identification by LC-MS. This method has been successfully applied for protein identification from biofluids[115] and tissues.[116] The gel-based workflow is especially useful as it can remove high molecular weight proteins that might generate many more peptide fragments than a low molecular weight protein of interest which complicates identification. Unfortunately, the direct link

to the protein is lost in this case because the intact mass of the enriched protein on the gel cannot be easily determined prior to digestion. To match the peptides to the intact mass of the protein, high sequence coverage and mapping of post-translational modifications may be required which can be difficult. Therefore, an alternative strategy for protein identification directly from serial sections of the imaged tissue was developed, enabling tracking of the protein throughout the protein identification workflow via its mass.

Results

Automated Matrix Deposition Using the ImagePrep

An automated reagent sprayer for matrix coating of tissues using a prototype vibrational sprayer has been developed. The ImagePrep (Bruker Daltonics) controls matrix deposition by actively monitoring the tissue surface during matrix deposition while providing a controlled atmosphere in the spray chamber. Figure 7A shows a schematic of the sprayer. A prototype of this sprayer was optimized to coat mouse brain with sinapinic acid. A transparent sample support such as an ITO-coated glass slide is placed on top of a light scattering sensor. A computer controlled vibrational sprayer attached to a matrix reservoir generates a fine mist of matrix droplets that settles by gravity onto the tissue. The size of the matrix spray droplets is controlled by the diameter of the pinholes, which are ~ 20 µm. To determine the area wetted by a single solvent drop, 60 % acetonitrile was sprayed onto water sensitive paper and the resulting circular areas were measured with a light microscope to yield a typical diameter of 65 µm.
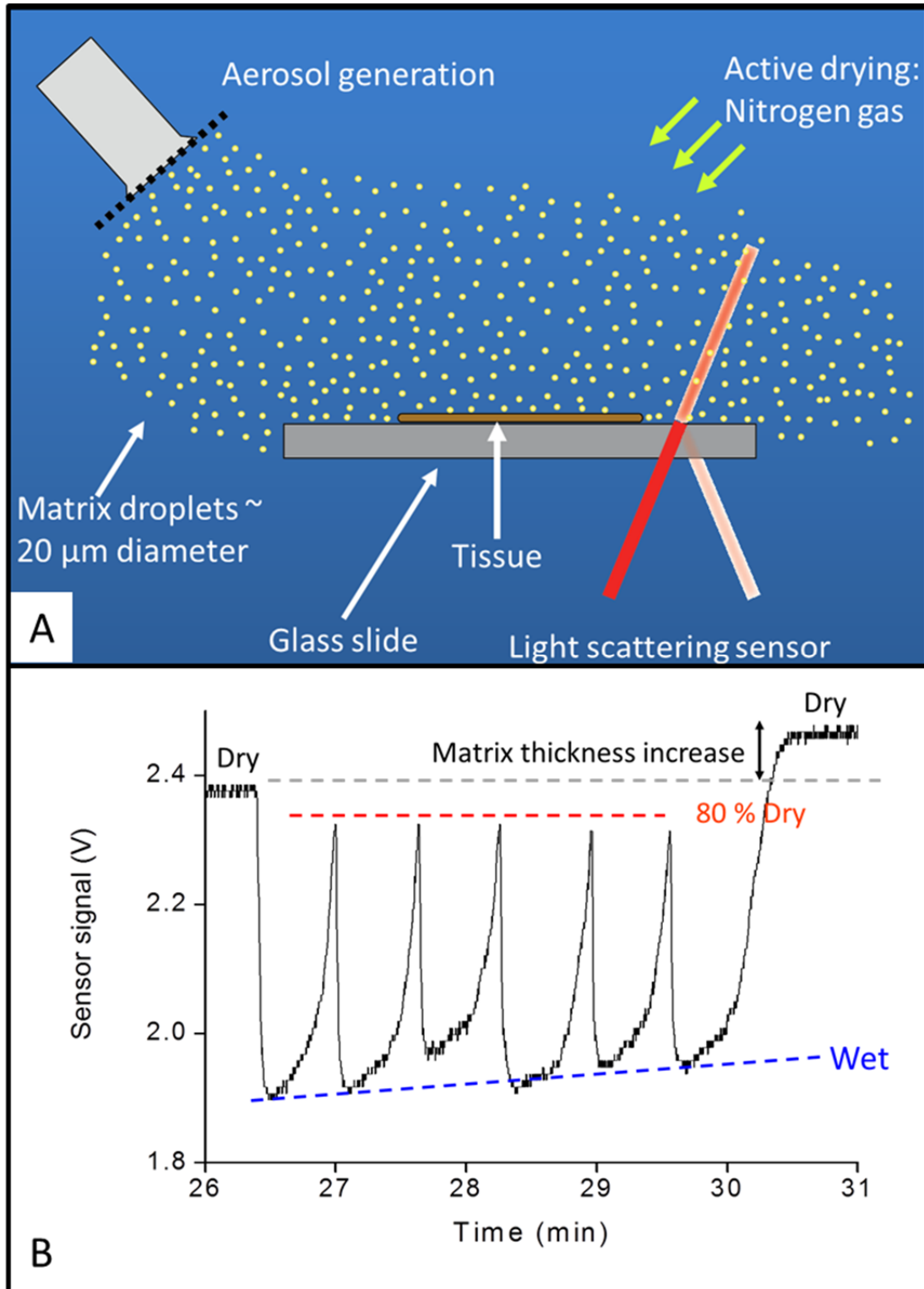
Figure 7: Matrix application using the ImagePrep. (A) Schematic of the sprayer. (B) Sensor signal monitored during spraying of sinapinic acid matrix solution showing 6 consecutive spray cycles followed by a complete drying step.

The spray duration and intensity is actively controlled using real-time feedback from the light scattering sensor beneath the sample. Light scattering is measured on the glass slide next to the tissue. A higher voltage signal indicative of more scattering is recorded as the thickness of the dried matrix layer increases (Figure 7B). Sensor control has the advantage of providing consistent amounts of matrix solution to the sample. This can compensate for potential matrix crystal build up on the sprayer which is common if matrix solutions > 10 mg/ml are used. Typically, a series of controlled matrix sprays are applied and nitrogen gas is supplied to the chamber to assist with drying. In this way, the drying process can be controlled enabling extraction of proteins for prolonged time periods. After several such cycles, the sample is completely dried and the process is repeated until the desired matrix coating quality is obtained. By providing feedback from the sensor to the sprayer, controlled matrix deposition can be achieved. The time required for coating tissue is method dependent but is typically 1-2 h. In case of sinapinic acid, hundreds of spray cycles are needed to build up sufficient matrix for analysis. Systematic optimization of all parameters results in reproducible coatings for serial tissue sections showing excellent MALDI signal quality. Importantly, by controlling the wetness of the tissue, delocalization of proteins can be controlled. The optimized protocol can be saved for future use enabling unsupervised matrix application.

Figure 8A shows a plot of the sensor signal for the optimized coating of mouse brain with sinapinic acid. Note that matrix is applied in several spray phases each consisting of a series of controlled matrix sprays to limit protein delocalization. As the method proceeds, the amount of matrix deposited is increased. This coating strategy limits protein delocalization especially if the initial spray phases are rather dry.

Overall parameters for 7 different spray segments were optimized for this method. A detailed description of the coating method can be found in Appendix A. The optimized coating showed good crystal homogeneity and coverage with crystal sizes between 20-50 μm. Tissue imaging was carried out with a raster with of 75 μm. Figure 8B shows the averaged mass spectrum from the ion image of the mouse brain. Proteins with *m/z* up to 33,000 were detected, but most were in the 3-15 kDa range. Ion images revealed localization of proteins to distinct tissue regions of the mouse brain (Figure 9) that matched anatomical structures revealed on a stained serial section. Advantages of this sprayer are that the matrix deposition is completely automated requiring minimum user interaction. Imaging at spatial resolutions of 50-100 μm is routine for a sinapinic acid matrix although tuning of the method may be required for different tissue types. The sprayer generates a homogeneous coating in close proximity to the sensor. However, the coating at the periphery of the slide tends to be too wet or too dry. Hence, placement of the tissue within 1.5 cm of the sensor is recommended. Under these circumstances, the coating process is completely automated, producing reproducible coatings between tissues which eliminate the need for time consuming manual matrix application.
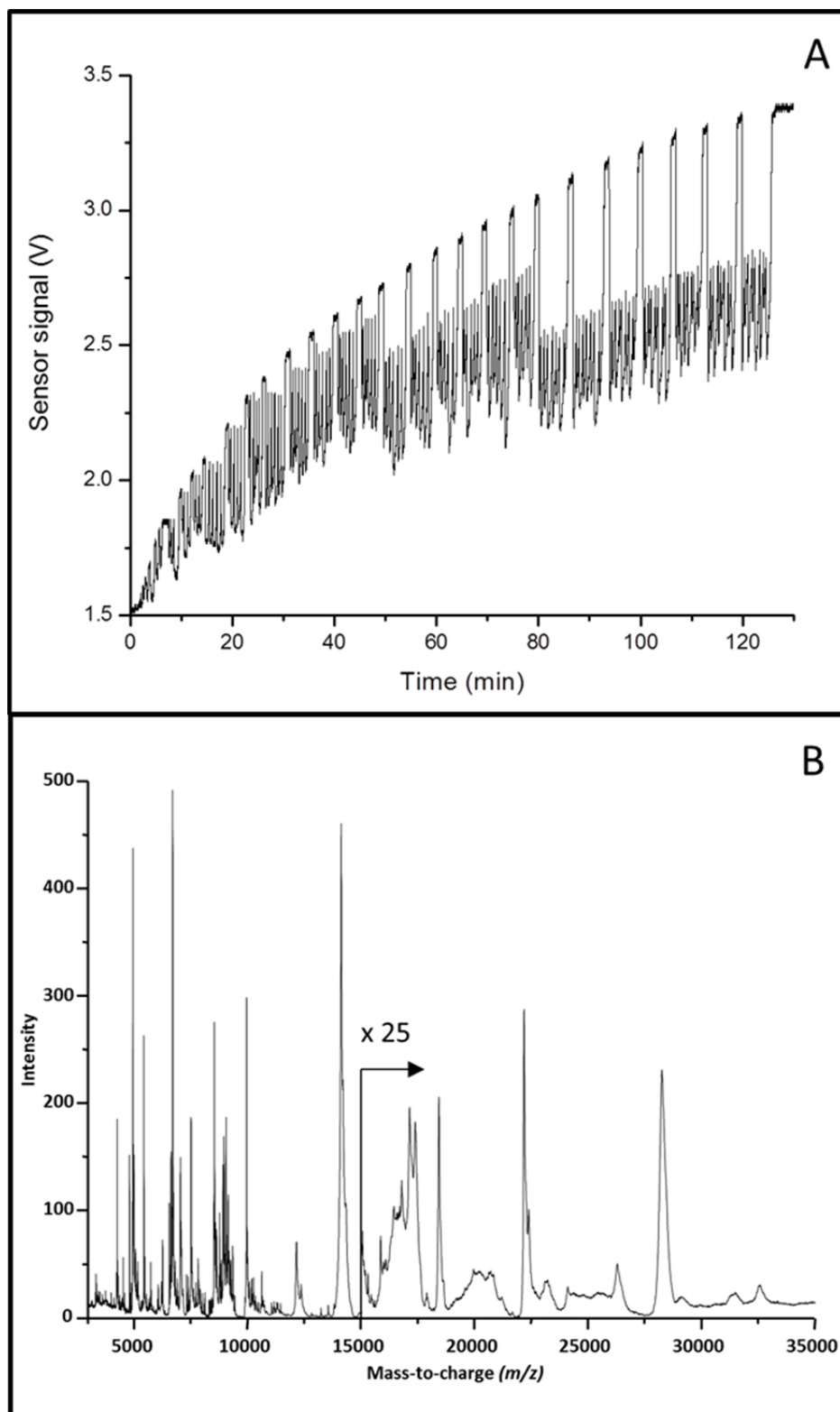
Figure 8: Coating of mouse brain tissue with the ImagePrep using sinapinic acid. (A) Measured light scattering during matrix application. (B) Summed mass spectrum from the brain image showing the mass range from 2500-35000 Da.
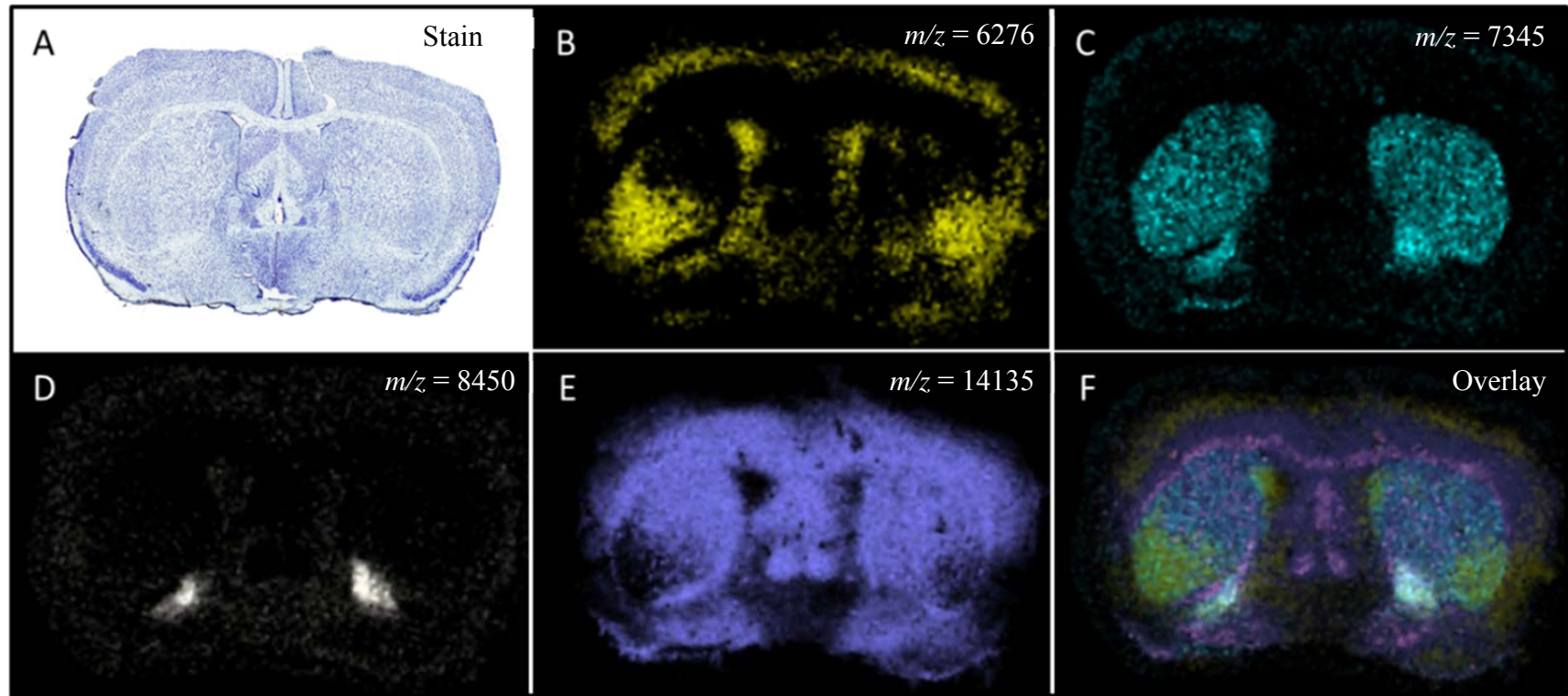
Figure 9: Imaging of mouse brain after matrix coating with the ImagePrep showing localization of proteins to distinct brain regions. (A) Cresyl violet stained serial section. (B-E) Ion images showing m/z = 6276, 7345, 8450, 14135. (F) Overlay of ion images B-E.

Automated Matrix Deposition Using the ARM

Matrix application by matrix solution printing has the advantage that protein delocalization is limited to the area wetted by the matrix spot. However, nozzle-based methods such as inkjet printers tend to clog, resulting in poor performance for matrix printing. Recently, an automated reagent multispotter (ARM) was developed and optimized for protein imaging.[113] This spotter uses a nozzle-free acoustic ejector for reagent printing allowing continuous matrix deposition with concentrated matrix solutions without clogging. Figure 10 shows a schematic of the ARM with translational stage, sample- and drop imaging systems and an acoustic ejector for matrix dispensing.

Matrix deposition requires that a tissue sample is first mounted to a motorized stage and placed above a macro lens attached to a color camera. Using the control software, an optical image is acquired and a rectangular array or discrete regions of interest are marked for matrix deposition. Matrix solution is filled into a reservoir and mounted above a focused transducer. An imaging system consisting of an adjustable stroboscopic light for back-light illumination and a long distance video microscope is used for real time monitoring of the surface of the matrix solution in the reservoir during tuning of acoustic ejector. The focal position and rf power supplied to the transducer are optimized to obtain stable droplet ejection as shown in Figure 11. The droplet volume is solvent dependent, with increased droplet size for higher percentages of acetonitrile in the matrix. For a 50 % acetonitrile solution the droplet volume was determined to be 121 ± 16 pl resulting in a calculated droplet diameter of 62 μm. Once the ejector is optimized for stable droplet ejection, the sample is transferred above the matrix reservoir for solvent deposition. The droplet ejection rate can be systematically optimized, and the number of

droplets dispensed in a printing cycle has been performed. Readers seeking a detailed description of the optimization may refer to Aerni *et al.*[117] For proteins, excellent results can be obtained with 3 dispensing cycles consisting of 13 droplets deposited at 10 Hz in start/stop printing mode. This generates matrix spots with 243 μm spot diameter on average. The spotter has shown promise for mapping proteins in tissues. For example, ion images from mouse brain were obtained that showed localization of proteins to distinct anatomical brain regions (Figure 12). Matrix printing reduces sample delocalization to the area wetted by the matrix solution and spotting conditions can be optimized for each tissue resulting in an excellent MALDI signal.

Several hundred laser shots can be obtained from each matrix spot increasing the signal-to-noise ratio of low abundance peaks. The performance of the spotter was compared with manual matrix deposition using a capillary. The average spot diameters were 230 μm with a CV of 7.6 % for the spotter and 370 μm with a CV of 22.1 % for the spots deposited with the capillary, indicating robotic spotting can improve the reproducibility of the matrix application process. In addition, comparison of the resulting spectra on tissue showed improved spectral quality from tissues coated with the ARM. The placement accuracy of the spotter is high allowing deposition of matrix droplets within 8-26 μm depending on the spotting conditions used.[113]

The spotter was used for mapping protein distributions in mouse epididymis. The epididymis displays a highly regionalized pattern of gene expression which is critical for the maintenance of a fully functional organ.[118] Therefore, one would expect localization of proteins to distinct regions of the epididymis.
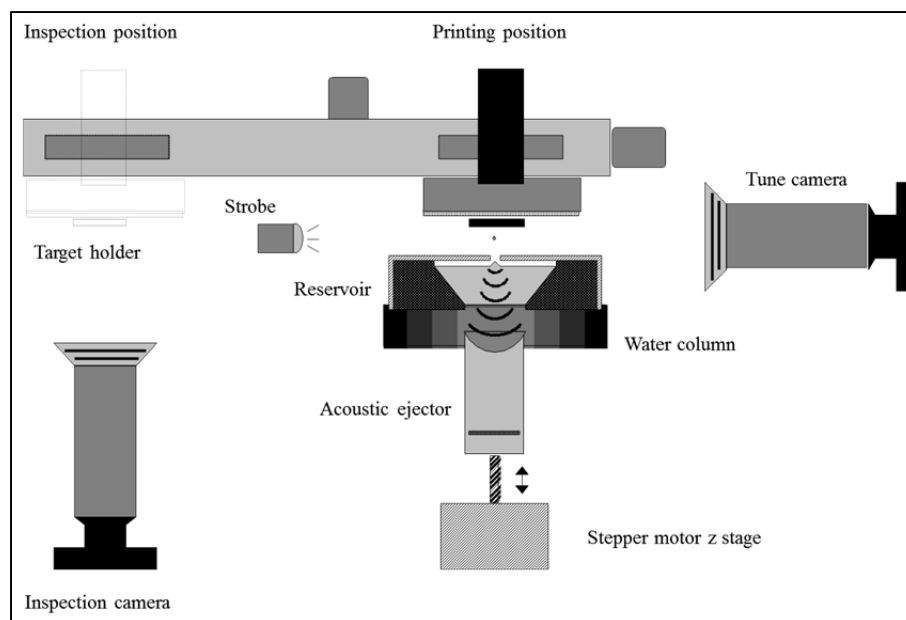
Figure 10: Schematic of the acoustic reagent multispotter.[113]
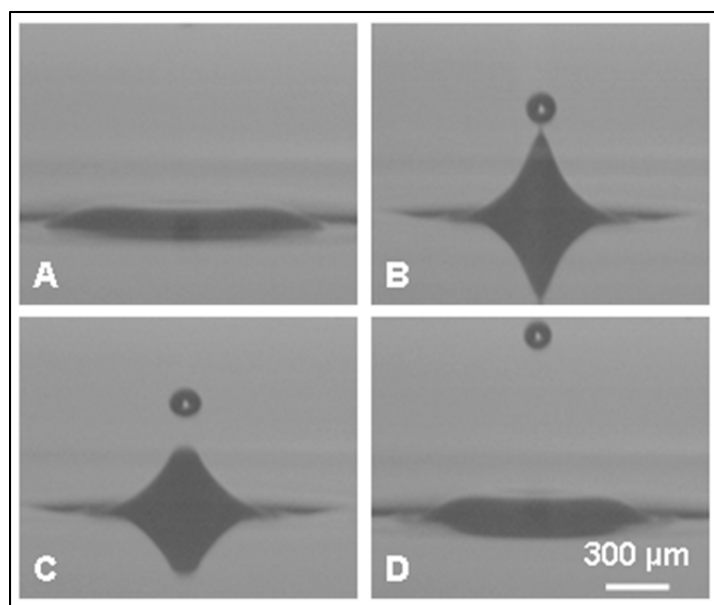
Figure 11: Photo micrographs obtained from the surface of the matrix reservoir during tuning of the acoustic transducer.[113] (A) The focal spot and amplitude of the acoustic wave produced by the transducer is adjusted to the point where a droplet is formed at the top of the liquid column (B) but not ejected (threshold energy). Adjusting of the energy above the threshold value ejects (C) a droplet toward the sample to be spotted (D) Matrix printing.
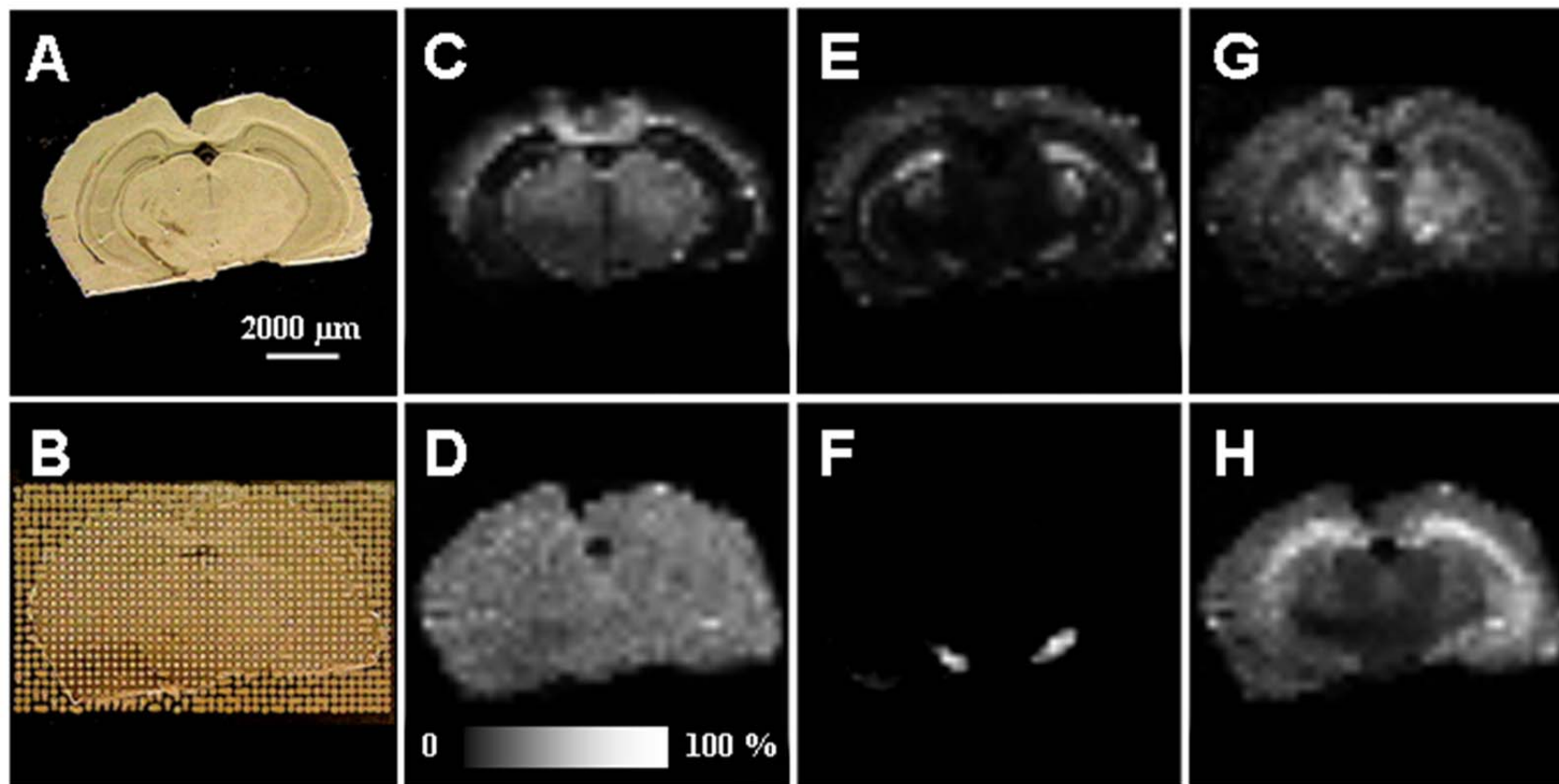
Figure 12: Matrix spotting and MALDI imaging of an adult mouse brain tissue section. (A) Matrix spots were printed as a rectangular array with a total of 1118 spots and 240 μm spot to spot distance. (B) Example ion images reveal the structure within the brain: (C) 14132 Da (D) 17885 Da (E) 6720 Da (F) 7338 Da (G) 11839 Da (H) 11790 Da. White represents the highest measured intensity.

Mapping of the distribution of proteins in this tissue is important to gain insight into spermatogenesis and may assist in the development of male contraceptives. Figure 13 shows ion images obtained from a mouse epididymis after matrix application with the ARM. Proteins are localized to distinct regions of the epididymis. For example the protein with $m/z = 5613$ was found only in the caput while the protein with $m/z = 11206$ was mostly located in the cauda and corpus. Several hundred ion images could be generated from such a dataset which makes this approach extremely valuable for discovery. One challenge that remains is the identification of proteins. In the mouse epididymis study, identification of proteins from this tissue had been carried out previously[119] and proteins could be matched via their corresponding m/z. Proteins with $m/z = 7285$, 8434, and 11206 were identified as ESPI (epididymal serine protease inhibitor), CRIP1(cysteine-rich protein 1), ACRBP (proacrosin-binding protein), respectively, while the protein with $m/z = 5613$ remains unknown.

While the spatial resolution of this approach is lower compared to the spray based approach, it provides spectra that show generally higher numbers of peaks thereby providing a more comprehensive inventory of the protein in the tissue. The nozzle-free design of the acoustic ejector allows printing of concentrated matrix solutions without the risk of clogging, a common problem with nozzle based printers used for matrix printing. Because the coordinates from each spot can be exported to the mass spectrometer, automated analysis of selected tissue regions spotted with discrete matrix spots becomes feasible. Cornett showed that such a workflow can be advantageous if high-throughput and cellular specificity are desired.[120]

.
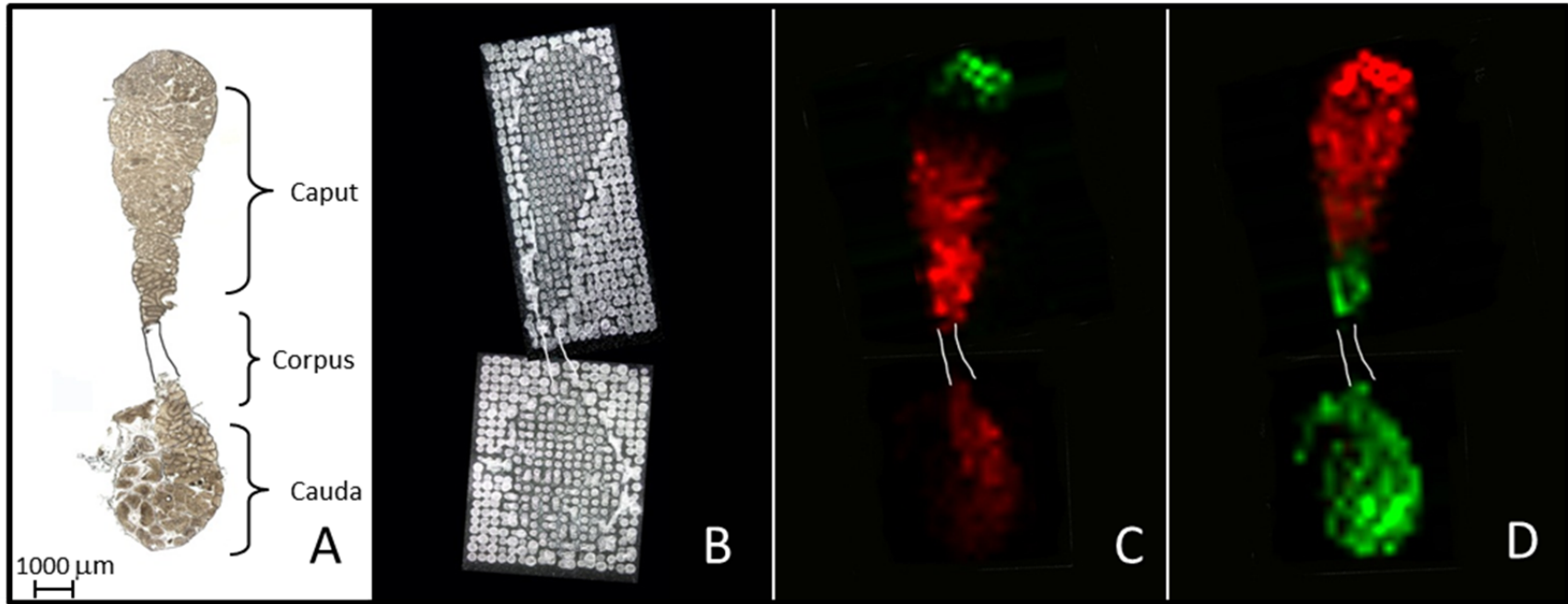
Figure 13: Imaging of mouse epididymis after matrix application using the ARM. (A) Optical image of an unstained serial section showing the distinct tissue regions. (B) Optical images for the spotted tissue. (C) Distribution of the protein with $m/z = 5613$ (unknown, green), and $m/z = 7285$ (ESPI, red). (D) Distribution of protein with $m/z = 11206$ (ACRBP, green) and 8434 (CRIP1, red).

Strategy for Protein Identification for MALDI IMS

The high sensitivity of MALDI IMS makes it a powerful technique for biomarker discovery in clinical tissues. As discussed earlier, protein identification is required to match the *m/z* value of a peak in the ion image to its corresponding protein. Homogenization of whole tissues and protein fractionation can be used in protein identification but homogenization of the whole tissue may increase the complexity of the sample rendering the identification more difficult.

Ideally, proteins would be identified from a tissue region where it is highly expressed, providing the first step of enrichment for subsequent fractionation steps. A workflow for the identification of proteins from serial tissue sections was developed and applied for discovery of differentially expressed proteins in a human clear cell renal cell carcinoma tissue. First, protein imaging of the tissue was carried out to identify differentially expressed proteins between tumor and tumor-free kidney tissue. Figure 14A shows an H&E stained tissue section where the distinct tissue regions corresponding to the tumor, the medulla and the cortex have been marked by a trained pathologist. The tissue was coated with a matrix spot array with 450 μm array pitch using the ARM (Figure 14B). Imaging of the coated tissue revealed a number of differentially expressed proteins (Figure 14C-F). For example, the unknown protein with *m/z* = 12343 is localized throughout the tissue but its relative intensity is increased in the tumor region. Using this protein as an example, a new workflow for protein identification was optimized. First, the tumor region of 4 serial tissue sections was excised by macro dissection.
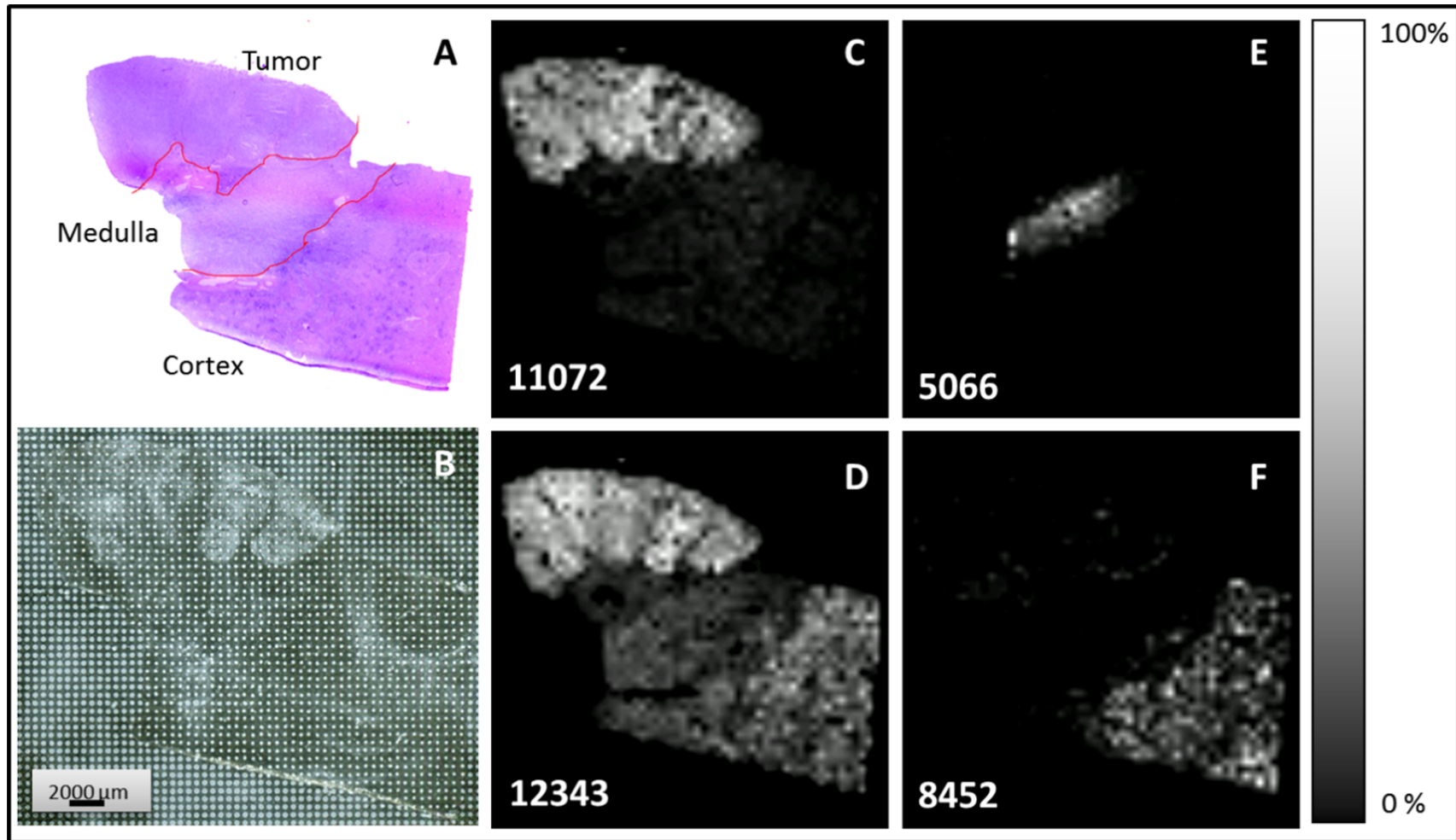
Figure 14: Discovery of proteins in a human kidney with clear cell renal cell carcinoma. (A) H&E stained serial section of the tissue. (B) Tissue after matrix application using the ARM. (C-F) Ion images showing the relative abundance of several proteins in the tissue.

Following protein extraction, a two dimensional fractionation protocol that combines off-line strong cation fractionation (SXC) and reversed phase chromatography using a C4 column was used to separate the complex protein mixture. Interestingly, even after two modes of separation, several proteins peaks which were close in mass to the protein of interest were detected (Figure 15).

Digestion of this fraction could make identification of the protein difficult especially if the protein was modified or if other high mass proteins were present in the sample. The low quantity of protein precludes the use of additional chromatographic fractionation steps which can severely diminish protein purification yields. Therefore, an alternative strategy using gas phase fractionation and top-down sequencing on a Qq-FT-ICR MS was implemented. To improve sensitivity, a microspray ESI set-up consisting of a 2 µl injection loop connected to a low dead volume nano injection valve was optimized allowing detection of proteins with high sensitivity. For example, detection of 250 fmol/µl ubiquitin delivered at 7µl/h could be demonstrated.
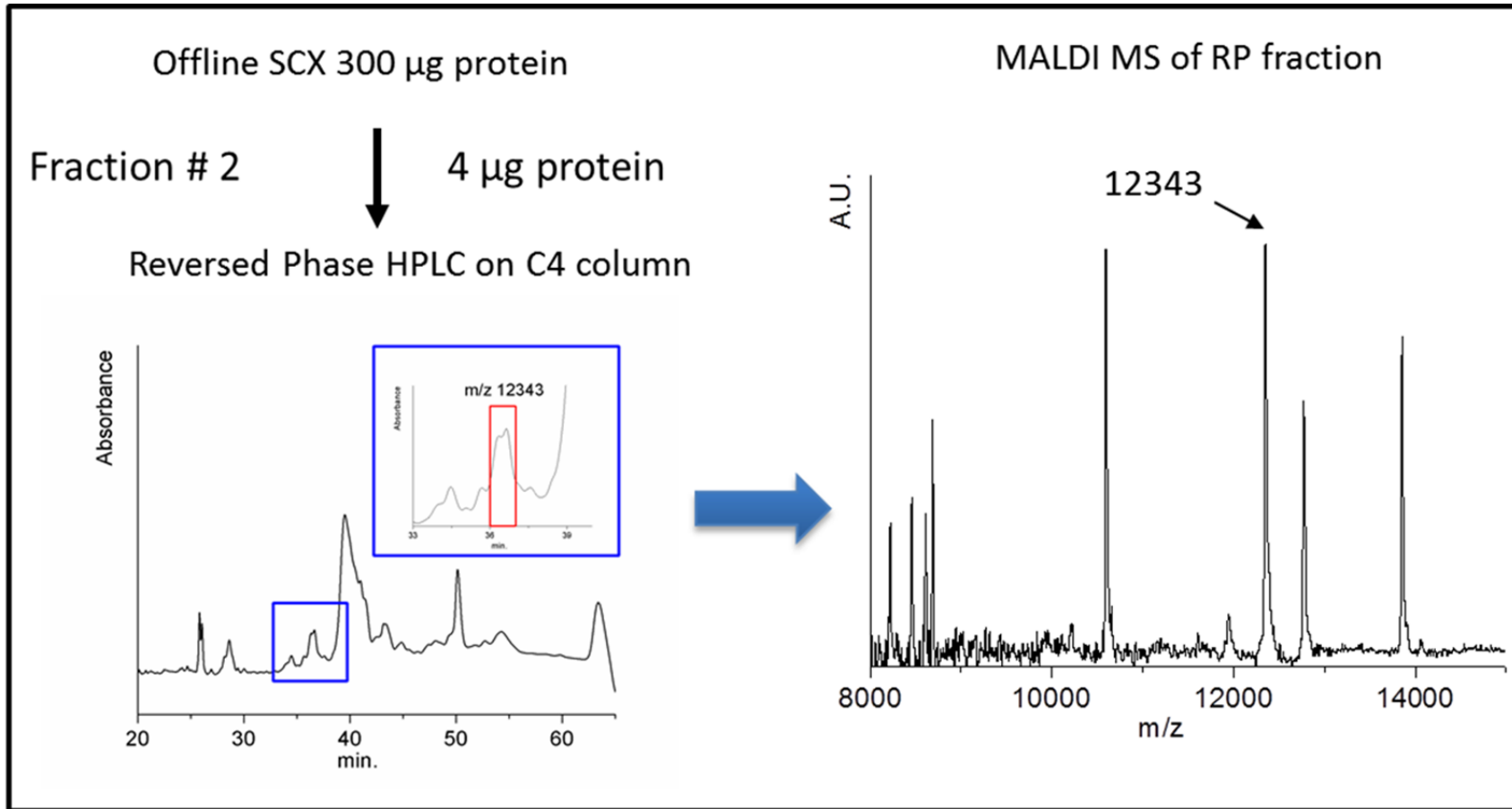
Figure 15: Workflow for protein identification from tissue. The protein with *m/z* = 12343 is enriched in one of the reversed phase fractions eluting around 36 min.

The ESI MS spectrum in Figure 16A shows the fraction of interest containing several multiply charged peaks. The complexity of the spectrum confirms the presence of several other proteins in this sample. Thus, the $[M+12H]^{12+}$ peak in the quadrupole was isolated and the ions were fragmented in the external collision cell. The resulting fragmentation spectrum (Figure 16B) was deconvoluted and submitted to database searching with ProSight PTM.[121] The protein was identified as macrophage migration inhibitory factor MIF, Swiss-Prot P14174. This identification yielded a significant score, with the measured mass of the precursor ion and the calculated mass of the identified protein were within 0.16 ppm. Along with the several characteristic fragment ions detected, successful identification of the protein could be achieved (Appendix B). Several other proteins were identified with this workflow indicating that using 4 modes of separation (selective protein enrichment from the tissue, SCX, reversed phase and gas phase fractionation) provide a powerful strategy for protein identification in MALDI IMS projects. In the future, the sensitivity and versatility of this workflow could be improved by implemented of chip based nanospray[122] which is expected to further improve sensitivity while reducing sample consumption. Alternative fragmentation techniques such as electron capture dissociation[123] could be implemented which could provide additional sequence coverage and assist in identification of modified proteins.
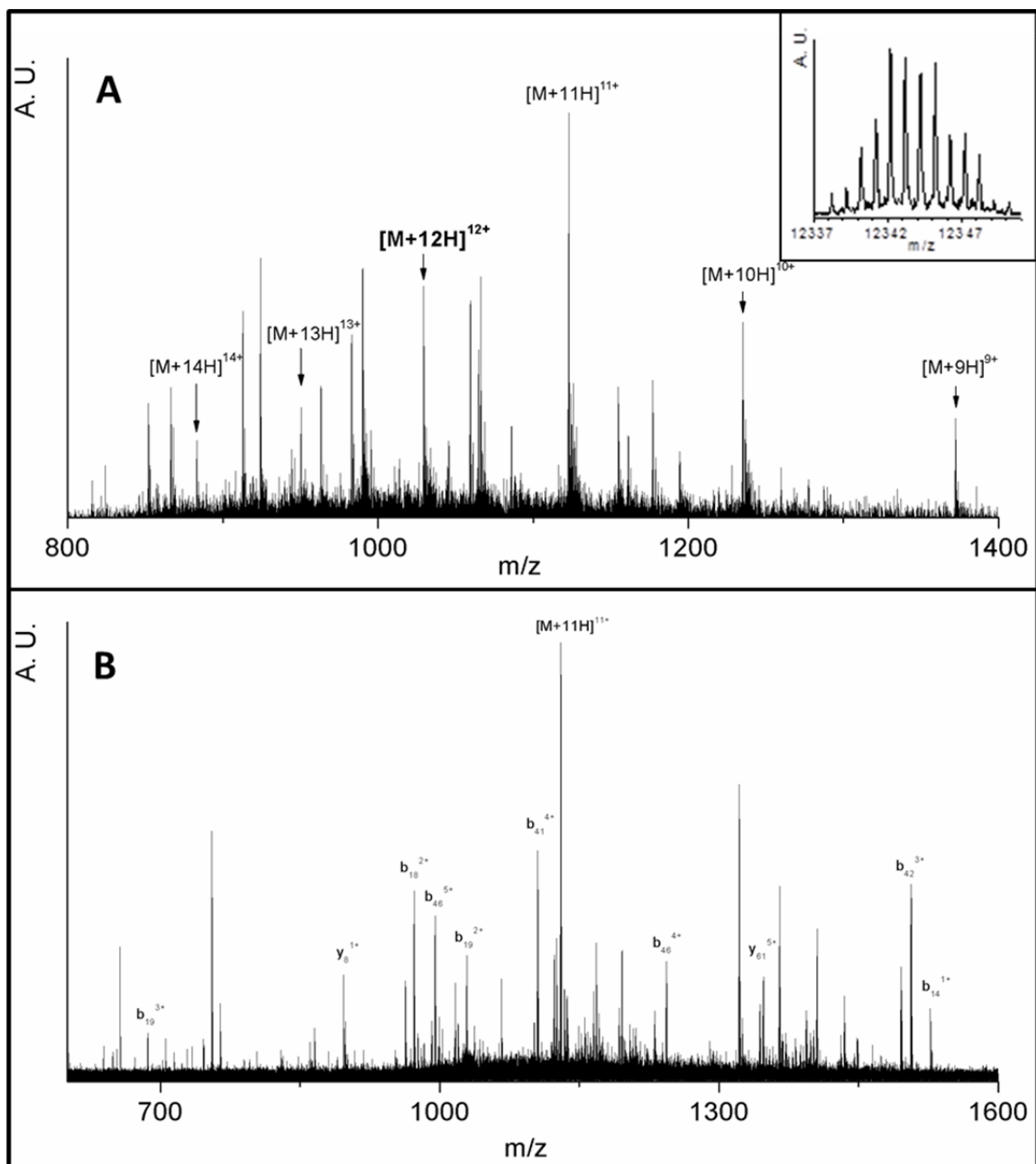
Figure 16: ESI-MS and MS/MS of protein fraction containing the protein with m/z = 12343. (A) ESI-MS spectrum showing multiply charged ions corresponding to the protein of interest. The inset shows the deconvoluted spectrum region for the protein of interest. (B) Fragment ion spectrum from $[M+12]^{12+}$ showing annotated ions corresponding to MIF.

Conclusions

Successful application of MALDI IMS for mapping of proteins in mouse brain and in human kidney tumor tissue has been demonstrated. First, tissue coating conditions were optimized for the analysis of proteins showing that robotic matrix deposition can generate high quality ion images which can reveal the relative abundance of proteins in a tissue. The ability to resolve small features is limited by the crystal size and matrix coverage for the spray-based technique and by the area covered by the matrix solution in the spotting approach. Typical spatial resolutions are 50-243 μm for the ImagePrep and ARM respectively. In general, the overall spectral quality seen with the ImagePrep compared with the ARM is probably due to less effective extraction of the proteins. IMS enables rapid detection of protein peaks in tissue regions that provide insight into the underlying biology. In that context, identification of the proteins is especially important as it links the *m/z* values in the ion images to a protein. A new highly sensitive workflow for protein identification has been described which can keep track of the proteins via their mass throughout the tissue purification steps. Top-down sequencing implemented here enabled gas phase enrichment of selected ions prior to fragmentation which provided additional selectivity.

Materials and Methods

Material

HPLC grade acetonitrile, trifluoroacetic acid (TFA), Freeze'it, halt protease cocktail, the Bradford protein assay kit and reagent grade ethanol were purchased from Thermo Fisher Scientific (Pittsburgh, PA). Protein standards, TRIS (2-Amino-2-(hydroxymethyl)-1,3-propanediol), ammonium acetate, NaCl and the polypropylene SPE tubes with frits were from Sigma-Aldrich (St. Louis, MO). Sinapinic acid (3,5-dimethoxy-4-hydroxycinnamic acid, 99% purity) was purchased from Fluka (Buchs, Switzerland) and used without further purification. The C_4 HPLC column and C_4 resin were obtained from The Nest Group (Southborough, MA) and the Sepax resin was from (Sepax Technologies Inc., Newark, Delaware).

Tissue Sectioning and Staining

Brain and epididymis tissue from adult CD1 mice was surgically removed and immediately snap frozen in liquid nitrogen or liquid Freeze'it, and stored at -80 °C until use. Human clear cell renal cell carcinoma tissue was obtained from the Vanderbilt University Ingram Cancer Center-Human Tissue Acquisition and Pathology Resource. This tissue was frozen in liquid nitrogen within 30 min of tissue harvest. Tissue sectioning was carried out in a microtome with section thicknesses of 12 μm. The tissue was thaw mounted onto cold ITO-coated glass slides[106] or gold-clad stainless steel MALDI targets. The targets were immediately transferred to a vacuum desiccator and allowed to equilibrate to room temperature (10 min). Serial sections of the tissue were mounted onto glass slides and stained with H&E or cresyl violet according to a protocol

described earlier.[106] Tissue for MALDI MS was subjected to a series of ethanol/water washes to fix the tissue while simultaneously removing MALDI contaminants such as physiological salts and other soluble low molecular weight compounds. Washing consists of gently agitating the plates in two successive 30 s baths of 25 mL of 70:30 % v/v ethanol/water followed by a 15 s wash in 25 mL of ethanol. Excess solvent was removed with a gentle blow of compressed dry air. The tissue was stored for at least 10 min but not longer than 24 h in a vacuum desiccator prior to matrix application. Magnified images from the spotted tissues were obtained on an Olympus BX 50 (Melville, NY) microscope equipped with a Q-Imaging 3.3 megapixel digital camera. Image-Pro-Plus Software from Media Cybernetics (Silver Spring, MD) was used for image analysis.

Matrix Application

ImagePrep: Matrix application with the ImagePrep (Bruker Daltonics, Billerica, MA) was carried out using sinapinic acid prepared at 10 mg/ml in 1:1 v/v mixture of ACN 0.2 % TFA as the matrix. The sensor signal was recorded using a 12 bit analog to digital converter (ADC) model NI USB- 6008 (National Instruments, Austin, Texas) operated with 5 Hz sampling rate and controlled by NI-DAQmx software provided with the ADC. A detailed description of the optimized method used for matrix application can be found in Appendix A.

ARM: A detailed description of the method for protein imaging with the ARM can be found here.[113] The spotting conditions for the clear cell renal cell specimen were 3 x 13 DPS at 10 Hz and 450 μm array pitch. The epididymis tissue was spotted with 2 x 13 DPS at 10 Hz with a 230 μm array pitch.

Protein Identification

     Protein extraction: Tissue was sectioned at 12 μm section thickness and the tumor region of the tissue was macro dissected with a razor blade. A total of 133 mg frozen tissue obtained from 4 tissue sections was transferred into a Kontes Dual 20 tissue grinder with glass pestle and protein was extracted with 1 ml cold extraction buffer consisting of a 50 mM, pH = 7.5 TRIS buffer with EDTA-free halt protease cocktail as recommended by the manufacturer. The lysate was spun down for 5 min at 16000 x g in the cold and the pellet was discarded. The protein yield was 777.5 μg as determined by the Bradford assay. An aliquot of the extract was diluted tenfold with the MALDI matrix for MALDI MS analysis to identify fractions containing the protein of interest.

     Fractionation of proteins: Fractions containing proteins of interest were separated by off-line SCX chromatography and reversed phase HPLC. For the SCX fractionation, a 3 ml polypropylene SPE cartridge was custom packed with 80 mg of Sepax SCX-NP5 resin with 5 μm particle size. The cartridge was conditioned with 2 x 1 ml loading buffer consisting of a 20 mM ammonium acetate prepared at pH = 4.5. Active sites on the column were blocked with 500 μl loading buffer containing 170 μg bovine albumin followed by a 1.5 ml wash with loading buffer and 2 washes with 1.5 ml of a 1.2 mol/l NaCl solution prepared in 20 mM ammonium acetate buffer with pH = 5.5. The column was then washed with 5 x 1.5 ml loading buffer. A total of 300 μg protein was dissolved in 1 ml loading buffer and loaded onto the SCX cartridge. The cartridge was washed with 3 x 350 μl of the loading buffer. Proteins were sequentially eluted with 2 x 200 μl of each elution buffer consisting of 20 mM ammonium acetate (pH = 5.5) with 0, 50, 150, 400, 650 and 1200 mmol/l NaCl respectively. The protein recovery for the SPE fractionation

was 31.5 % as determined by the Bradford protein assay. The pH of the salt fractions was adjusted to ~ 2.5 using TFA and fractions were subjected to reversed phase clean-up on 3 ml SPE cartridges containing 75 mg C4 reversed phase material with 20 μm particle size (Vydac # 214 TPB 1520). Each cartridge was conditioned with 2 ml of 70:30 % v/v ACN/water with 0.1 % TFA and 2 ml washing buffer consisting of 5:95 % v/v ACN/water with 0.1 % TFA. Each SCX salt fraction was loaded onto a separate column and washed with 2x500 μl washing buffer. Finally, the protein was eluted with 2 x 300 μl 50:50 % v/v ACN/water with 0.1 % TFA. The samples were dried in a rotary centrifuge operated for 15 min at 60 °C and then reconstituted in 15 μl of 5 % ACN 0.1 % TFA for MALDI MS analysis. The protein recovery as determined by the Bradford assay was 115 % for the reversed phase clean-up step. Fractions were analyzed by MALDI MS to identify the fractions containing the protein of interest.

Further fractionation was carried out using reversed phase HPLC carried out with an Agilent 1100 system which was equipped with a 25 cm, 2.1-mm ID C_4 column with 5 μm particle size. Four micrograms of protein were injected and the column was operated with a flow rate of 350 ul/min at 28 °C collecting fractions with an automated fraction collector with 1 min fraction collection intervals. Details of this set-up have been described earlier [124]. Briefly, a binary gradient consisting of 0.1% TFA in water or acetonitrile (solvent B) was used for elution of the proteins. The separation was carried out using the following linear gradient program: 0-3 min 5 % B; 10 min 25 % B, 20 min 35 % B, 59 min 55 % B, 62 min 95 % B followed by a 5 min wash at 95 % B. Chromatography was monitored by UV detection at 214 nm. Fractions were dried in a rotary centrifuge and reconstituted in 10 μl of solvent consisting of 50 % methanol and

2 % acetic acid. MALDI MS was carried out to identify the fractions containing the protein of interest.

MALDI TOF MS

Imaging of mouse epididymis: MALDI TOF MS for the epididymis image was performed on a Voyager-DE STR (Applied Biosystems, Framingham, MA) in linear positive mode using 25 kV acceleration voltage. Delayed extraction conditions were optimized for protein analysis between 2-70 kDa with a resolution of 1000 (FWHM) for m/z = 15000. Spectra were recorded at 20 Hz using a nitrogen laser with 337 nm wavelength focused to 100 μm. Signals between 2 and 70 kDa were recorded with 4-ns time bins. External calibration of the instruments was performed using a mixture of porcine insulin $[M + H]^+$ = 5778.6 Da, horse heart cytochrome c $[M + H]^+$ = 12361.2 Da and horse ampomyoglobin $[M + H]^+$ = 16952.5 Da deposited with the dried droplet method. Spectra acquisition was accomplished manually or under instrument control using the Sequence Editor module of the Voyager Control software package. To facilitate automated spectrum acquisition, custom plate files based on the matrix spot locations were generated. Absolute stage coordinates for the center of a number of registration spots were transferred from the mass spectrometer software into a spreadsheet where a bilinear fit was performed to interpolate the coordinates of all spots in the array. The resulting list of interpolated spot coordinates was exported into a plate file format and submitted to Voyager Control for automated acquisition. For each matrix spot, 400 individual spectra were summed in 40 spectra/location segments using a random search pattern confined within the area of the spots. Exclusion criteria rejected spectra with poor signal intensity (base peak <1000 counts) or containing peaks with intensity greater than

the 16-bit dynamic range of the digitizer. Programs written in our laboratory were used for automated processing of the spectra in Applied Biosystems Data Explorer software version 4.4. Operations performed on the data include a Gaussian smooth and removal of the baseline using the advanced baseline subtraction function. Individual spectra were then rendered into a modified Analyze 7.5 format (Mayo Clinic, Rochester, MN) compatible with the BioMap software (Novartis, Basel, Switzerland) package, 14 which was used for image analysis and extraction of selected ion images.

Imaging of mouse brain and ccRCC: Mass spectrometry was performed on Bruker Daltonics Ultraflex II MALDI-TOF/TOF and Autoflex II Billerica, MA instruments equipped with SmartBeam technology and dedicated imaging software. Spectra were recorded over the mass range from 2-70 kDa using linear positive mode and 4 ns time bins. Calibration of the instruments was carried out as described for the Voyager instrument. If not mentioned otherwise FlexAnalysis 3.0 and FlexImaging 2.0 were used for data processing. A custom script in FlexAnalysis was used for baseline subtraction and Gaussian smoothing. All images were normalized in FlexAnalysis using the TIC normalization algorithm.

The mouse brain image was acquired on the Ultraflex II instrument with a spherical laser beam focused to a diameter of 50 μm. Imaging was carried out in microprobe mode using 75 μm pixel pitch while summing 60 spectra from each sample location. The human kidney image was acquired on the Autoflex II instrument using a custom plate file generated as described above for the Voyager system. The spectra were the sum of 420 individual laser shots obtained in 60 shots increments randomly sampled within each

matrix spot. Data were baseline subtracted and normalized by TIC normalization with a custom MATLAB script creating a BioMap compatible file format.

MALDI TOF MS for protein identification: Samples for MALDI MS were prepared with the dried droplet sample preparation using sinapinic acid prepared at 20 mg/ml in a 1:1 v/v mixture of ACN and 0.2 % TFA. The spectra were the sum of 1000 individual laser shots obtained in 50 shots increments randomly sampled within each matrix spot. All spectra were baseline subtracted using automated scrip in FlexAnalysis

ESI-FT-ICR MS for top-down protein sequencing: Top-down sequencing of proteins was carried out on an apex-Qe instrument (Bruker Daltonics, Billerica MA) equipped with an actively shielded 9.4 T magnet and Apollo II Dual ESI/MALDI source. ESI was performed using a custom micro ESI set-up consisting of a PicoTip emitter model # FS360-20-10-D-5 (New Objective, Woburn, MA) that was mounted into the Bruker nanospray source. The emitter was connected with a 50 cm fused silica capillary (360 OD, 50 μm ID) to a micro injection valve (Upchurch Scientific, Oak Harbor, WA) equipped with a 2 μl injection loop. The valve was used for sample injection into a continuous flow of ESI solvent consisting of a 1:1 v/v mixture of 50 % methanol and 2 % acetic acid which was delivered using an external syringe pump operated at a flow rate of 7 ul/h. Calibration of the ICR cell was performed with bovine ubiquitin prepared at 250 fmol/ul in the ESI solvent. At least 4 multiply charged ions spanning the mass range of interest were used for calibration providing mass accuracies better than 1.5 ppm. Top-down sequencing was carried out by Qq-FT-ICR. First, ions were accumulated in the source hexapole for 2-5 s seconds to increase sensitivity and multiply charged precursor ions were isolated in the first mass selective quadrupole using an isolation window of 10

Da. Fragmentation of the selected ions was carried out in the in the external collision cell using Argon as the collision gas and a collision energy of 10-20 eV which was optimized individually for each precursor ion. Fragment ions were analyzed in the ICR cell using a 256 kpoint transient and a mass range from 400 to 1500 Da. Between 10-40 scans were accumulated into a single file. Spectra were deconvoluted using DataAnalysis software provided with the instrument and subjected to database searching against a human database using ProSight PTM[121]. An intact mass tolerance of 2000 Da and fragment ion mass tolerance of 25 ppm was used for all searches. Significant protein hits were manually verified with help of the Biotools data software package (Bruker Daltonics).

CHAPTER III

High-Throughput Profiling of FFPE Tissue Using Parallel Electrophoresis and MALDI MS[*]

Abstract

Analysis of formalin-fixed and paraffin-embedded tissues (FFPE) is increasingly recognized as a strategy for the discovery and validation of clinically useful biomarker candidates. Large tissue collections including tissue microarrays (TMA) are available but current analytical strategies for their characterization have limited throughput. In this chapter, a workflow for rapid analysis of hundreds of FFPE tissue specimens is described. The strategy combines parallel sample processing and on-chip electrophoresis with automated MALDI MS analysis. The method is optimized for small quantities of clinically valuable tissues allowing detection of hundreds of peptides from a single core in a TMA section. Results from the optimization of the method are described and the strategy is applied for the analysis of tissue microarrays containing formalin fixed tissue specimens from human kidney.

Introduction

Vast archival collections of formalin-fixed paraffin embedded (FFPE) tissue samples are a valuable discovery source for biomarker discovery since in many cases patient outcomes are known. FFPE procedures are routinely used to prepare surgical specimens for histological analysis and to render the tissue suitable for long-term storage. Unfortunately, direct protein analysis from FFPE specimens are not directly amenable to MS analysis as the chemical fixation with formalin creates a network of insoluble cross-linked proteins.[125] Recovery of proteins from FFPE tissue can be achieved through a procedure known as antigen retrieval (AR), which was developed to restore antigen-antibody reactivity in immunohistochemistry.[126] Antigen retrieval has been successfully adapted for analysis of FFPE tissue using MS[127, 128] but can introduce MS-incompatible reagents such as detergents and buffers, making time consuming sample clean-up necessary prior to mass spectrometric analysis. In turn, sample clean-up and fractionation steps severely limits throughput.

A new device for parallel electrophoretic sample processing for proteins and peptides has been developed[129] and I have employed it in our FFPE tissue analysis strategy as a clean-up stage. Using native electrophoresis as the separation principle, up to 96 samples can be processed in parallel with typical run times of less than an hour. The charge and electrophoretic mobility of analytes is controlled by the sample buffer, the polarity of the electric potential applied and the pore size of the polyacrylamide gel plug in each separation well. By keeping the running buffer constant and using multiple individual wells, separation into distinct fractions can be achieved. Compounds such as proteins and peptides are then captured on a monolithic reversed phase capture chip

directly below the electrophoresis gel. The capture chip is removed, mounted into an extraction device and analytes are eluted with the MALDI matrix solution or solvent into microvials for direct MALDI MS or ESI MS analysis. MALDI MS is especially useful if large numbers of samples need to be analyzed as it offers extremely high-throughput.

This chapter describes the protocol and its optimization for high-throughput analysis of FFPE tissues using parallel electrophoresis and analysis by MALDI FT-ICR. Uniquely, after completion of the dissection step, the optimized workflow is capable of analyzing several hundred samples per day, permitting rapid screening of vast FFPE tissue depositories for markers in disease of clinically relevant queries.

Results and Discussion

A new workflow for protein biomarker discovery in FFPE tissues is presented (Scheme 1). The strategy combines parallel sample processing and on-chip electrophoresis with MALDI-FT-ICR to enable high sample throughput. Differentially expressed peptides can be sequenced and identified using LC MALDI MS/MS. In this case, peaks from the profiles are linked to the sequence of the peptide using accurate precursor ion mass measurements on the FT-ICR instrument. Here we present this protocol and its optimization and apply it for the analysis of small FFPE tissue biopsies and TMAs.

Scheme 1: Workflow for high-throughput molecular discovery from FFPE tissue.

1: Discovery: Profiling

FFPE Tissue
↓
Microdissection
↓
Antigen Retrieval
↓
Tryptic digestion
↓
Electrophoresis
↓
MALDI-FTICR

2: Identification: LC-MALDI

LC-Fractionation
↓
MALDI-FTICR
↓
m/z of Peptide of interest
↓
MALDI-TOF-TOF
↓
Molecular Candidates
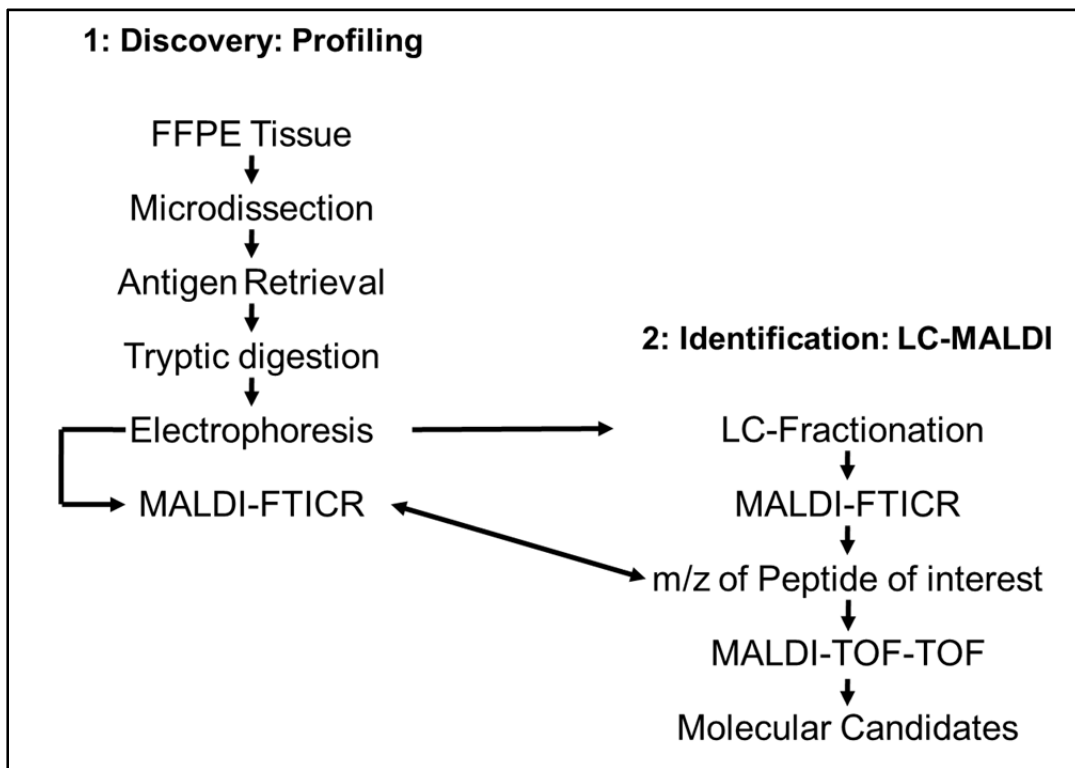
Tissue Microdissection

Microdissection with a tissue micropunch was used for tissue isolation from selected regions of the specimen determined from histology. Previous work used sections of 200-300 μm thickness mounted on glass slides and a tissue micropunch for dissection.[66] In the current paper, we modified this protocol to allow use of thinner sections, typically 5-40 μm thick. Tissue is placed onto a layer of laboratory parafilm and the membrane is mounted onto a self-healing punching mat. Stained serial sections can be used as a guide for dissection. Punching accuracy and the size of the punch, typically 0.35 to 4 mm defines the spatial resolution. The ability to rapidly obtain relatively large amounts of tissue combined with the possibility to visually track the dissected material during sample handling make this approach a valuable tool for tissue collection in high-throughput applications.

Antigen Retrieval and Tryptic Digestion

Optimization of the antigen retrieval protocol was performed using a TRIS buffer which is commonly used for antigen retrieval in immunohistochemistry. The basic composition of the buffer before optimization was 10 mM TRIS (pH 8.6 at 20 °C), 1 mM EDTA, 10 mM DTE and 0.05 % (6.7 x CMC) Tween-20. TRIS[18] and EDTA[19] are common AR buffer components and their efficiency has been discussed extensively. DTE was added for reduction of cysteines, reducing the number of steps in the workflow. Optimization of antigen retrieval conditions was carried out using a FFPE mouse liver tissue that was dewaxed and then homogenized with a mortar and pestle. The average particle size of this homogenized material, determined by microscopic analysis of 50 randomly selected particles, was 2 μm ± 1 μm, rendering this material useful for all

subsequent optimization experiments. The first set of experiments investigated the effect of temperature and incubation time on tissue solubility. FFPE standard tissue was mixed with the antigen retrieval buffer and subjected to antigen retrieval at 95 °C in a sand bath or in a laboratory autoclave operated at 121 °C. Visual inspection of the samples showed that tissue treated for 1 or 2 h in the sand bath was mostly intact while a single 50 minute autoclave treatment at 121 °C successfully dissolved most of the tissue. Hence, AR in the autoclave was used for all further experiments. The effect of sample pH and detergent was also investigated. Lowering the pH from 8.6 to 4.0 did not improve tissue solubility as judged by both visual inspection of the reaction and by analysis of peptides after subsequent digestion. These results support evidence that the pH of the antigen solution may be optimized for different tissue types.[130] The effect of the detergent was studied by varying the concentration of Tween-20 (CMC = 0.06 mM) and octyl-β-D-maltoside (CMC = 0.17 mM) at 0, 6.7, 27 and 270 × the detergent CMC. Detergent was found to improve tissue solubility when compared to the negative control. No improvement of tissue solubility was observed above 27 × the CMC. Follow-up experiments studying digestion of BSA in the presence of the detergents were performed. Improved sequence coverage was observed for Tween-20 compared with octyl-β-D-maltoside which showed lower performance at all detergent concentrations tested probably due to interference with the digestion. Hence, Tween-20 at a concentration of 27 × its CMC was selected as the detergent. The final composition of the antigen retrieval solution was 10 mM TRIS (pH 8.6), 1 mM EDTA, 10 mM DTE and 0.2 % (27 x CMC) Tween-20. The advantage of this buffer is that it is compatible with downstream sample processing including tryptic

digestion and electrophoresis. This eliminates potential sample loss and improves the speed of the analysis.

Detergent Removal and Peptide Fractionation with Parallel On-Chip Electrophoresis

Tolerance of MALDI MS toward salts and detergents is limited and efficient sample clean-up can increase sensitivity and remove spectral interferences. Direct MALDI MS of peptides obtained from antigen retrieved and digested FFPE tissue showed poor matrix crystallization and the mass spectra were dominated by detergent-related peaks. Removal of the detergent together with peptide fractionation was initially attempted using strong cation exchange (SCX) chromatography. Peptides were distributed between several fractions and the approach was difficult to automate, resulting in limited throughput. Therefore, electrophoretic on-chip sample preparation[129] was investigated as an alternative. For this purpose, samples were mixed with a pH 5.35 running buffer and loaded into wells of an electrophoresis cartridge consisting of 96 individually controlled wells. Electrophoresis was carried out under constant current control (1 mA). Charged molecules were separated on a short acryl amide gel plug and captured on a hydrophobic monolithic capture column for subsequent extraction with the MALDI matrix solution. Fractionation of the peptides can be controlled by the duration of electrophoresis and the polarity and potential applied to the sample reservoir; positive for cation capture and negative for anion capture. Initial optimization of the process was carried out using a tryptic digest of BSA mixed with the antigen retrieval solution. Figure 17A shows successful removal of the detergent and fractionation of the peptides into two complementary fractions. It is noted that detergent-related peaks were completely absent

after electrophoresis. Detailed analysis of the data (Figure 17B) revealed that peptide fractionation can be predicted by the theoretical pI of a peptide. Importantly, detergent removal and fractionation allowed detection of 42 peptides from BSA while only 19 peptides were identified in the detergent containing raw sample.

Electrophoresis running conditions were further optimized for the analysis of a tissue digest from antigen retrieved mouse liver FFPE tissue. Aliquots corresponding to 5 μg FFPE tissue digests were loaded into each well and the charge applied for electrophoresis was varied between 1 and 3 coulombs. The number of detectable monoisotopic ions for each polarity is reported in Table 1

Table 1: Optimization of running conditions for electrophoresis of 5 μg of FFPE mouse liver tissue.

Mode	Cation			Anion		
Charge C	# peaks	Confidence Interval N=4	Confidence Interval %	# peaks	Confidence Interval N=4	Confidence Interval %
1	319	36	11	289	53	19
2	282	33	12	269	30	11
3	285	60	21	245	42	17

Sample processing time and reproducibility of the data were used as criteria for selection of optimized running conditions; 1 coulomb for cation and 2 coulombs for anion capture respectively. Under these conditions, 588 ions could be detected from the combined cation and anion fractions. Importantly, the spectra showed that most of the peptides in the individual fractions were unique (Figure 18) thereby maximizing peak capacity of the mass spectrometer.
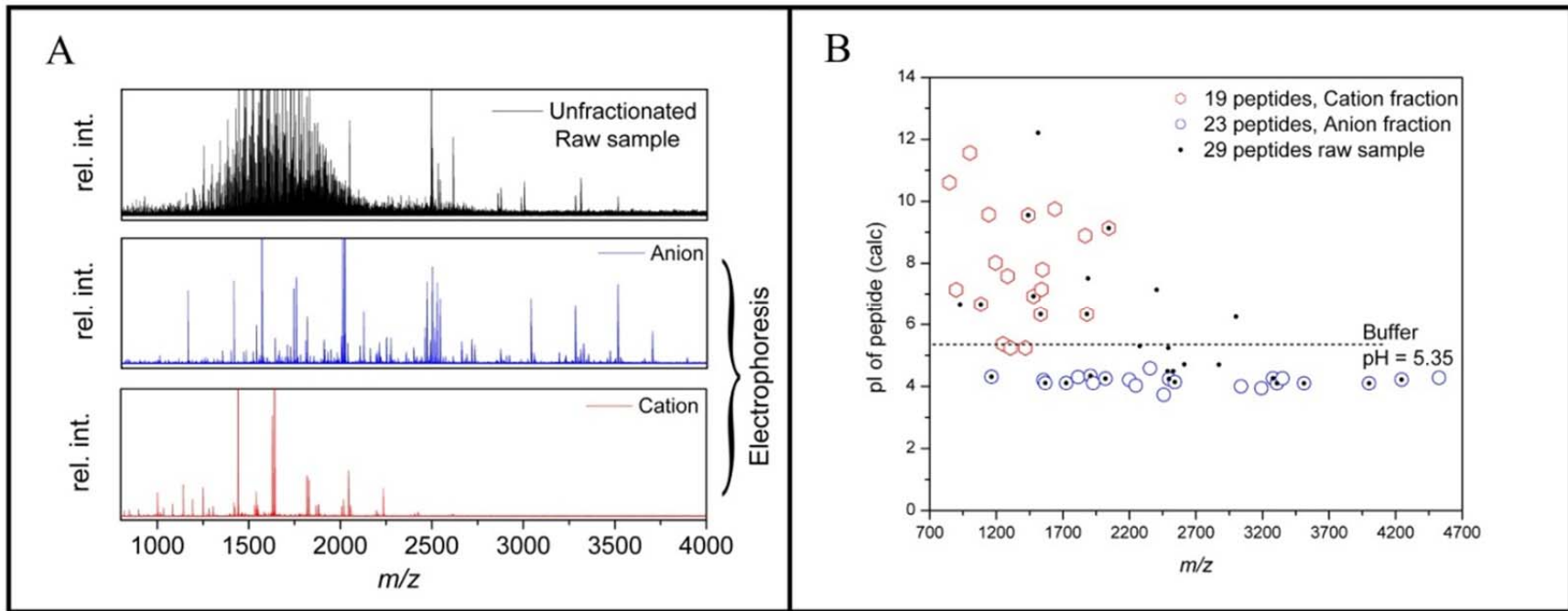
Figure 17: Electrophoretic fractionation of a BSA raw digest containing tween-20 detergent. (A) The raw sample shows a strong interference in the mass spectrum from the detergent which is completely absent after electrophoresis. (B) BSA peptides are fractionated into two complementary fractions defined by the pH of the electrophoresis running buffer. The total number of detected BSA peptides increases from 29 in the detergent containing raw sample to 42 after fractionation.
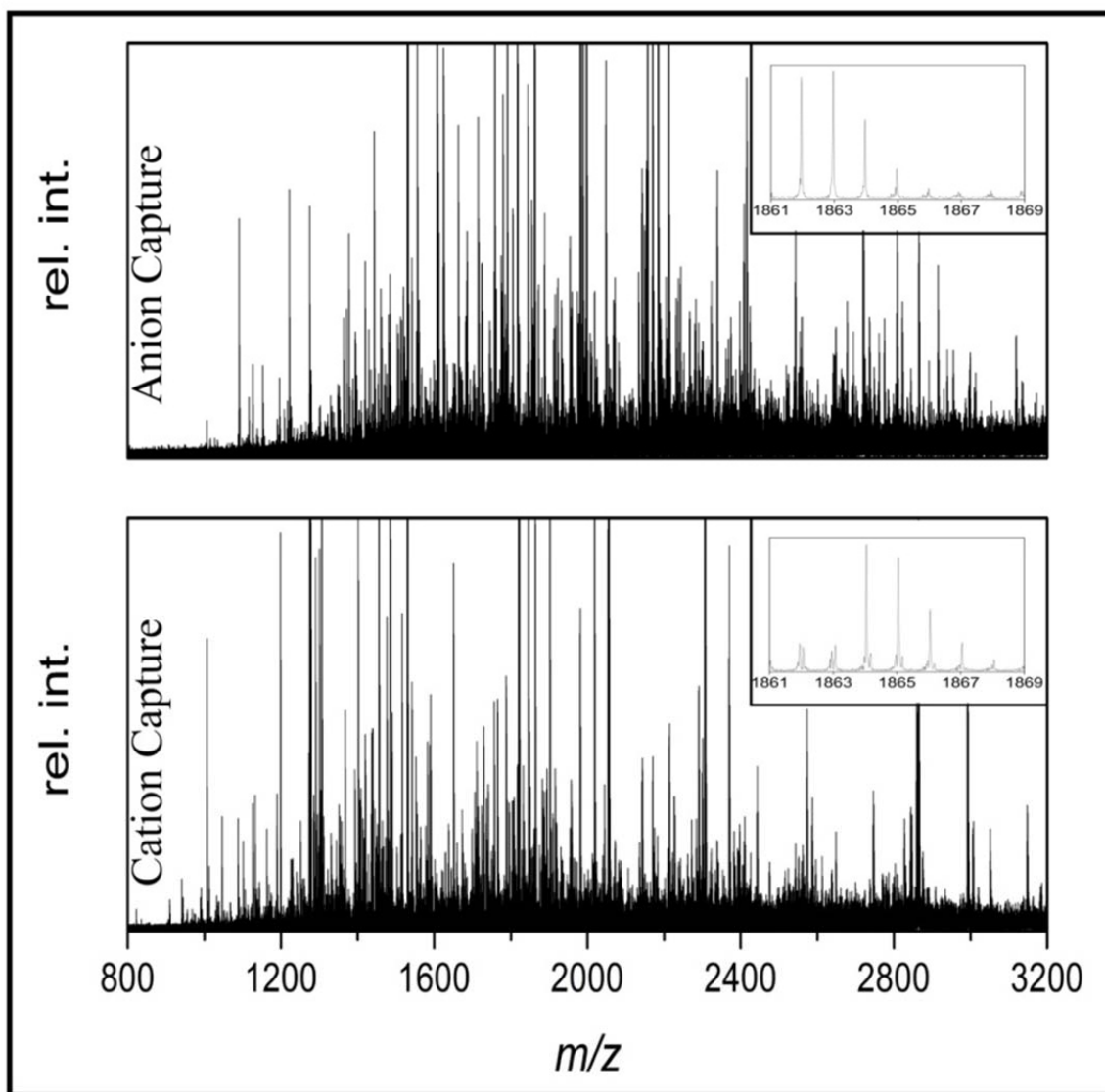
Figure 18: Complementary peptide patterns are observed from the analysis of 5 µg FFPE mouse liver in both anion and cation capture mode maximizing peak capacity in the mass spectrometer. The total number of detected monoisotopic peptides was 588.

Performance Evaluation

The performance of the method was assessed by comparing fresh frozen and FFPE mouse liver tissue. It is reasonable to expect that similar peptide profiles should be obtained assuming that the antigen retrieval step is optimized. Sections of 30 μm thickness were subjected to microdissection using a 600 μm diameter punch. Six punches from each tissue were combined and processed using the workflow described above. The protein concentration and cell numbers for this experiment were estimated by assuming that 18 %[131] of the total mass of a cell is protein and the average diameter of a cell is 10 μm. In this case, 97,200 cells corresponding to 9.2 μg of protein were used in each experiment. Electrophoresis was performed in cation capture mode and spectra from 3 technical repeats were averaged (Figure 19A). Automatic peak picking using the SNAP-2 algorithm resulted in detection of 422 ions from fresh frozen and 366 ions for FFPE tissue. A total of 114 common peaks were detected by binning the peak lists with a 0.01 Da window and common bins were identified by filtering the data in Excel. It is understood that this approach may reduce the number of common peaks, as common peaks split between two bins may be lost. Nevertheless, the average peak intensity ratio of the selected peaks was evenly distributed around the expected value of 1 (Figure 19B). This indicates that this method can successfully generate peptide patterns from FFPE tissue that are similar the peak patterns from fresh frozen tissue.
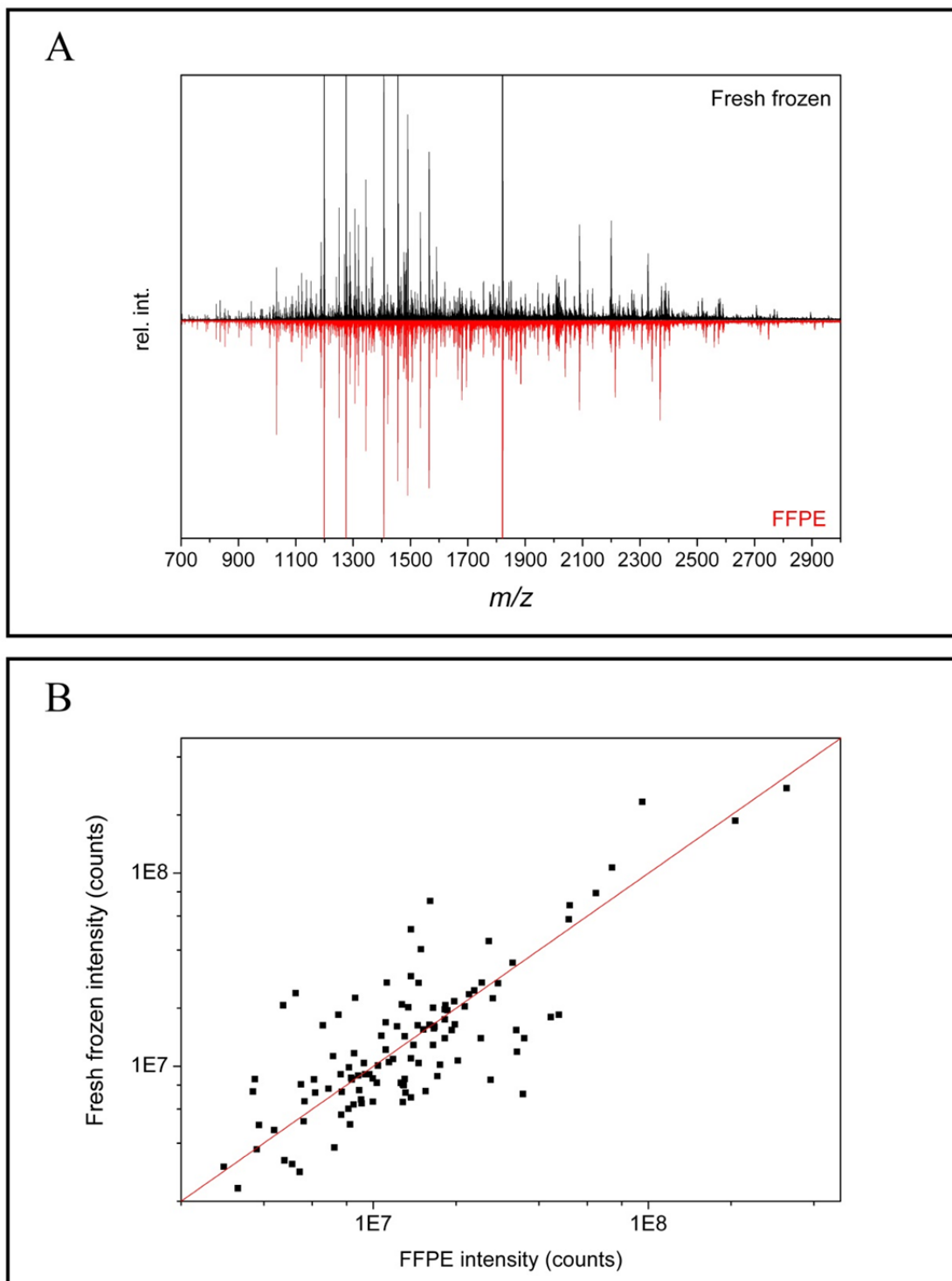
Figure 19: (A) Comparison of MALDI FT-ICR spectra obtained after electrophoretic clean-up of fresh frozen and FFPE mouse liver tissue after antigen retrieval and digestion. Spectra from cation capture experiments are presented showing similar peak patterns. (B) Distribution of the peak intensity ratios of common peaks are centered around the expected peak ratio of 1.

The sensitivity and reproducibility of the method was investigated using single tissue micropunches obtained from serial 10 μm thick FFPE mouse liver tissue. Micropunches with 500 μm and 2 mm diameter were used to isolate an estimated 15,000 or 60,000 cells corresponding to 1.4 and 5.7 μg of protein respectively. The sensitivity of the method permits detection of peptide signals from as little as 15,000 cells, although the quality of the spectra was improved if 60,000 cells were used. In this case 423 and 303 peptides were detectable from cation and anion capture fractions, respectively. Repeated analysis of single punches consisting of 60,000 cells generated spectra that were extremely similar. The 95 % confidence interval for the number of detected peaks was better than 12 % for both anion and cation capture mode (N=4).

We also applied this protocol for the analysis of TMA specimens and tissue biopsies. For this purpose, a 3 x 3 TMA from FFPE mouse liver and kidney tissue with 1 mm diameter tissue cores was used. The TMA was cut at 10 μm thickness and individual array spots were isolated using a 2 mm tissue micropunch resulting in isolation of an estimated 15000 cells. Mass spectra obtained from these samples showed organ specific peptide patterns indicating that the method has the potential to identify tissue specific peptides. FFPE tissue biopsies from the clinic were also investigated. Figure 20 shows the results from the analysis of a human clear cell renal cell carcinoma after microdissection with the micropunch. Spectra from the tumor and adjacent healthy control tissue show distinct peak patterns indicating that this method can discriminate pathologically relevant tissue regions.

Identification of Differentially Expressed Peptides.

Identification of differentially expressed peptides was achieved using a modified LC MALDI workflow. Scheme 1 shows the overall process. Peptides are eluted from the electrophoresis chip and subjected to LC fractionation, spotting onto anchor chip and accurate mass measurement using MALDI FT-IRC followed by automated sequencing from the same target using MALDI TOF/TOF MS. A detailed summary of the identified peptides from a LC MALDI experiment of mouse liver tissue is included in Appendix D showing the identification of 240 peptides. This corresponds to 138 proteins assuming a false discovery rate of 5 % at the peptide level and a minimum of 2 peptides for each protein as a criterion for successful protein identification. The identified peptides can be linked to the profiling data using accurate mass measurement. This process was tested using FFPE mouse liver. It was possible to identify nominally isobaric peptides as they were separated during the LC experiment. As an example, the peptides KHHLDGETEEER from glutathione S-transferase and LGEYGFQNAILVR and GLVLIAFSQYLQK, both from serum albumin, with calculated monoisotopic *m/z* of 1479.6823, 1479.7954 and 1479.8570, respectively, were identified.
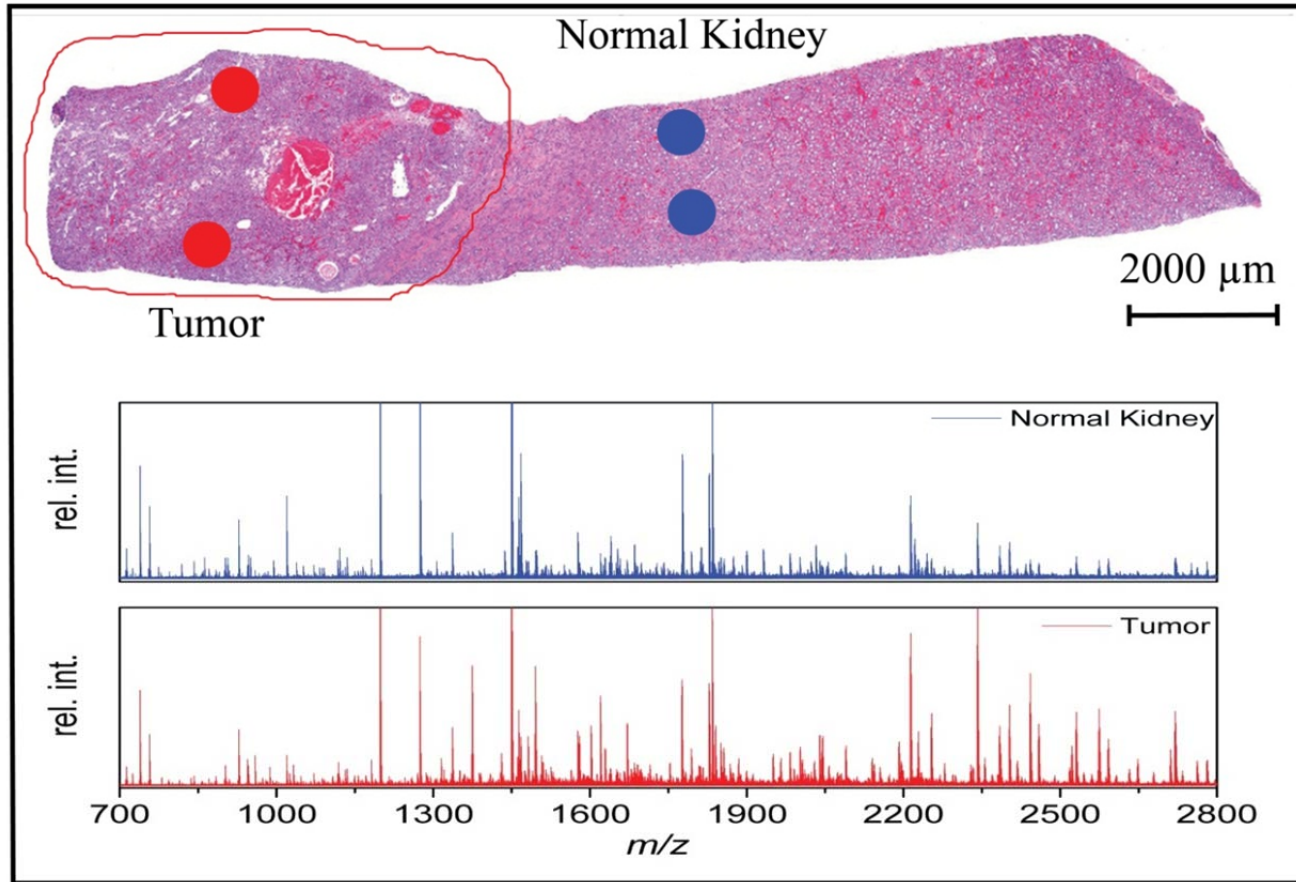
Figure 20: H&E stained section of a human clear cell renal cell carcinoma sample (Fuhrman grade III) obtained from a FFPE tissue repository with the punched regions marked. Representative spectra after electrophoresis in cation capture mode show distinctly different peak patterns.

Conclusion

A high-throughput workflow for the analysis of FFPE tissues is described. The method takes advantage of parallel on-chip electrophoresis and MALDI-FT-ICR allowing rapid sample processing. We estimate that several hundred samples can be processed per day making this method an ideal choice for screening of large tissue archives. Over 700 peptides were detected starting with only 60,000 cells but peptides could be detected from as few as 15,000 cells. Peptide profiles from FFPE tissue were similar to profiles obtained from fresh frozen tissue, allowing this technology to be used with large collections of FFPE tissues which have long-term clinical data. A modified micropunching technique was developed allowing rapid microdissection from tissue sections as thin as 5 μm. Situations requiring higher dissection accuracy may require LCM, but this can lower throughput. Detergent removal and pI based fractionation using on-chip parallel electrophoresis was critical for efficient sample preparation prior to MALDI MS analysis. Electrophoresis generates peptide fractions that are complementary which reduces spectra complexity, maximizes peak capacity and simplifies downstream data interpretation. Mass spectrometers that provide high mass accuracy and resolving power like FT-ICR, QTOF and Orbitraps are ideally suited for this application. Identification of the differentially expressed peptides is an important part of overall process as it enables linking of the data to underlying biological processes.

Materials and Methods

Reagents. All chemicals were purchased from Sigma-Aldrich (St. Louis, MO, USA) and were of highest purity available. HPLC grade acetonitrile (ACN) and ethanol, enzyme grade Tween-20 detergent, histological grade xylenes, diammonium citrate and parafilm M were purchased from Fisher Scientific (Air Lawn, NJ). Trifluoroacetic acid (TFA) and α-cyano-4-hydroxycinnamic acid (CHCA) were purchased from Fluka (Buchs, Switzerland). TRIS base was from J.T. Baker. (The CHCA matrix was 2x recrystallized from ethanol and water. Ammonium bicarbonate (AMBIC), iodoacetamide (IAA), 1,4-Dithioerythritol (DTE) and neutral buffered formalin solution 10 % were obtained from Sigma-Aldrich. Sequencing grade modified trypsin was purchased from Promega (Madison, WI, USA). Peptide standard mix and protein standard mix for MALDI-TOF-(TOF) calibration were from Bruker-Daltonics (Billerica, MA).

Tissue processing. Adult CD-1 mice were sacrificed and dissected organs were immediately snap-frozen in liquid nitrogen or subjected to fixation in 10 % neutral buffered formalin. Sectioning of the fresh frozen tissue was described in detail elsewhere[102]. Formalin fixation was performed on tissue specimens not thicker than 500 μm to allow rapid penetration of the fixative. Fixation was carried out for 41.5 h at room temperature and tissue was transferred into 70 % ethanol. Further tissue processing including paraffin embedding and sectioning was carried out at the Vanderbilt Human Tissue Acquisition Core. Sections were cut with a microtome with section thicknesses of 5-40 μm. The tissue was mounted onto 1-8 layers of laboratory Parafilm M for punching experiments or standard glass slides for H&E staining. The tissue micropunch consisted of a 21.5 gauge guide wire assembly (Small Parts, Inc, Miramar, FL) or commercially

77

available 0.35 and 2 mm diameter Harris uni-core punches (Ted Pella Inc, Redding, CA). Punching was carried out on a self-healing punching mat from the same manufacturer and the punch was carefully cleaned between punching to prevent cross contamination.

Antigen retrieval and digestion. Tissue punches corresponding to roughly 60,000 cells or up to 15 µg of FFPE tissue were collected in a 150 µl well of an Eppendorf (Hamburg, Germany) 96 well twin.tec PCR plate. Twenty µl of the antigen retrieval solution consisting of 10 mM TRIS, 1 mM EDTA, 10 mM DTE and detergent (see results section for details) was added. Antigen retrieval was carried out in a sand bath at 95 °C or in a STERIS (Mentor, OH) model SV120 laboratory autoclave operated with the standard liquid cycle at 121 °C. In this case, samples were covered with aluminum foil allowing pressure exchange and preventing sample spill during autoclaving. The reaction was allowed to cool for 15 min and 2 µl of a 300 mM IAA$_{(aq.)}$ was added. Alkylation was carried out for 15 min in the dark. Excess IAA was quenched by adding 5 µl of 100 mM DTE$_{(aq.)}$. Finally, 20 µl 100 mM AMBIC (pH = 8.0, 20 °C) and trypsin was added and digestion was carried out at 37 °C for 15 h. Note that the protein to enzyme ratio was 20:1 but enzyme concentration was at least 1 µg/100 µl if the protein concentration was low. The sample was taken to dryness in a vacuum centrifuge operated at 60 °C. It is noted that this protocol scales well for processing of up to 500 µg tissue.

Electrophoresis. Electrophoresis was carried out on a Passport 1200 instrument from Protein Discovery (Knoxville, TN) using Passport RP sample prep cartridges. A detailed description of this instrument can be found somewhere else.[129] Briefly, a sample cartridge comprised of 96 individually controlled wells was filled with the running buffer consisting of 689 mM MES pH 5.35 (20 °C). Peptides were reconstituted in 40 µl of the

sample buffer, 30 % (w/v) sucrose and 45 mM octyl β-D-glucopyranoside prepared in running buffer, and aliquots of this mixture were transferred into the sample cartridge. Electrophoresis was carried out at 1 mA with a total of 2 coulombs passed-charge for cation and anion capture mode respectively. Cation and anion capture experiments were performed in series using a single sample cartridge. Sample buffer (350 µl) was exchanged at 0.5 coulomb for cation capture and 1 coulomb for anion capture experiments. The cartridge was disassembled and the capture chip located beneath the gel plug and the sample well was removed. All 96 capture surfaces were washed simultaneously by immersing the capture chip for 4-6 h in 0.1 % TFA. The capture chip was allowed to dry and mounted into the extraction device provided with the instrument. Peptides were extracted with 3 µl of the matrix solution consisting of 12 mg/ml CHCA and 10 mM diammonium hydrogen citrate prepared in 1:1 acetonitrile/0.2 % TFA (aq.). The extraction was carried out for 60 s prior to 5 aspiration/dispensing cycles with a mechanical pipette for mixing the well content. Finally, 1.5 µl of the well content was directly spotted onto a Bruker MTP 384 polished steel target for MALDI MS analysis. Calculation of peptide pI values was carried out using GPMAW software ver. 8.1 (Lighthouse Data, Denmark) with the Skoog-Wichman algorithm.

Mass Spectrometry. MALDI FT-ICR MS was carried out on a 9.4 T Bruker Apex Qe equipped with an Apollo 2 ion source and a modulated Nd : YAG laser[86] operated at 100 Hz. External calibration was performed using a custom peptide mixture consisting of Bradykinin 1-7, Angiotensin II, [Glu[1]]-Fibrinopepdide β, ACTH fragment 18-39 and Insulin chain B oxidized with theoretical *m/z* ratios of 757.39915, 1046.54179, 1570.67684, 2465.19833 and 3494.65077, respectively. Typical mass accuracy was better

than 5 ppm over the observed mass range from 600-4000 Da. The external storage quadrupole was used to accumulate 250 laser shots from a single sample position prior to FT-ICR analysis. A total of twenty scans were accumulated from each sample spot and saved into a file. Data acquisition was automated using custom software tools written to generate sequences files for the Hystar software (ver. 3.4) supplied with the instrument. Spectra were processed using customized scripts for Bruker DataAnalyis version 4.0 which performed peak picking and export of the peak lists and raw spectra in ASCII format for further processing in OriginPro 7 and MATLAB. Monoisotopic peaks were determined using the SNAP-2 algorithm with a minimal signal-to-noise (S/N) of 3:1 and a quality factor of 0.4.

LC MALDI for peptide identification. LC-MALDI was carried out on a Agilent 1100 binary pump attached to a flow splitter, manual injection valve with 2 μl sample loop and a 125 μm ID capillary column packed with 8.5 cm 3 μm Monitor C_{18} resin (Column Engineering. Ontario, CA). The column was attached to an Accuspot spotter (Shimadzu Biotech) for eluent deposition onto a 384 well, 600 μm stainless steel anchor chip from Bruker Daltonics. The chip was prepared with CHCA according to the instructions provided by the manufacturer. The fraction collection interval was set to 30 s and a sheath flow of 0.1 % TFA at 2.8 μl/min was delivered with the matrix pump to assist deposition of the eluting peptides. Peptide separation took place at a flow rate of 1 μl/min using water and acetonitrile with 0.1 % TFA as the eluent. The gradient was ramped from 2-45 % acetonitrile in a 45 minute time window resulting in collection of 90 fractions. MALDI FT-ICR MS was performed to determine the accurate mass of the peptides and peptides were automatically sequenced from the same target using an

Ultraflex II MALDI TOF/TOF instrument from Bruker Daltonics equipped with Warp LC v 1.1. Finally, database searching was performed using Myrimatch[132] and search results were filtered using IdPicker[133] software ver. 2.2.2 with a peptide false discovery rate of 5 %. Detailed information about the software parameters used for peptide identifications can be found in the Appendix C.

CHAPTER IV

Combining LCM and On-Chip MALDI MS for the Analysis of Selected Cells in Tissue

Abstract

Enrichment of cells with single cell type specificity for proteomics is desirable because it allows cell type specific protein discovery in tissues. Not only does this reduce the complexity of the sample but it provides increased sensitivity and dynamic range as large numbers of cells can be accumulated prior to analysis. However, isolation of single cells from a tissue using LCM can be time-consuming which renders proteomic analysis tedious or impractical especially if the availability of tissue is limiting. This led to the development of new workflows for the analysis of LCM captured cells from fresh frozen and FFPE tissue. By combining the spatial selectivity of LCM with on-chip processing, high sensitivity and unprecedented tissue resolution was achieved. Dissection and on-chip capture of dissected tissue on a Zeiss MicroBeam LCM were optimized. Antigen retrieval, protein extraction, digestion, clean-up and analysis of peptides were directly carried out on the capture chip which reduced the potential for sample loss. Special care was taken to ensure compatibility of on-chip chemistry with downstream MALDI FT-ICR MS analysis. The high peak capacity and sensitivity of this technique allowed detection of 3,000 peaks from less than 100 dissected cells. The overall reproducibility and sensitivity of the workflow was determined for the fresh frozen and the formalin fixed tissue allowing detection of proteins from as few as 20 cells.

Introduction

Spatial proteomics of tissue samples using MALDI MS is an emerging tool for molecular pathology because it enables discovery of diagnostically useful protein markers that can be correlated with disease.[134, 135, 136, 137, 138] An ongoing challenge is mapping protein changes in tissues with morphologically complex architecture, which requires methods with high spatial resolution to distinguish between the cells. As the spatial resolution of surface sensitive methods such as MALDI MS is increased, its sensitivity is reduced.[38, 139] One solution to this problem is to enrich cells prior to analysis. In order to maintain single cell selectivity, a method capable of isolating single cells from tissue is required. Laser capture micro dissection (LCM) is widely used for this purpose.[68, 72, 140, 141] The advantage of LCM is that it combines the function of a microscope with the ability to dissect cells with single cell specificity. Proteomic studies typically require several thousand[127] cells for analysis as the overall sensitivity is limited by sample loss occurring during processing and sample analysis. Indeed, sample losses in proteomics can be significant. As an example, I have developed a new workflow for protein marker discovery in tissues[87] (Chapter III) which required at least 15,000 cells for analysis because of sample losses during sample clean-up and fractionation. Sample losses in proteomics are most likely the result of multistep workflows where sample losses accumulate for each processing and transfer step resulting in overall poor sensitivity.[142, 143] These sample losses are relevant for single cell population proteomics as enrichment of large cell numbers by LCM is extremely time-consuming especially if single cells need to be dissected from a morphologically complex tissue. For example, dissection of 15,000 single mammalian cells with 20 μm diameter from a heterogeneous

tissue would require at least 8 h for the dissection alone using current LCM technology. Clearly, this limits the usability of this technique for potential clinical applications where high-throughput and cellular specificity are desired. In addition, there are many cases where the availability of pathologically interesting cells is limited such as in small tissue biopsies or in cytology.[144] Therefore, there is a clear need to develop methods that can analyze small numbers of isolated cells with high sensitivity. I hypothesized that sensitivity could be improved if contact of the tissue with surfaces could be reduced throughout the analysis. The ongoing miniaturization of sample handling devices is promising as this is an effective way to reduce the surface in contact with the proteins which maximizes sensitivity.[145] Indeed, lab-on-a-chip devices are being developed for protein analysis including protein enrichment, processing[146] and detection.[147, 148] At this time, most platforms focus on cultured cells or protein extracts and analysis of cells dissected from tissues remains a novelty. Here I describe a new workflow that combines on-chip processing and MALDI MS for profiling of cell populations from fresh frozen and FFPE tissue enabling protein analysis from less than 20 cells.

Results

Systematic optimization of an on-chip workflow for mapping proteins from laser captured cells was performed. Figure 21 summarizes the individual steps of the workflow. Cells of interest are marked for cutting with a focused laser. Dissected cells are transferred onto a capture chip above the tissue using contact-free laser pressure catapulting (LPC). A hanging droplet of a capture fluid is used for cell capture ensuring effective cell transfer from the tissue onto the chip. These cells can be directly analyzed from the chip using MALDI MS if desired. In turn, on-chip processing of the cells, such as antigen retrieval, protein extraction, reduction and alkylation and digestion with trypsin, can be performed. If necessary, on-chip clean-up can be carried out if reagents incompatible with MALDI MS are required. Here, we combine MALDI with FT-ICR MS which provides high sample throughput while taking advantage of the high peak capacity and mass accuracy of the FT-ICR analyzer. This strategy provides high information content without the need for time consuming protein fractionation. The optimization of the individual steps of this workflow is described below.
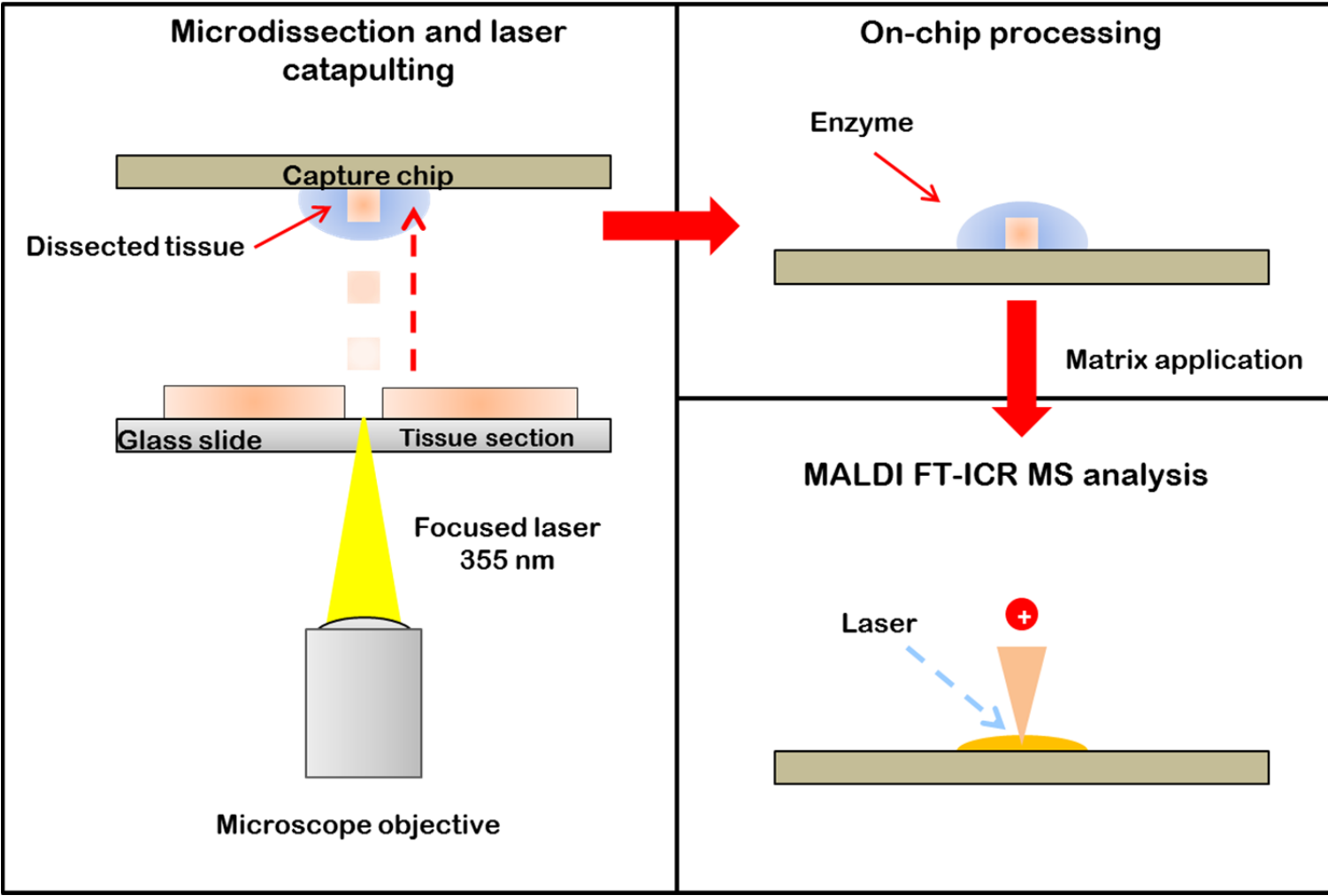
Figure 21: Workflow for cell type specific protein profiling using LCM and MALDI FT-ICR MS.

Optimization of LCM for On-Chip Cell Capture

A Zeiss MicroBeam LCM instrument was optimized for dissection and contact-free transfer of single cells onto newly developed chips for cell processing. The use of chip technology was necessary to increase sensitivity. Initial studies with standard LCM collection devices such as PCR tube caps showed poor sensitivity. I dissected up to 5,000 cells into caps of 200 and 500 µl PCR tubes using the hanging droplet approach for cell capture. After evaporation of the capture buffer, cells were extracted with the MALDI matrix and analyzed using MALDI MS. It was discovered that at least 5,000 cells were required for reliable protein detection. Visual inspection of the collection vessel showed that dissected cells tend to adhere to the walls of the cap and are not accessible during extraction with the matrix solution. Clearly, the high surface area of these devices promotes sample loss, and it was hypothesized that sensitivity could be increased if cells could be directly captured on a surface suitable for protein processing and analysis. Obviously, isolation of cells directly onto a MALDI target would be ideal as this would eliminate the need for sample transfer. Therefore, I modified the robotic sample stage of the LCM system with a custom holder (Figure 22A-B). This allowed capture of cells directly onto a standard MALDI target (alternative capture devices will be discussed in detail below). Importantly, the full functionally of the robomover for cell capture was maintained enabling accurate positioning of the chip for cell capturing during dissection and LPC.

The sensitivity of a MALDI MS experiment depends on the analyte density on the target[41, 149] and thus focusing cells to a small area on the capture chip is desired. The overall spread of LCM-dissected material after LPC on the capture chip was investigated.

A glass slide fitted with double-sided tape was used to capture and immobilize cells that were transported by LPC from a 100 x 150 μm rectangular area of 10 μm thick mouse liver tissue that was mounted onto a Director slide (Figure 22C). In this experiment, the capture chip was positioned 1-1.5 mm away from the tissue, which is typical for LCM using caps as a capture device. Figure 22D shows that the catapulted material is deposited over an area almost 1400 μm in diameter (note that the black features in the picture are an artifact of the double-sided tape). For clarity cell debris were marked by yellow dots. LPC tends to dissociate the tissue into small pieces that may be beneficial for subsequent processing. Previous studies show that a plume of dissected cell debris is formed during laser catapulting which radially expands from the point of dissection.[76] One way to reduce sample spread would be to place the chip closer to the glass slide. This was tested by reducing the distance between the glass slide and the capture chip to 284 μm, the minimum distance that can be achieved with this holder design. It is noted that the spread of the dissected cells on the capture chip depend on dissection conditions and the power applied for laser catapulting. However, the reduced distance between tissue and the chip enabled capturing of cells within a sample well of 1 mm diameter.

Cell capture for subsequent MALDI MS analysis does not permit the use of adhesive tape as a capture strategy as it can interfere with the experiment. Therefore, I investigated whether cells can be captured in a hanging droplet of capture fluid attached to a glass slide. Aqueous buffers were not suitable due to rapid evaporation; for example, a 1 μl water droplet evaporated within 1-2 min of cell capturing. Moreover, as the droplet was undergoing evaporation, it would physically move which resulted in poor cell capture. Consequently, alternative capture fluids were explored. The high boiling point

solvent 1,2-propanediol (bp = 188.2 °C) proved superior for this application. Using only 0.3 µl of this solvent enabled dissection of cells for hours while providing a 2 mm wetted area that is ideal for cell capture. This solvent can be rapidly removed in a vacuum centrifuge to prevent signal suppression for downstream MALDI MS analysis.

Sample preparation is an important factor that affects dissection accuracy and cell transfer during LCM. I optimized tissue processing protocols including tissue staining and washing that enabled effective dissection from 3 different sample supports, namely positively charged microscope slides, Zeiss membrane slides and Director slides. Dissection of fresh frozen and FFPE tissue was feasible for all slides tested. The best performance was observed with tissue thicknesses between 6-8 µm, although tissue as thick as 40 µm could be dissected. Dissection with the charged microscope slide required higher laser power than with the other slides. Cutting accuracy is limited with the charged slides as cells close to the area cut by the laser tend to detach and catapult nearby cells, probably due to a shockwave caused by the laser impact on the glass slide. This is undesirable as it can contaminate the sample with unwanted cells. The Zeiss PEN membrane slides showed excellent performance for dissection of fresh frozen and FFPE tissue, providing that areas larger than ~ 20 µm in diameter were dissected. Large tissue regions can be rapidly dissected as the cells adhere to the PEN membrane which requires a single laser pulse for tissue transfer with LPC. Importantly, the PEN membrane is compatible with subsequent MALDI MS analysis. Dissection of cells smaller than 20 µm is difficult with these slides because cells adhere to the edge of the melting PEN membrane and are partially lost from the analysis. Therefore I tested a new type of LCM slide which are layered with a thin energy absorbing coating.
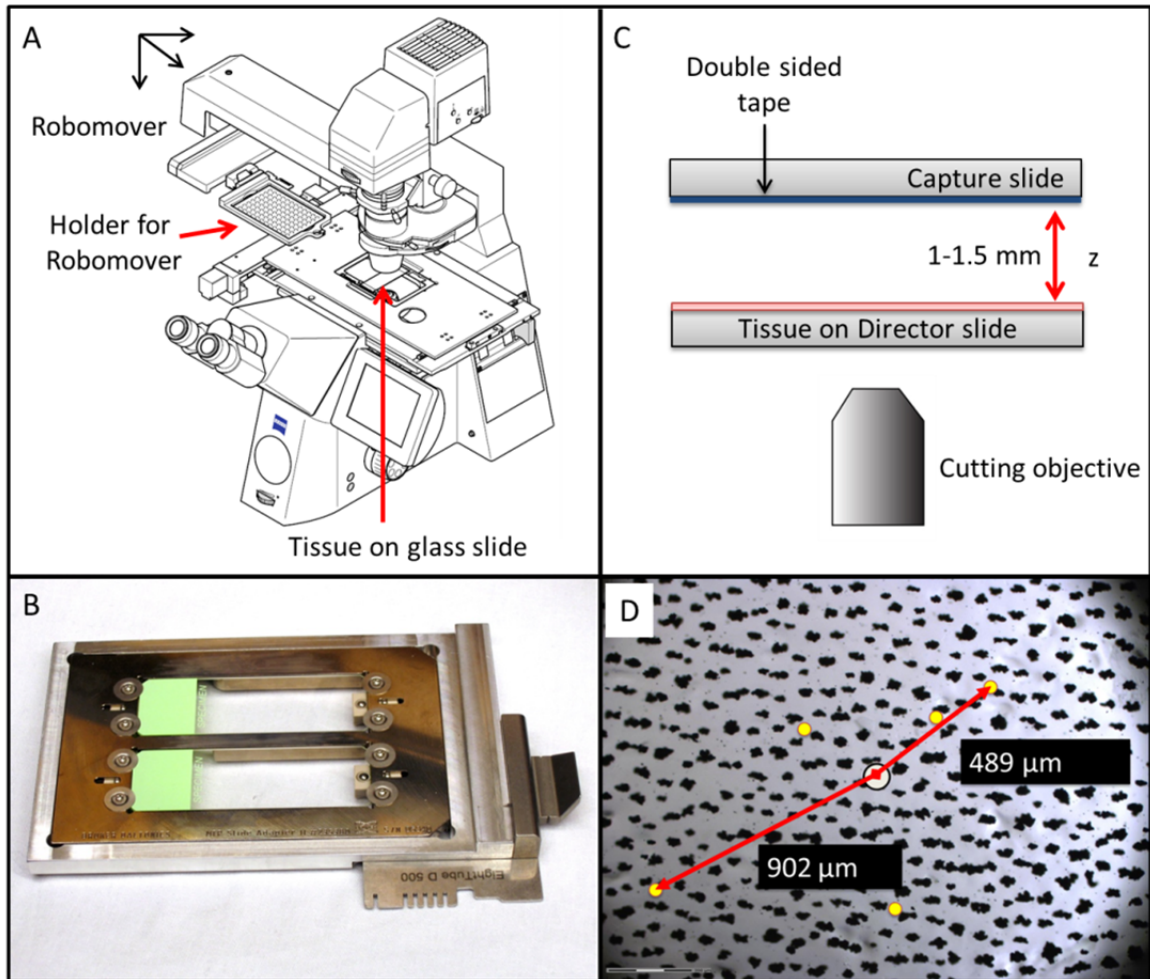
Figure 22: Modification of the Zeiss MicroBeam LCM system with a custom holder for on-chip cell capture. (A) Schematic of the LCM system showing the robomover with the capture holder attached. (B) Capture devices such as glass slides are mounted into the custom holder using a MALDI target plate adapter. (C) Experimental set-up for testing of cell spread on capture chip. (D) Cell debris (yellow) are scattered almost ~ 0.9 mm away from the center of point of dissection (white mark).

These so-called Director slides showed the best performance for single cell dissection (Figure 23), providing excellent cutting accuracy for single cells smaller than 10 µm while enabling efficient tissue transfer onto the capture device. Using these slides, dissection conditions for the LCM system were optimized for each cutting objective available (Table 2).
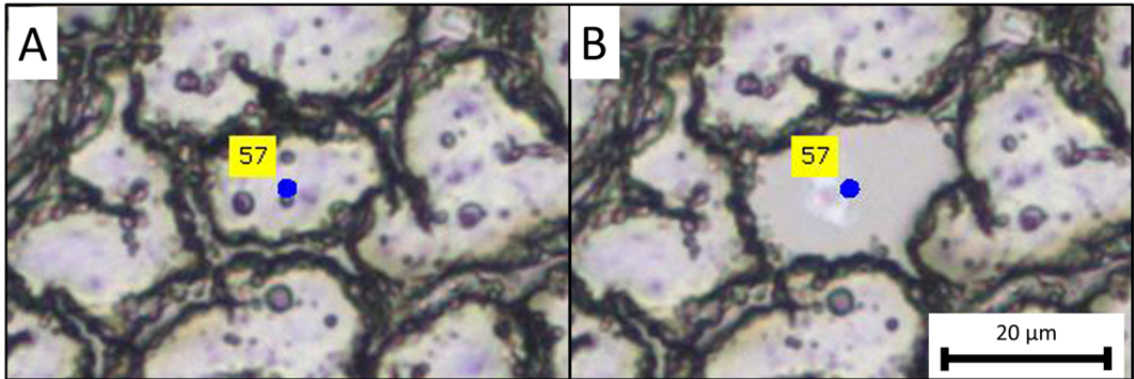
Figure 23: LCM of a single mouse liver cell from fresh frozen mouse liver tissue on a Director slide. (A) Cell marked for dissection. (B) Tissue after dissection of a single cell.

Table 2: Optimized cutting conditions for dissection of mouse liver tissue from Director slides. Single cell dissection was performed with the 40x or 63x objectives.

Magnification	Focus setting	Cutting Energy %	Energy Delta LPC %	Focus Delta LPC μm	Dist. AutoLPC Shots μm	Dist. AutoLPC from line μm
10x	82	31	15	3	5	3
20x	70	29	8	0	3	2
40x	55	24	10	0	2	1
63x	16	19	12	-2	8	2

Chip Designs for Cell Capture

The performance of 3 different capture chip designs was evaluated for cell capture and on-chip processing. The first design was a commercially available stainless steel anchor chip with 600 μm diameter hydrophilic anchors. Successful capturing of fresh frozen mouse liver cells could be demonstrated using a hanging droplet consisting of 2 μl of 1,2-propanediol as the capture fluid. However, the chip is non-transparent which made its accurate positioning difficult as the chip is placed between the objective and the light source. On-chip processing including digestion with trypsin showed extensive peptide oxidation characterized by a mass shift of 16 Da. Oxidation of peptides has been cited previously as a known problem with anchor chips.[149]

The second chip investigated was a polydimethylsiloxane (PDMS) chip (Figure 24). It was manufactured by cast molding of PDMS followed by plasma oxidation of the chip and mounting it to an oxidized glass slide. The capacity of each sample well was 4.8 μl. Using the hanging droplet method successful cell capture could be demonstrated. Digestion protocols with trypsin were optimized, allowing digestion of the captured cells. Unfortunately, the design of this chip did not facilitate direct analysis of the reaction products by MALDI MS as the laser beam was unable to reach the matrix at the bottom of the well. The laser angle of incidence on the Apollo II ion source is estimated to be ~ 30 ° and calculations confirmed that the laser beam would be intercepted by the walls of the chip. Therefore, removal of the chip from the glass slide was attempted but this proved difficult due to the tight bound between the two. Transfer of the peptides to a standard MALDI target was necessary for analysis. Hydrophobic pipette tips (ZipTips) were used for sample transfer that enabled desalting of the sample prior to MALDI

analysis. The overall sensitivity of this chip was lower than the anchor chip probably due to the large surface area in contact with the sample and the additional sample processing steps required for MALDI MS.

The third chip design investigated was a commercially available Teflon printed glass slide with 2 mm well diameter (Figure 25A). Up to 10 µl of reaction buffer can be deposited into each well of the chip. The wells are optically transparent which is useful for positioning of the chip during cell capture, allowing inspection of the dissected cells. Control experiments showed that peptides can be detected with high sensitivity directly from the chip using MALDI FT-ICR MS. On-chip digestion of BSA protein was carried out to test the sensitivity of on-chip digestion. Detection of several peptides from as little as 10 fmol could be demonstrated (Figure 25B). The high sensitivity and versatility of this chip are advantageous for cell capture and on-chip processing. Therefore, this chip was used for all subsequent experiments.
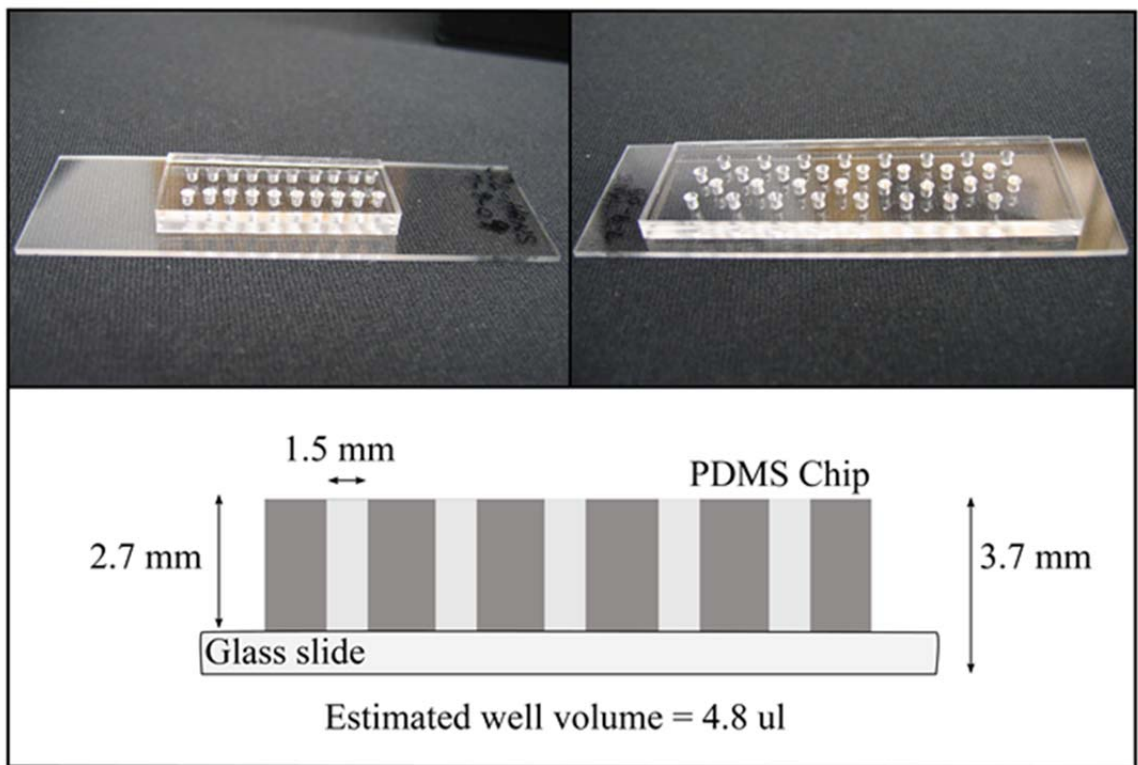
Figure 24: PDMS chip for processing of LCM captured cells.

Optimization of Chemistry for On-Chip Processing of LCM Captured Cells

Strategies were optimized that supported direct on-chip processing of captured cells using chemical approaches. One challenge of working with an open chip design and small reaction volumes is the rapid evaporation of the reaction buffers. For example, spotting of 1 µl of aqueous reaction buffer resulted in evaporation of the fluid in 1-3 min depending on the relative air humidity in the laboratory. Therefore, active humidity control using a humidified chamber for chip processing and incubation was implemented. This was sufficient to enable digestion of proteins for 18 h in as little as 2 µl buffer. Even longer incubation times were possible if the high boiling point solvent 1,2-propanediol was used as a buffer additive. At a concentration of 30 % successful digestion of protein could be achieved without concern for sample evaporation with incubation times exceeding 30 h.

Workflow for On-Chip Digestion of Fresh Frozen Tissue

A protocol for on-chip digestion of LCM captured cells with trypsin was developed. Cells are digested directly on the chip using a digestion buffer containing ammonium bicarbonate (AMBIC) that is removed upon drying to allow direct MALDI MS analysis of the peptides from the chip with high sensitivity. Optimization of the digestion buffer was carried out using BSA as a model protein. I observed that the digestion of BSA was improved if 30 % of 1-propanol was added to the digestion buffer (Figure 26). Control experiments with this new buffer were carried out in PCR tubes demonstrating similar performance improvements. This buffer showed excellent performance for on-chip digestion enabling detection of peptides from as little as 10 fmol BSA (Figure 25B).
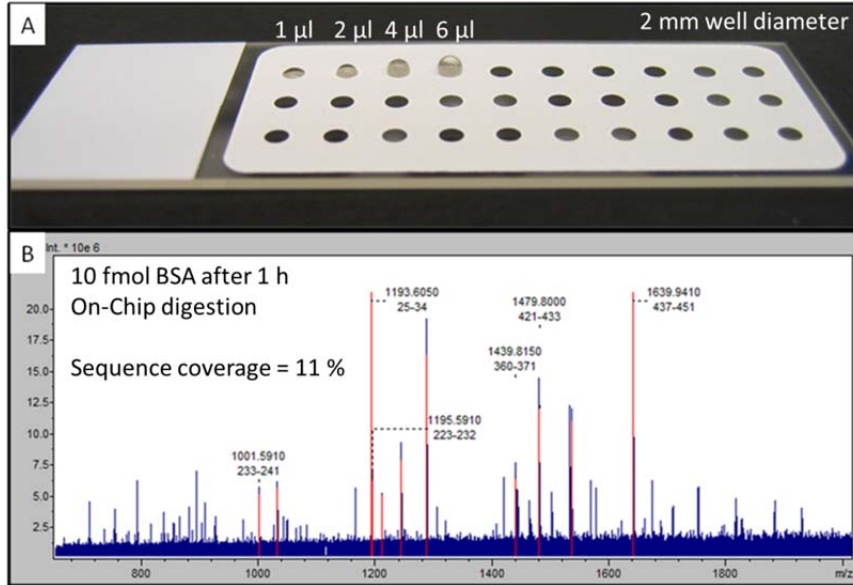
Figure 25: Testing of Teflon printed glass chip for on-chip digestion with trypsin. (A) Teflon printed glass chip showing efficient trapping of 1, 2, 4 and 6 μl of aqueous buffer. (B) MALDI-FT-ICR MS analysis of a 10 fmol BSA digest carried out of the chip. Six BSA matching peptides were detected with a sequence coverage of 11 %.
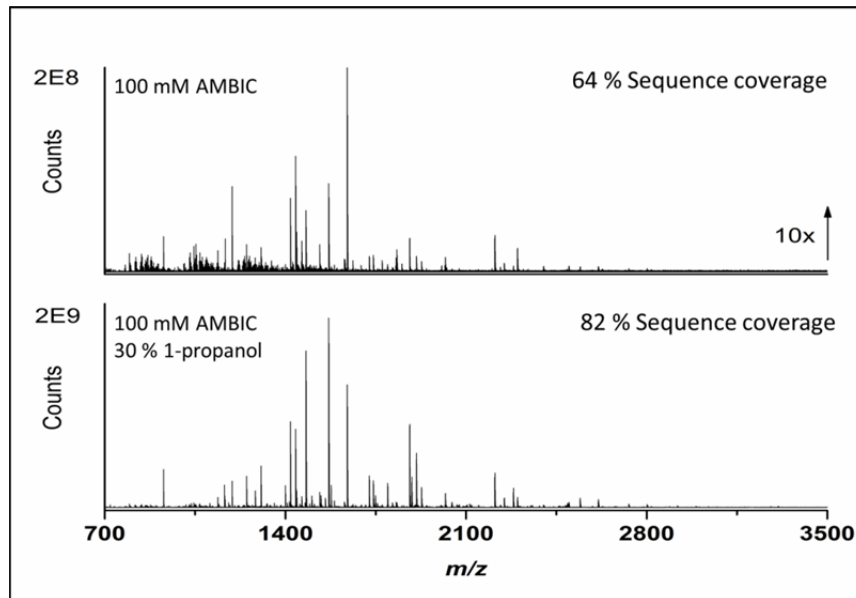
Figure 26: MALDI FT-ICR MS spectra obtained from a 1 h on-chip digests of 200 fmol BSA. The use of 30 % 1-propanol in the digestion buffer increased sequence coverage and sensitivity.

This workflow was applied for on-chip digestion of proteins from LCM captured fresh frozen mouse liver tissue. Spectra with several thousand peaks could be detected for the analysis of tissue corresponding to 100 cells (see below). The number of detectable peptides decreased as fewer cells were analyzed but detection of peptides from as few as 9.6 fresh frozen mouse liver cells could be demonstrated (Figure 27).

On-Chip Processing of FFPE Tissue

The optimized protocol for on-chip digestion was applied to FFPE mouse liver tissue. Figure 28A shows a comparison of spectrum obtained after on-chip digestion of an estimated 99 cells from fresh frozen and FFPE mouse liver tissue from the same animal. Antigen retrieval of the FFPE tissue was carried out on the glass slide using a standard protocol and tissue was dissected. As expected, lower numbers of peaks were observed for the FFPE tissue using the workflow developed for the fresh frozen tissue (Figure 29A). I hypothesized that the offline antigen retrieval step, developed for histological applications, is only partially effective for proteomic applications as it has to preserve the morphology of the tissue on the glass slide. Therefore, an improved antigen retrieval protocol for on-chip processing was developed. As described in chapter 3, heat and detergent are important factors for successful antigen retrieval. However, the antigen retrieval buffer in this work contained the MALDI incompatible detergent Tween-20 which required extensive sample clean-up prior to MALDI MS reducing sensitivity.
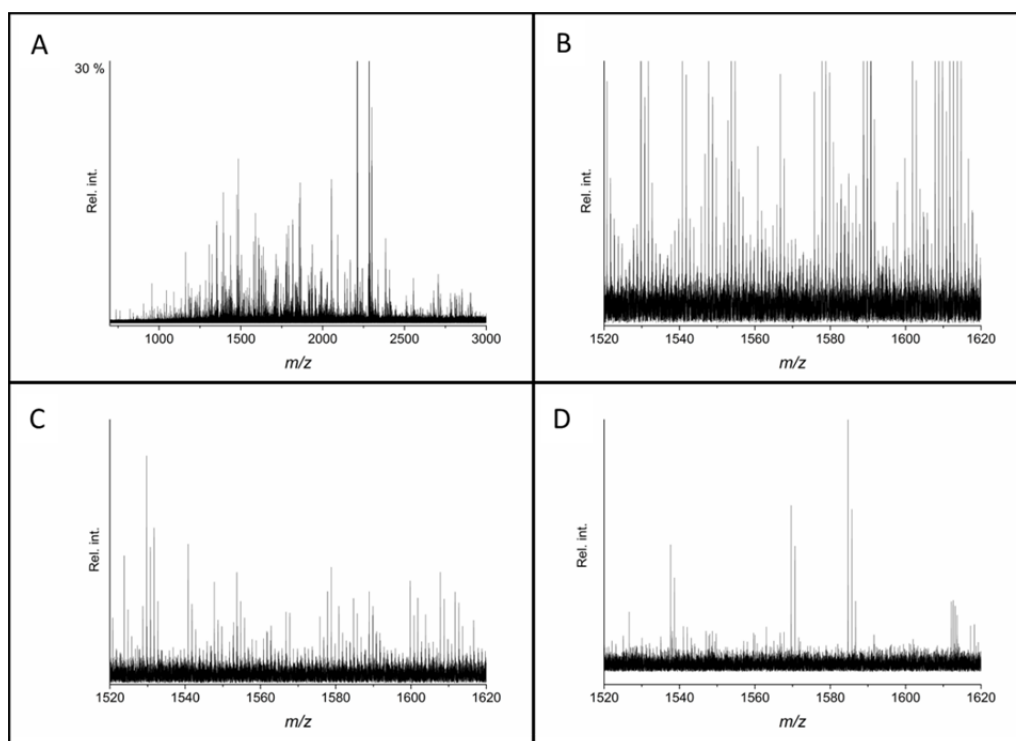
Figure 27: Profiling spectra of LCM captured mouse liver tissue after on-chip digestion and analysis by MALDIFT-ICR MS. (A) Spectrum obtained after on-chip digestion of tissue dissected from an estimated 19 cells resulting in detection of 143 ions. (B) Magnified region showing the *m/z* range from 1570-1620. C) Spectrum from the on-chip digestion and analysis of an estimated 9.6 cells. (D) Spectrum from a control digest carried out without the tissue.

To eliminate the need for extensive detergent removal, we tested whether the acid-cleavable detergent ALS-II could replace Tween-20 during antigen retrieval. Experiments demonstrated that cleavage of ALS-II with acid can be achieved directly on the chip in as little as 10 min. Cells from FFPE tissue were mixed with the new AR buffer and incubated for 1 h at 90 °C for antigen retrieval. Subsequently, alkylation of cysteines was carried out on the chip and the detergent was cleaved prior to digestion with trypsin. Direct detection of peptides from the chip was feasible although a reverse phase clean-up with C_{18} ZipTips was added to remove salts and detergent artifacts. This significantly improved sensitivity compared to experiments carried out without clean-up. Figure 28 shows photomicrographs of cells during on-chip cell capture and processing. As observed earlier, LPC generates cell debris that are amenable for protein extraction. Note that the structure of the captured material changes significantly as it is being processed by chemical and enzymatic means.

The optimized protocol for processing of FFPE tissue was compared with the workflow for fresh frozen tissue. As shown in Figure 29B, significantly higher numbers of peaks could be detected for FFPE tissue with peak numbers similar to the analysis of fresh frozen tissue. Importantly, most of the peaks detected in the fresh frozen tissue sample were also detected in the FFPE tissue indicating that proteomic discovery in FFPE tissue using this workflow is feasible.
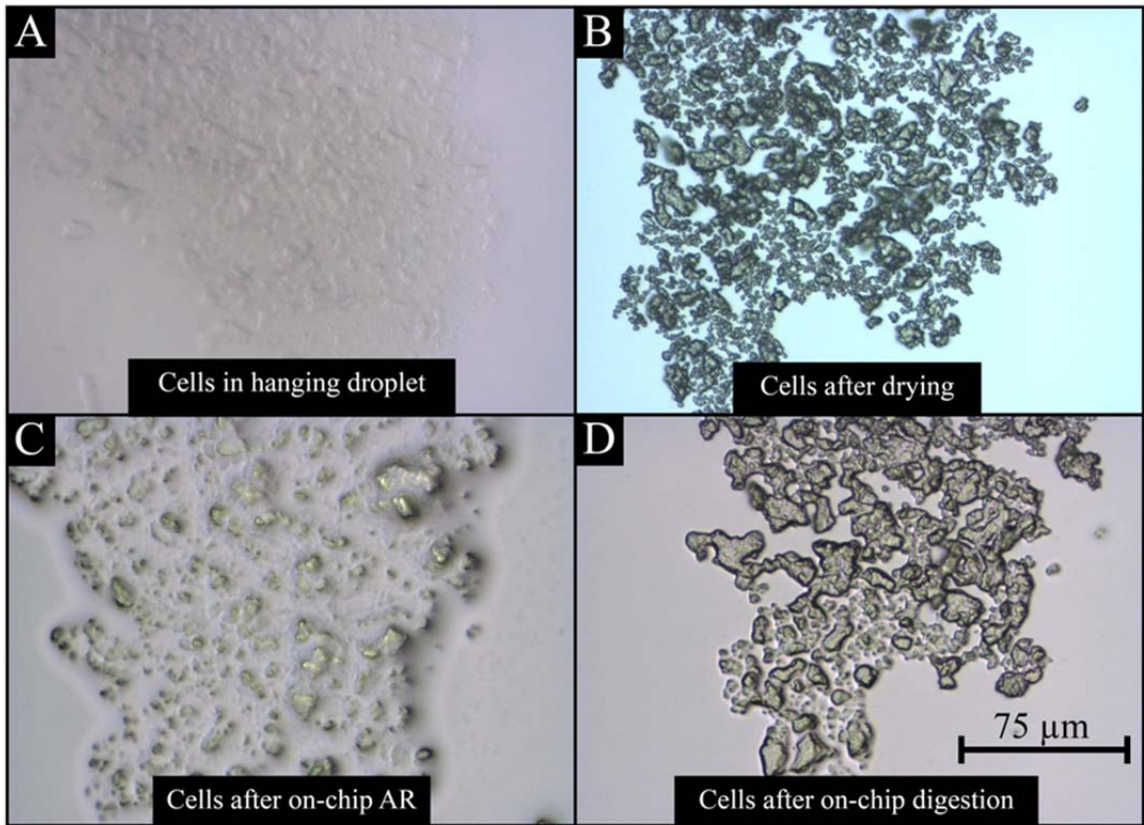
Figure 28: On-chip processing of FFPE mouse liver tissue. (A) Capturing of LCM-dissected cells in a hanging droplet. (B) Cells on the chip after evaporation of the capture buffer. (C) Cells after antigen retrieval. (D) Extracted cells after digestion.
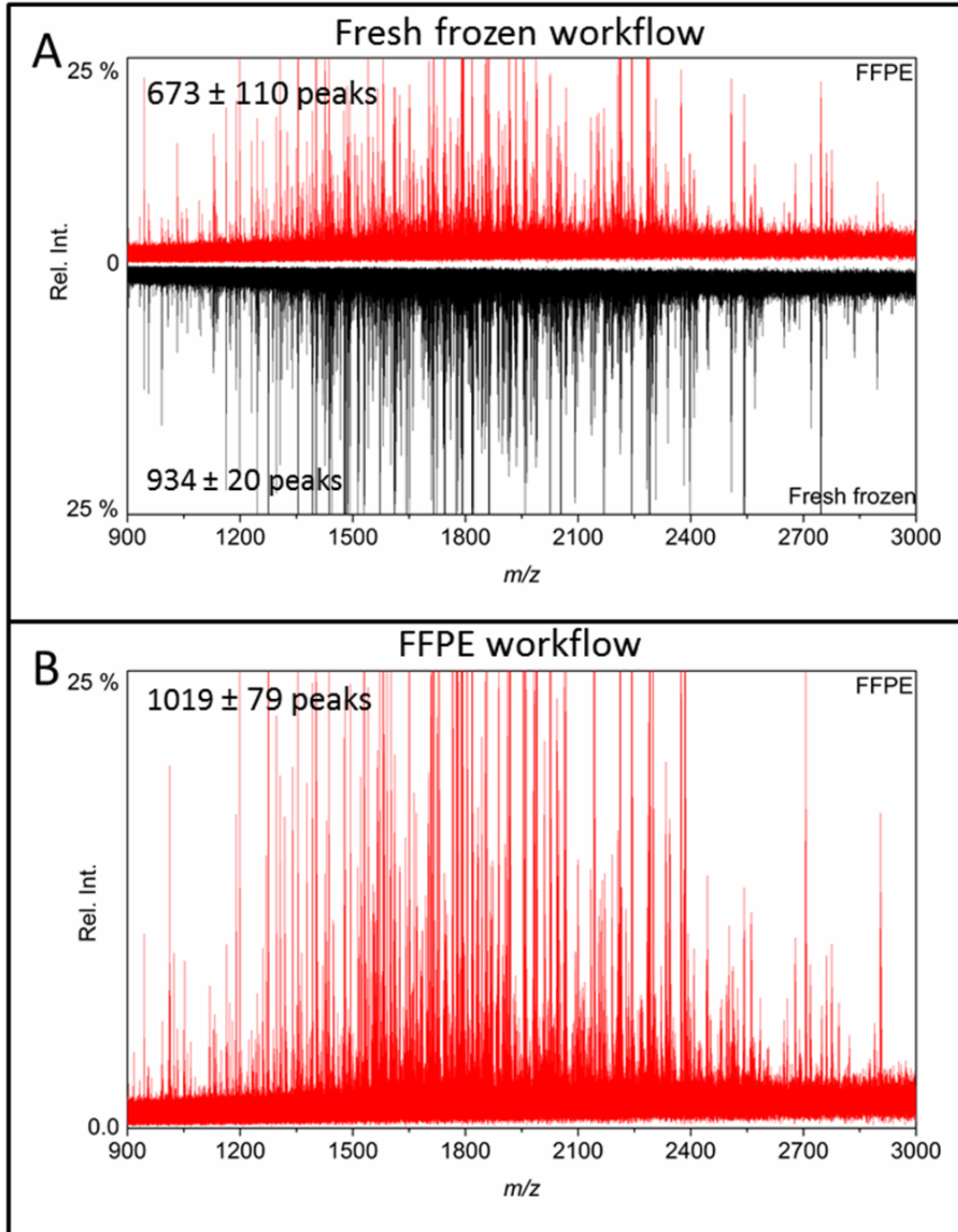
Figure 29: Comparison of average spectra (N = 3) from the processing of fresh frozen and FFPE mouse liver tissue with two optimized workflows for on-chip processing of LCM captured cells. Peaks were detected with a minimal signal-to-noise ratio of 6:1. The confidence interval was calculated at the 95 % confidence level. (A) Comparison of spectra from FFPE and fresh frozen tissue processed using the fresh frozen workflow without antigen retrieval. (B) Analysis of FFPE tissue with on-chip AR and alkylation of cysteines improves the number of detected peptides.

Performance Evaluation

The performance of the FFPE workflow for on-chip processing of cells was evaluated for the analysis of fresh frozen and FFPE tissue. Table 3 summarizes the results obtained from 3 technical repeats of the analysis of FFPE and fresh frozen mouse liver tissue from the same animal. For FFPE tissue, up to 2,774 peaks were observed from an estimated 196 cells with a standard deviation of only 1 %, indicating good reproducibility. Slightly lower numbers of peaks were detected for the analysis of 98 cells. Importantly, peaks observed in the blanks were not present in the spectra from 98 cells. However, for the 19 FFPE cells, only peaks identified in the blank samples were detected while peaks detected from 196 and 98 cells were not present. The fresh frozen tissue showed higher peak numbers compared with the FFPE tissue but overall reproducibility was similar.

The day-to-day performance of the assay was tested for the analysis of FFPE tissue. Figure 30 shows representative spectra obtained for the analysis of 99 FFPE mouse liver cells processed several days apart from the experiment presented in Table 3. The number of detected peaks is within 11.2 % of the early measurements and the overall reproducibility judged by inspection of the spectra is excellent. These results demonstrate that reproducible and analysis of LCM-dissected tissue is feasible showing outstanding reproducibility between analyses.

Table 3: Sensitivity and reproducibility for on-chip processing of FFPE and fresh frozen (FF) mouse liver tissue using the FFPE tissue workflow. Peak detection was carried out using a signal-to-noise cut-off of 4:1.

Sample	FFPE			FF	Blank
# of cells	196	98	19	98	0
Analysis # 1	2743	2639	1665	3138	1479
Analysis # 2	2804	2763	1621	3279	1426
Analysis # 3	2774	2646	1506	3253	1758
Average	2774	2683	1597	3223	1554
sx	31	70	82	75	178
sx (%)	1	3	5	2	11
Confidence	35	79	93	85	202
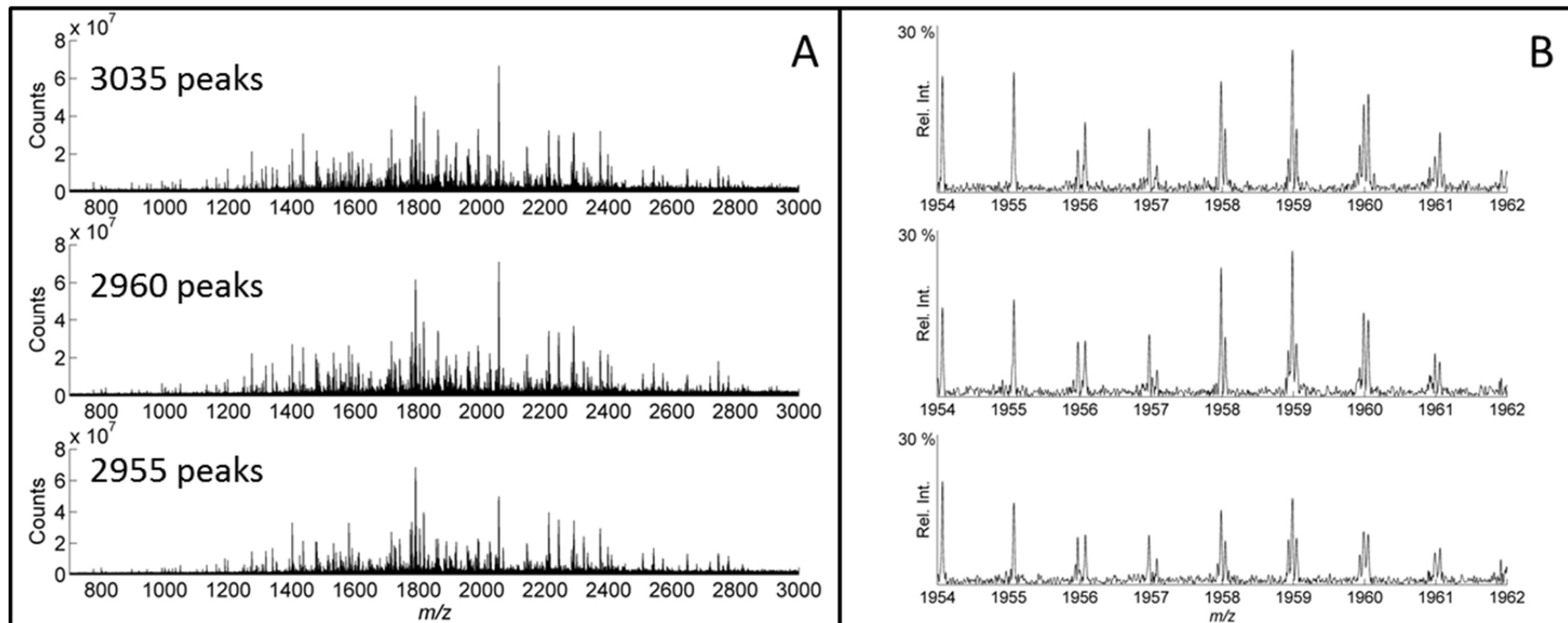
Figure 30: (A) Reproducible MALDI-FT-ICR MS profiles obtained from 3 technical repeats from the analysis of 99 LCM-dissected FFPE mouse liver cells after on-chip processing with the FFPE workflow. The average number of detected peaks with signal-to-noise > 4:1 prior to deisotoping was 2983 ±51. (B) Expanded 8 Da window from (A).

Discussion

New tools for molecular analysis of tissue samples that enable single cell type protein discovery are needed for the development of the next generation of proteomic technology. Single cell type protein profiling in tissues has remained difficult because of the need to dissect several thousand cells prior to analysis. Here, a new workflow for protein discovery in selected cell populations was optimized, allowing cell type specific protein analysis from less than 20 cells. This innovative work can lead to future discoveries in the identification of distinct cell subpopulations from seemingly similar cell types.

Systematic optimization of the workflow was necessary to approach single cell sensitivity. Modification of the LCM system with a custom holder was necessary to reduce nonspecific cell losses to the wall of the collection container during laser catapulting of dissected cells. This improves sensitivity and has the advantage that sample transfer steps are eliminated. Several chip designs were tested for cell capture and processing including a Teflon printed chip with a 2 mm well diameter. The hydrophilic wells of this chip supported effective cell capture as the capture fluid is anchored in place above the tissue. Moreover, Teflon printed slides are chemically inert while providing a defined reaction zone thereby controlling the risk of well-to-well contamination. Up to 30 reactions can be carried out in parallel and custom chips are available if higher throughput is required. Chips with 3 mm and 60 μm well diameters were tested to study the effect of the well size on sensitivity. As expected, sensitivity was reduced for the chip with larger wells. Interestingly, experiments with the chip with 60 μm wells enabled detection of protein signals from fewer than 10 cells. In this case, a large droplet of

capture fluid was attached to the hydrophilic well, enabling effective cell capturing while concentrating the cells in the hydrophilic well upon evaporation of the capture fluid. The improved sensitivity is expected because of the higher analyte density achieved using the smaller well. Unfortunately, liquid handling for these small reaction wells remains tedious and microdispensing of reagents and matrix solution is necessary for on-chip manipulations. This will require additional optimization in future studies to enable reasonable throughput.

A surprising discovery was the improved digestion performance when using 1-propanol in the digestion buffer (Figure 26). Solvent additives such as trifluoroethanol,[150] methanol[151] and acetonitrile[152] are known to improve the digestion of protein with trypsin but the use of 1-propanol for this purpose has not been reported. 1-Propanol has a higher boiling point compared with the other solvents, which is especially useful for on-chip applications where evaporation of solvents is a concern.

Two workflows for on-chip processing of fresh frozen and FFPE tissues have been optimized that show similar peak patterns. Up to 3,000 peaks could be detected from the analysis of either fresh frozen or FFPE mouse liver from the same animal. The resulting peak patterns were similar for both tissue types. This indicates that the newly developed antigen retrieval protocol is effective. Compared with antigen retrieval carried out on the tissue section before LCM, higher numbers of peaks could be detected after on-chip antigen retrieval. This highlights the ability for effective on-chip processing of cells prior to MALDI MS analysis.

Protocols for the analysis of FFPE tissues provide access to large collections of FFPE tissues that are often associated with long-term clinical follow-up data, which is

critical for the development of new diagnostic strategies. This new approach compares favorably with direct approaches such as *in situ* tissue digestion.[153] In this case, the spatial resolution is limited by the size of reaction zone (typically 175 μm). The LCM-based workflow enables parallel processing of many samples indicating that this would be a good complement for the analysis of TMAs, which are increasingly used for proteomic studies.[153, 154, 155]

The reproducibility of the method is excellent, generating similar spectra and numbers of peaks for analyses carried out on the same or separate days. Thus the method is robust, providing opportunities for large scale protein marker discovery carried out over extended periods of time.

The overall sensitivity of the method was assessed with fresh frozen and FFPE tissues and generated meaningful spectra from less than 20 and 100 cells, respectively. This is a significant improvement over currently available methods because dissection of such few cells can be done within the timeframe demanded in clinics. Depending on the complexity of the samples, dissection of 100 cells can be achieved within 10-30 min for each sample, and this is likely to be further shortened as new LCM platforms capable of automated cell recognition and dissection emerge.

Conclusion

Systematic optimization of workflows for the isolation, processing and analysis of cells from fresh frozen and FFPE tissues has been demonstrated for protein analysis of LCM-dissected cells. Cells of interest can be enriched with single cell specificity onto a capture chip for processing and analysis. The chip is disposable, reducing the potential for carryover. Up to 30 samples can be analyzed in parallel with the possibility of on-chip chemistry automation. On-chip antigen retrieval, protein extraction and digestion have been optimized with the goal to minimize sample loss. The high sensitivity of the method allows single cell type specific protein marker discovery with the advantage that cells can be sampled from relevant regions of a tissue. A method with such sensitivity and resolution provides opportunities for development of improved diagnostic tools. Importantly, one or more cell populations can be isolated, opening up the possibility to study the interactions of cells within their microenvironment. Compared with our earlier work, a significant increase in sensitivity is achieved, reducing the minimum number of cells for FFPE tissue analysis from 15,000[113] to less than 100 cells.

Materials and Methods

Reagents. All chemicals were purchased from Sigma-Aldrich (St. Louis, MO, USA) and were of highest purity available. HPLC grade acetonitrile (ACN) and ethanol, histological grade xylenes, diammonium citrate (DAC) were purchased from Fisher Scientific (Air Lawn, NJ). Tris base and calcium chloride was from J.T. Baker. The acid cleavable detergent ALS-II was obtained from Progenta (Morgantown, WV). Trifluoroacetic acid (TFA) and α-cyano-4-hydroxycinnamic acid (CHCA) were purchased from Fluka (Buchs, Switzerland). The CHCA matrix was 2x recrystallized from ethanol and water. Ammonium bicarbonate (AMBIC), iodoacetamide (IAA), 1,4-Dithioerythritol (DTE) were obtained from Sigma-Aldrich. Sequencing grade modified trypsin was purchased from Promega (Madison, WI, USA). Peptide standard mix and protein standard mix for MALDI-TOF-(TOF) calibration were from Bruker-Daltonics (Billerica, MA).

Tissue processing for fresh frozen tissue. Adult CD-1 mice were sacrificed and dissected organs were immediately snap-frozen in liquid nitrogen and stored at -80 °C until use. A sample of each tissue was formalin fixed as described in Chapter 3. Sections were cut with a Leica cryomicrotome with section thicknesses of 5-40 μm and thaw mounted[102] onto superfrost slides obtained from Fisher Scientific (Air Lawn, NJ), 1 mm PEN membrane slides from Carl Zeiss Inc (Thornwood, NY) or Director slides received from Expression Pathology (Rockville, MD). Note that the PEN slides were activated with a UV lamp for 30 min prior to mounting of fresh frozen tissue. For protein work, tissue was washed using sequential 2 minute washes in 70, 95, 100 % ethanol followed by an additional 2 minute wash in 100 % ethanol. The dehydrated tissue slides were

stored in a vacuum desiccator until use or subjected to staining with cresyl violet. For this purpose, tissue was rehydrated for 1 minute in 70 % ethanol followed by a 15 s dip in water. Staining was performed for 30 s in 0.5 % cresyl violet stain[106] followed by 3 consecutive 30 s washes in 70, 70 and 95 % reagent grade ethanol.

Tissue processing for FFPE tissue. Sections were cut with a microtome with section thicknesses of 6-8 μm and tissue was mounted onto Director slides. Slides were dried overnight at 37 °C. In the morning a washing protocol for paraffin removal and stepwise hydration was performed using a series of solvent washes: 2 x 5 min xylenes, 2 x 3 min ethanol, 1 x 3 min 95 % ethanol, 1 x 3 min 70 % ethanol and 2 x 5 min Milli-Q water. At this stage, staining of the tissue can be performed as described above for the fresh tissue. If no stain is necessary, tissue is stepwise dehydrated using a 70 % ethanol (1 min) and reagent grade ethanol (1 min). Tissue is stored for at least 1 h in a vacuum desiccator prior to LCM.

LCM. LCM was carried out using a ZEISS MicroBeam instrument. Objectives with 10, 20, 40 and 63x magnification were used for sample inspection and LCM. Optimized dissection conditions for Director slides are provided in Table 2. Cells were dissected using the close cut & AutoLPC method with the following settings for AutoLPC: Distance of AutoLPC shots = 5 and Distance of AutoLPC shots from line = 3. Cells were captured on the 2 mm Teflon chip using 0.3 μl 1,2-propanediol as the capture fluid or in 200 μl PCR tube caps using 20 μl water for cell capture. The distance between the capture chip and the tissue was 284 μm during dissection. The capture buffer was removed by placing the chip into a closed petridish followed by a 25 min drying step in a

rotary centrifuge operated at 45 °C and 1-4 mbar pressure without spinning (rotor removed).

Estimation of protein content and cell numbers based on area. A rough estimation for the protein content of tissue can be obtained by assuming that 18 %[131] of the wet weight of a cell is protein. It is assumed that a cell is spherical and there is no space between the cells. For mouse liver, we measured an average cell diameter of 17.2 µm. In this case, dissection of an area of 44328 µm^2 from a tissue section cut at 6 µm thickness corresponds to 100 cells or 47.9 ng protein.

On-chip digestion for the PDMS chip. BSA protein was dissolved in the digestion buffer consisting of 10 mM Tris, 1 mM EDTA, 10 mM DTE, 2 mM CaCl$_2$, 30 % 1-propanol and 0.5 % ALS-II. Two µl of this mixture was loaded into each well of the chip during digestion. The chip was briefly spun in a centrifuge to remove air bubbles. The chip was covered with aluminum foil and subjected to heating in an autoclave using the liquid program which heated the sample to 121°C for 20 min The chip is immediately removed after completion of the autoclave program and 2 µl of the digestion buffer was added. Alkylation of the protein is performed by adding 0.4 µl of freshly prepared, aqueous iodoacetamide solution prepared at 150 mmol/l. The reaction is allowed to proceed for 15 min in the dark. Excess alkylation reagent was destroyed by adding 0.5 µl of a 50 mM DTE solution. Sequencing grade porcine trypsin is dissolve in 1 µl of digestion buffer and spiked into the well. The enzyme concentration was variable but a E/S ratio between 1/20 to 1/5 showed the best performance. The digestion is incubated in a humidified chamber with controlled temperature of 37.5 °C. After 1 h, 1 µl of a 2 % aqueous TFA solution was added to quench the reaction. The reaction mixture was

subjected to ZipTip clean up using Millipore P10 tips of the C_{18} variety according to the recommendations of the manufacturer. The peptides were eluted from the chip using 6 µl of the matrix solution consisting of 6 mg/ml CHCA prepared in 70 % ACN 0.1 % TFA and 2 µl of this sample were spotted onto a standard stainless steel Bruker plate for MALDI-MS analysis.

On-chip processing for Teflon printed slides with the fresh frozen tissue workflow. Teflon printed glass slides with 2 mm hydrophilic wells were obtained from Electron Microscope Science (Hatfield, PA). Protein and sequencing grade porcine trypsin were diluted in the digestion buffer consisting of 10 mM TRIS, 1 mM EDTA, 10 mM DTE, 2 mM $CaCl_2$, 30 % 1-propanol. A mechanical pipette was used to deposit 1 µl of the protein standard and 1 µl of the enzyme solution onto a hydrophobic region of the capture chip for digestion of BSA. For digestion of LCM captured cells, 2 µl of the digestion buffer were used. The enzyme concentration was adjusted to obtain a E/S ratio of 1:5. The chip is placed into a petridish lined with water soaked filter paper and incubated for 1-16 h in a temperature controlled oven operated at 37.5 °C. The reaction is quenched with 2 µl of 1 % TFA solution and the chip is placed in a vacuum centrifuge operated at a temperature of 45 °C and 1-4 mbar pressure without spinning (rotor removed). Complete evaporation of the droplets is typically observed after 5-8 min but extended drying for 20 min is carried out to ensure complete removal of all solvent. Finally, 2 µl of a 6 mg/ml CHCA matrix solution prepared in 70 % ACN 0.1 % TFA is deposited onto the chip and allowed to crystallize with the sample.

On-chip processing for Teflon printed slides with the FFPE tissue workflow. LCM-dissected cells captured on the Teflon printed chip were subjected to antigen

retrieval using 2 µl of antigen retrieval buffer consisting of 10 mM Tris buffer, 1 mM

EDTA, 10 mM DTE, 30 % 1,2-Propanediol and 0.5 % ALS-II. The chip is placed into a

humidified chamber (see above) and incubated for 1 h at 90 °C in a laboratory convection

oven. Upon removal of the chip from the oven, the chip is transferred into humidified

chamber that is operated at room temperature and allowed to cool for 10 min. This is

important to prevent excessive condensation of vapor on the chip. Alkylation of cysteine

containing peptides is carried out in the humidified chamber by adding 0.8 µl of a freshly

prepared aqueous IAA solution. The reaction is allowed to proceed for 20 min in the

dark. Excess alkylation reagent is quenched with 0.7 µl of a 25 mM DTE solution.

Following 5 min incubation, 1.3 µl of a 4 % formic acid solution is added and acid

cleavable detergent is allowed to cleave for 15 min in a humidified chamber. The chip is

placed into a petridish and subjected to 25 min of drying at 70 °C in a rotary centrifuge as

described above. For digestion of cells, 2 µl of the digestion buffer consisting of 30 % 1-

propanol, 70 mM TRIS with pH=8.1 (23°), 1.4 mM $CaCl_2$, and trypsin is spotted onto the

chip and the chip is incubated at 37.5 °C overnight in a humidified petridish. The trypsin

concentration in the digestion buffer was adjusted depending on the number of dissected

cells to obtain an E/S ratio of 1:5. For example, for the analysis of 100 mouse liver cells

we estimated 47.9 ng total protein. In this case 9.6 ng of trypsin were added for digestion.

The reaction is quenched with 1 µl of a 4 % formic acid solution and the chip is dried for

15 min in a vacuum centrifuge operated at 70 °C. On-chip clean-up is performed using

C_{18} micro ZipTips (Millipore). The tips are activated as recommended by the

manufacturer. Peptides are solubilized on the chip with 5 µl of a 0.1 % TFA solution.

Peptides are extracted from the chip using 10 aspiration and dispense cycles. The tip is

washed 4 x with 10 µl 0.1 % TFA for salt removal. Peptides are eluted into a 200 ul PCR tube containing 2 µl matrix solution consisting of 2mg/ml CHCA prepared in 70 % ACN with 0.1 % TFA and 1.7 mM DAC. For spotting of the peptides onto a stainless steel target, 1 µl of 0.1 % TFA is added to the tube and the whole tube content is deposited onto a stainless steel MALDI target for analysis.

Mass Spectrometry. MALDI FT-ICR MS was carried out on a 9.4 T Bruker Apex Qe equipped with an Apollo II ion source and a modulated Nd:YAG laser[86] operated at 100 Hz. External calibration was performed using a custom peptide mixture consisting of Bradykinin 1-7, Angiotensin II, [Glu^1]-Fibrinopepdide β, ACTH fragment 18-39 and Insulin chain B oxidized with theoretical *m/z* ratios of 757.39915, 1046.54179, 1570.67684, 2465.19833 and 3494.65077 respectively. Typical mass accuracy was better than 5 ppm over the observed mass range from 600-4000 Da. The external storage quadrupole was used to accumulate 250 laser shots from a single sample position prior to FT-ICR analysis. A total of twenty scans were accumulated from each sample spot and saved into a file. Data acquisition was automated using custom software tools written to generate sequences files for the Hystar software (ver. 3.4) supplied with the instrument. Spectra were processed using customized scripts for Bruker DataAnalyis version 4.0 which performed peak picking and export of the peak lists and raw spectra in ASCII format for further processing in OriginPro 7 and MATLAB. Monoisotopic peaks were determined using the SNAP-2 algorithm with a minimal S/N of 3:1 and a quality factor of 0.4. The total number of peaks were determined with the FTMS algorithm with a S/N cut-off of 4:1.

CHAPTER V

Applications: Profiling of LCM-Enriched Cells with MALDI FT-ICR MS

Introduction

The results in the previous chapter established innovative methods for the enrichment and analysis of selected cells populations from fresh frozen and FFPE tissues, but the suitability of the methods for morphologically complex tissues, and how specific labeling approaches for identification of specific cell populations affects the analysis remained unknown. This chapter addresses these challenges by describing the successful application of these methods to several protein profiling studies. Specifically, human prostate FFPE tissues and striatal medium spiny neurons (MSNs) in rat brain were profiled.

Prostate cancer (PCa) is the most common cancer in men[156] in the United States. The disease incidence is strongly correlated with age, and the lifetime risk of developing prostate cancer is 1 in 5 for African Americans and 1 in 6 for Caucasians. Diagnosis of PCa with digital rectal exams and blood tests which measure prostate specific antigen (PSA) are available. The usefulness of the PSA test is controversial due to its low specificity,[157] and often a subsequent invasive biopsy is required for PCa diagnosis. Radical prostatectomy, the surgical removal of the prostate, is invasive and can have severe side effects such as impotence and incontinence. Therefore, pathological risk

stratification using initial biopsies obtained for suspected PCa is important as it can often provide clues about the stage and severity of the disease, including the potential for invasion of neighboring tissues, which can influence treatment. Unfortunately, the samples obtained from these biopsies tend to be small so the number of cancer cells can be limiting. A method that could obtain unique molecular profiles from these few cells could provide the molecular clues needed to diagnose and appropriately manage the disease.

The second application presented here is the molecular profiling of striatal MSNs in rat brain. MSNs are striatal projection neurons into the basal ganglia that are involved in motor control and habit and reward learning.[158] These neurons have been associated with neurological diseases such as schizophrenia and Parkinson's disease.[159] At least two MSN types exist within the striatum, the striatopallidal (indirect pathway) and the striatonigral (direct pathway) neurons. The striatopallidal neurons project from the striatum to their corresponding output nuclei in the medial globus pallidus (GP), while the striatonigral neurons project from the striatum to the substantia nigra (SN).[160] The degeneration of nigrostriatal dopamine neurons causes a decrease in striatal dopamine concentrations, which gives rise to the motor defects in Parkinson's disease. Consequently, most of the research in Parkinson's disease has focused on the mechanism of degeneration of dopamine neurons in the SN. However, the consequences of dopamine loss on the striatal target cells of nigrostriatal neurons are not well understood. The two MSN cell types in the striatum are morphologically identical except in their projections to their corresponding output nuclei.[160] This makes molecular characterization of these MSN types difficult and new strategies for the analysis of these neurons are desired.

Results and Discussion

Analysis of Human FFPE Prostate Tissue

A method for protein profiling normal epithelial cells and tumor cells in FFPE prostate tissue was developed. Prostate tissue staining protocols were optimized for histopathological analysis to enable the marking of desired cell populations for LCM. Experiments with H&E-stained FFPE tissue showed that H&E staining significantly reduced the number of detected peaks compared with unstained tissue. We investigated whether cresyl violet could be used as an alternative stain to increase the sensitivity of the method. Peptide profiles from FFPE mouse liver tissue stained with cresyl violet showed similar peak patterns and intensities compared with non-stained tissue, indicating that this stain is compatible with our workflow. Figure 31A and B demonstrate that the quality of cresyl violet-stained prostate tissue is sufficient for identification of epithelial and tumor cells as judged by a trained pathologist.

One advantage of LCM is that tumor cells can be enriched from selected tissue regions, such as from nerve invading tumor cells (Figure 31C and D), which are a significant route of metastatic disease in PCa. This process, known as perineural invasion, has been associated with poor clinical outcome.[161, 162] The ability to enrich cells from pathologically relevant cell populations is an important advantage of this workflow because it enables specific cell type and location proteome analysis in the tissue.
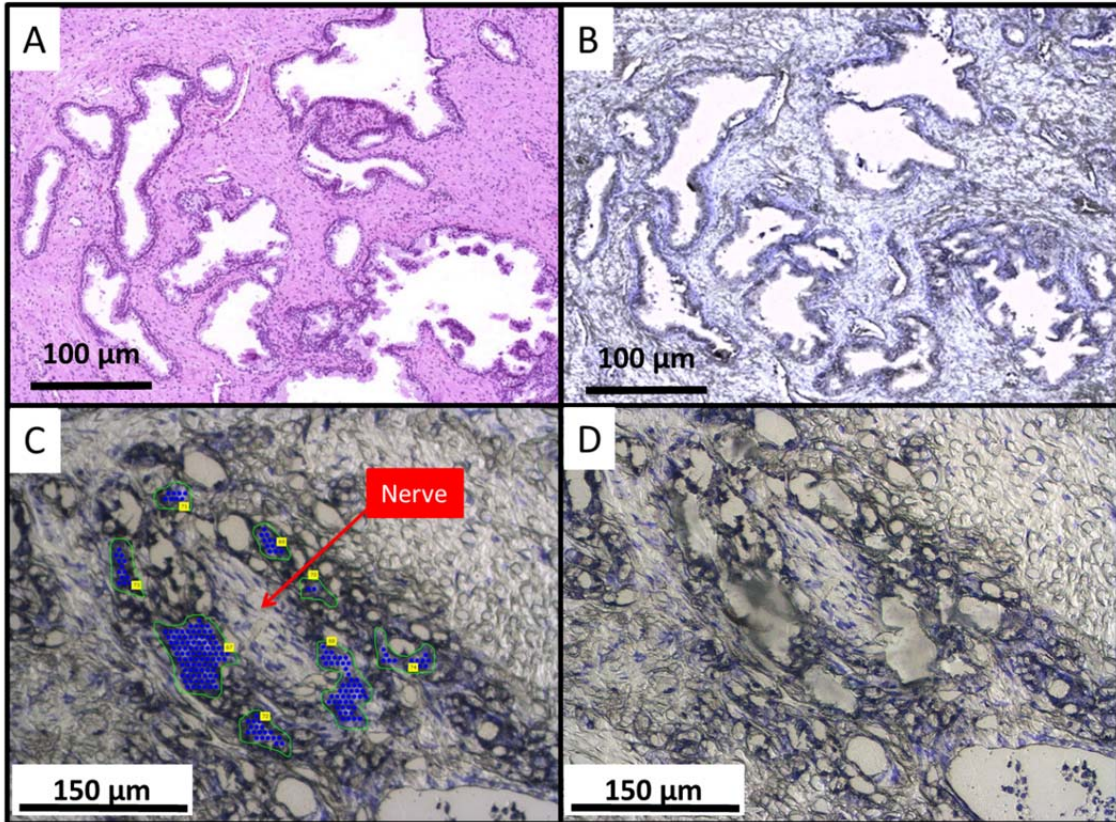
Figure 31: Staining and dissection of human prostate tissue. (A) H&E stain and (B) cresyl violet stain from serial sections. (C) Cresyl violet-stained tissue samples with tumor cells surrounding a nerve marked for dissection. (D) Tissue after dissection.

Dissected cells were subjected to on-chip processing using the FFPE workflow described earlier (chapter IV). Examples of the quality of peptide spectra from LCM-dissected normal epithelial cells and prostate cancer cells obtained from the same patient are shown in Figure 32A. Distinct peptide patterns could be obtained from only 98 LCM-dissected cells. The profiles differ significantly between the two cell populations as indicated by differential analysis of the spectra (Figure 32B). Clearly, a much larger study with a sample cohort that is correlated with long-term clinical outcome will be needed to establish a method for risk assessment for prostate tissue biopsies. It is noted that dissection of cells in the prostate is relatively fast as the tumor and normal epithelial cells tend to form large connected areas which improves the speed of LCM dissection. For example, dissection of 98 cells could be achieved in less than 10 min. The high sensitivity of this workflow combined with the ability to isolate pathologically relevant cells from selected tissue regions highlight the potential of this approach for future applications in clinical discovery and diagnostics.
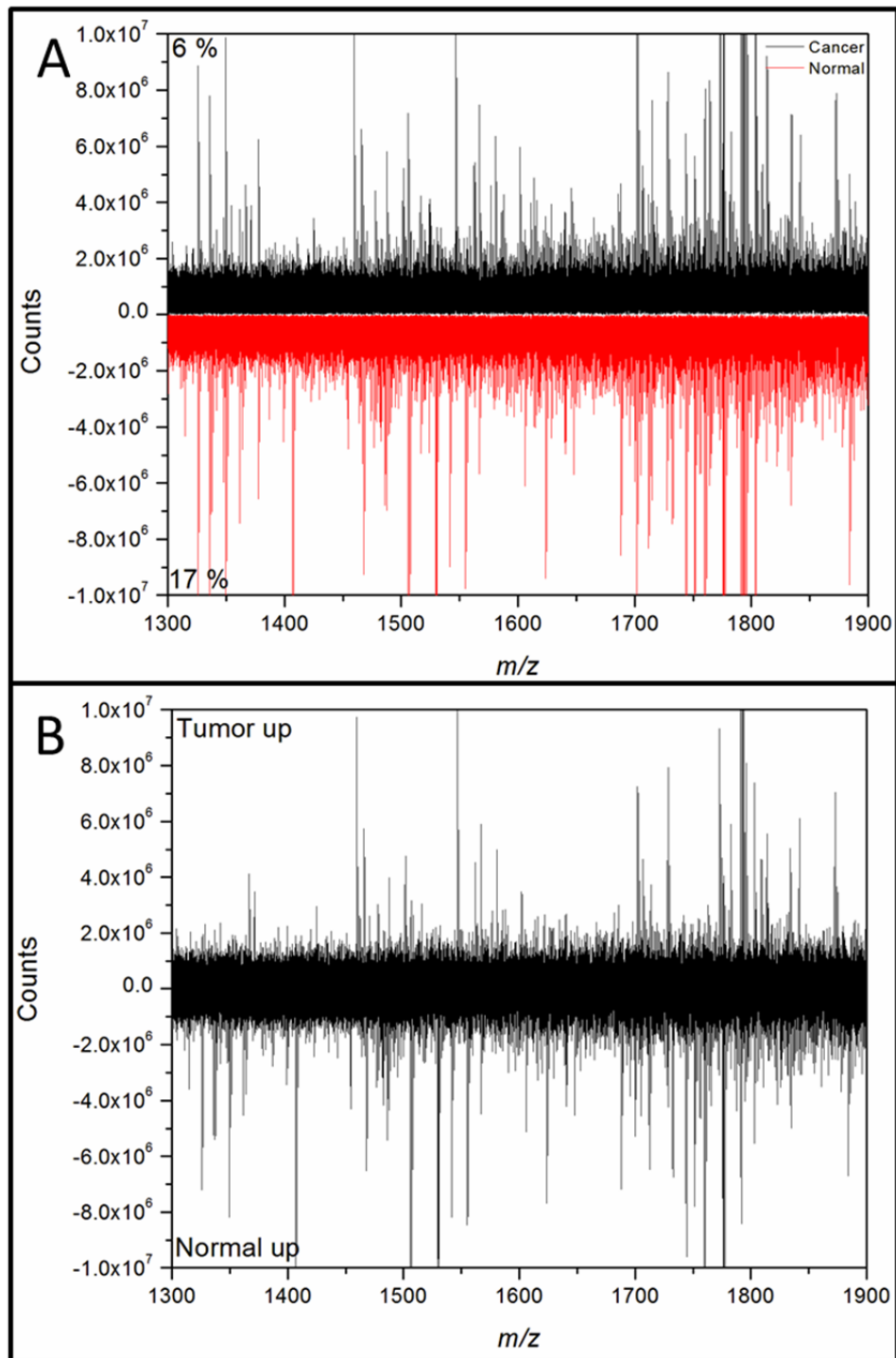
Figure 32: Marker discovery in human prostate cancer. (A) Comparison of averaged spectra (N = 3) from normal and cancer epithelial cells. (B) Differential spectrum from (A) revealing differentially expressed peaks.

Proteomic Profiling of MSNs in Rat Brain

Fresh frozen rat brain tissue with retrograde labeled MSNs were subjected to cell type specific dissection using fluorescence-assisted LCM. Figure 33 shows microscope images from the striatum obtained by bright field and fluorescence imaging, respectively. The two MSN populations can be easily identified based on the different fluorescent tracker dyes used for labeling. Dissection of MSNs was carried out using optimized dissection conditions described in chapter IV. MSNs were roughly 10-20 μm in diameter which allowed rapid dissection with single cell specificity (Figure 34). Tissue corresponding to 200 MSN cells was dissected for each MSN type. Dissection of myelinated axon bundles (Figure 33A) located between the MSN cells in the striatum was also performed to interrogate differences in the proteome of these two neurological structures. Processing of dissected cells was performed as described in chapter IV using the FFPE tissue workflow. Although fresh tissue was used for this project, on-chip reduction and alkylation improved protein extraction and digestion from fresh frozen tissue.

Peptide profiles obtained from the two MSN types did not show any statistically significant differences as judged by the t-test and a minimum two fold intensity difference indicating that they are molecularly similar (Figure 35A). However, distinct differences in the profiles from the MSN and myelinated axons (Figure 35B) demonstrated that cell type specific profiles can distinguish between different neurological structures in rat brain. Importantly, retrograde labeling was compatible with this workflow, enabling cell type specific enrichment with LCM.
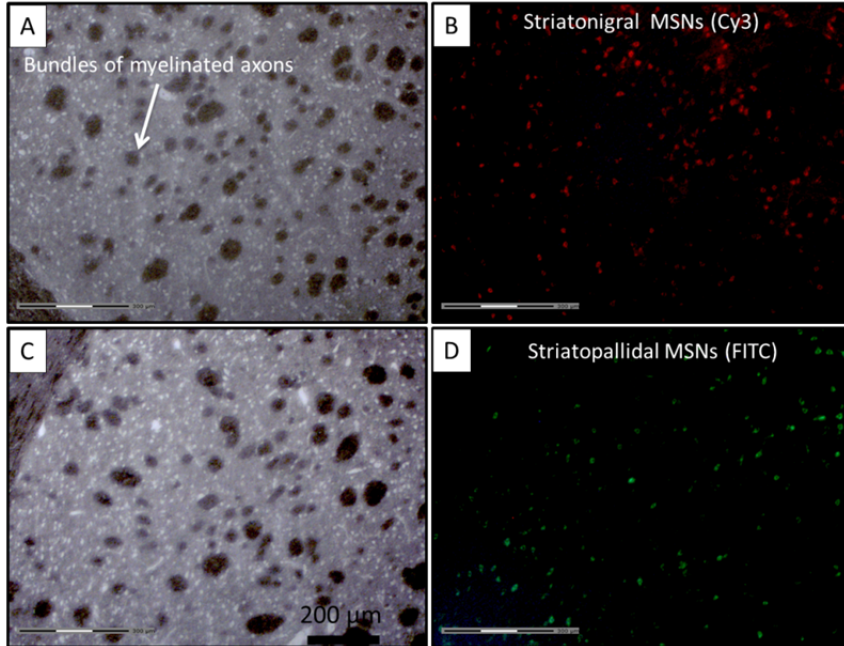
Figure 33: Bright field (A, C) and fluorescent images (B, D) of rat brain striatum showing retrograde labeled MSNs. Striatonigral neurons were labeled with a fluorescent probe detected with the Cy3 fluorescence filter (red) set and striatopallidal MSNs with a FITC filter set (green) respectively.
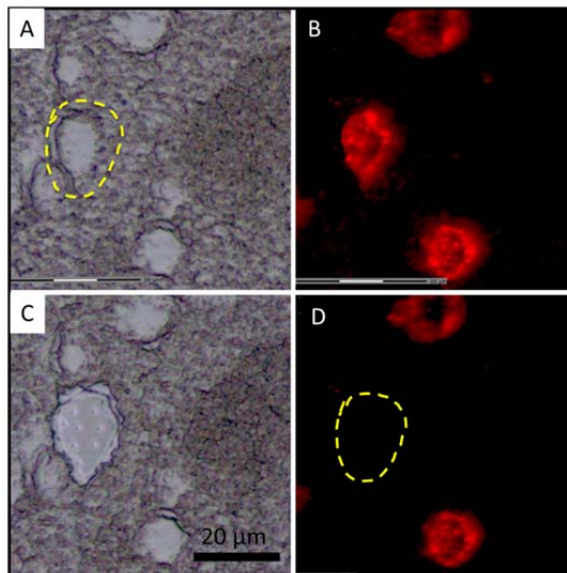
Figure 34: Dissection of a single striatonigral neuron from rat striatum. (A, B) Bright field images showing the tissue before and after dissection and (B, D) corresponding fluorescence images showing the tissue before and after dissection.
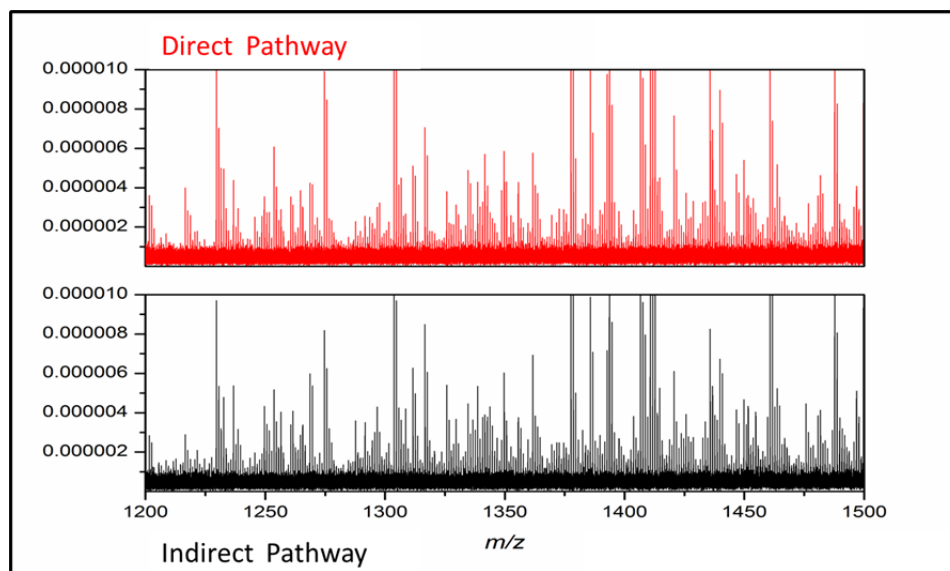
Figure 35: Average spectra from 200 dissected direct and indirect pathway MSNs from rat brain (N = 2).
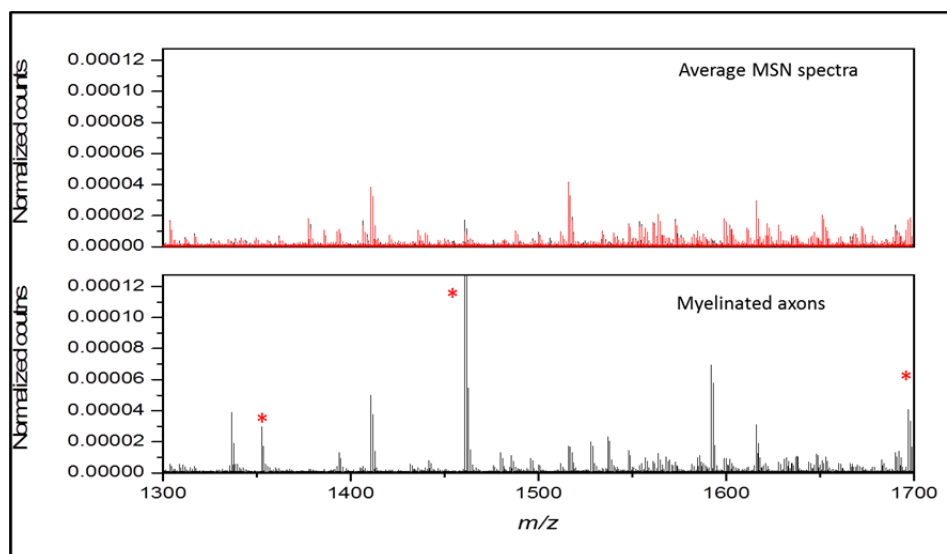
Figure 36: Comparison of averaged spectra from 200 MSNs (N = 3) and 100 myelinated axons (N = 2) after on-chip digestion. Peptides identified by MALDI TOF/TOF MS are marked (*). Spectra were normalized using TIC normalization.

Studies using microarray profiling from FACS-enriched MSNs have revealed only a few differentially expressed protein transcripts that are low abundance, supporting my findings at the protein level. It is expected that strategies to increase the dynamic range of the method (chapter VI) could increase the detection of lower abundance proteins.

Identification of some of the high intensity peptides in the myelinated axons was carried out using MALDI TOF/TOF followed by database searching with Mascot. Identification of myelin protein in the axon bundles could be confirmed (Table 4) along with other proteins such as tubulin and α-internexin which is involved in axon growth[163]. Direct identification of lower abundance peptides in the spectra proved more difficult as the ability to select precursor ions in the MALDI TOF/TOF instrument can be limiting. This resulted in complex fragmentation patterns from multiple peptide precursors that did not yield statistically significant hits. An identification strategy using LC-MALDI MS (chapter III) would be beneficial for identification of these lower abundance peptides. It is estimated that identification of these peptides with LC-MALDI MS could be achieved with as few as 400-500 neurons which can be readily dissected as sufficient tissue is available.

Table 4: Identification of peptides with MALDI TOF/TOF MS from an estimated 100 myelinated axons in rat striatum.

m/z	Protein
1130.5990	Tubulin beta-2C chain,
1352.6340	Myelin basic protein S (MBP S)
1460.7220	Myelin basic protein S (MBP S)
1701.9140	Tubulin alpha-1 chain (Alpha-tubulin 1)
1864.9230	Tubulin alpha-1 chain (Alpha-tubulin 1)
2175.0370	Alpha-internexin (Alpha-Inx)

Conclusions

Successful application of LCM and on-chip processing for protein profiling of human PCa and for profiling of morphologically indistinguishable neuron subpopulations in rat brain has been described. The PCa project demonstrates that the method has great potential for molecular analysis of small tissue samples such as biopsies that might be used for risk stratification in PCa patients. Distinct peptide profiles were obtained from FFPE tissue that distinguished between normal epithelial and cancer cells. The ability to analyze FFPE tissue will be critical to extend this study to a larger sample cohort for correlation with clinical outcome. The high sensitivity of the method indicates that it might be applicable for the study of tissue microarrays, which would enable analysis of large numbers of samples with high-throughput.

The use of fluorescent tracker dyes for retrograde labeling and dissection of MSNs in rat brain was demonstrated and peptides specific to neurological structures in the striatum could be identified. Fluorescent trackers are advantageous as they can provide high cellular specificity. Dissection of single cells was time-consuming because each cell had to be marked individually, requiring at least 1 hour for marking 200 cells. Initial studies with automated software scripts enabled automated cell marking for dissection of fluorescent cells, significantly reducing the time. Automated cell marking tends to fail at the edges of tissues and in regions with non-specific fluorescence. However, development of new multi-modal algorithms[164] for automated cell recognition have been described and it is anticipated that such approaches might be useful to improve automated single cell dissection.

Materials and Methods

Tissue samples

Rat brain tissue: Adult male Sprague Dawley rats (age 90-110d) were stereotaxically injected with the fluorescent retrograde tracers AlexaFluor 488-conjugated cholera toxin B (CTb; InVitrogen) and red fluorescent latex microspheres (FLMs; LumaFluor). 250 nl of the CTb tracer was injected into the SN, and 100 nl of the FLMs into the GP of the contralateral hemisphere. Two weeks later rats were deeply anesthetized with isoflurane and decapitated. The brain was removed within 30 s from the point of death and snap frozen in Freeze'it. Tissue was stored at -80 °C until use. Sectioning was performed in a cryostat with a section thickness of 8 μm. Sections were thaw mounted onto Director slides and dried for 10 min in a vacuum desiccator. Inspection of the sections using fluorescence microscopy demonstrated specific labeling of MSNs.

FFPE prostate tissue. FFPE prostate tissue was a gift from Dr. Axel Wellmann from the Pathologische Institut Zelle in Germany. All tissues blocks for this study had undergone prior histopathological analysis and only blocks with a Gleason score of 4-7 were selected for these experiments. Tissue was sectioned at a section thickness of 6 μm using a microtome. Paraffin removal and rehydration was carried out as described in Chapter IV. The cresyl violet staining protocol optimized for prostate tissue consisted of a 1 min staining step in in 0.1 % cresyl violet stain[106] and two 1 min destaining steps in 70 % ethanol and reagent grade ethanol respectively. Tissue was stored in a vacuum desiccator for at least 1 h prior to LCM. LCM and on-chip processing, using the FFPE workflow, was carried out as described in chapter IV.

Tissue processing and Fluorescence assisted LCM for dissection of MSNs. Tissue

sections were dehydrated with consecutive 2 minute solvent rinses in 70, 95 and 100 %

ethanol followed by an additional 2 minute wash in 100 % ethanol. Remaining solvent

was removed by storing the tissue in a vacuum desiccator for at least one hour before

LCM was carried out. A ZEISS MicroBeam LCM system, equipped for fluorescence

assisted LCM, was used for dissection. The 63x objective and the FS17C adv. (FITC) and

the FS00C adv. (Cy3) filter sets were used for fluorescence imaging and marking of the

cells. An estimated 200 MSNs corresponding to a tissue area of 66,492 μm^2 were

dissected for each MSN subpopulation as described in chapter IV. Dissection of the

myelinated axons in the striatum, on-chip processing of dissected cells using the FFPE

workflow and MALDI FT-ICR MS were carried out as described in chapter IV.

MALDI TOF/TOF MS for protein identification. MALDI TOF/TOF MS and database

searching for peptide sequencing was carried out as described in detail elsewhere.[153]

CHAPTER VI

Research Summary

Methods for mapping proteins using direct and indirect proteomic strategies with high cellular specificity have been optimized for protein discovery in tissues. In chapter II, the optimization of two matrix deposition robots for coating tissues with matrix for MALDI IMS has been described. Optimized protocols for matrix deposition onto tissues including brain and epididymis from the mouse and human clear cell renal cell carcinoma were developed which provided highly reproducible spectra. The resulting ion images revealed the location and relative abundance of hundreds of proteins in the tissue. Indeed, MALDI IMS provides very high sensitivity for protein detection because sample loss is minimal due to the few processing steps required prior to mass spectrometry analysis. Overall, MALDI IMS is a powerful tool for biological discovery with vast potential for clinical applications.[165, 166, 167] As demonstrated in chapter II, automated matrix application using a vibrational matrix deposition robot can generate highly reproducible protein spectra for routine IMS experiments with a spatial resolution in the range of 50 μm. This corresponds to an estimated 9 cells for mouse liver tissue (cut at a section thickness of 12 μm) highlighting the excellent sensitivity of this method. However, imaging of proteins with single cell resolution remains challenging. First, the sensitivity decreases due to the smaller laser spot size. Oversampling approaches, which are often used if the laser spot size is limiting, exacerbates this problem.[168] Second, acquisition of large datasets at high spatial resolution, especially if large tissue samples are analyzed, is

time consuming. Lastly, protein identification is difficult and requires separate experiments which have limited sensitivity and throughput. These challenges were addressed using a newly developed workflow for protein identification that combines multidimensional chromatography and top-down sequencing for identification of proteins with high sensitivity.

An alternative strategy for protein identification is *in situ* digestion with trypsin which has shown excellent performance for the analysis of FFPE tissues allowing direct identification of proteins from the tissue.[169] Unfortunately, the spatial resolution of this method is limited due to the need for robotic spotting of trypsin, and the placement accuracy for reagent deposition can be influenced by the tissue microenvironment. Consequently, protein profiles obtained by this approach may represent an average from several different cell types limiting the specificity of these profiles.

To address this issue, several new strategies for protein analysis from tissue sections have been developed. In chapter III, a high-throughput method for rapid profiling of FFPE tissue was described. The method combines off-line tissue processing and electrophoretic peptide fractionation for detergent removal enabling detection of differentially expressed peptides in selected tissue regions. At least 15,000 cells were needed for this workflow although 60,000 cells provided improved performance. Sample losses during processing and fractionation were identified as the source for the relatively low sensitivity. It was concluded that this approach is advantageous for the analysis of samples that show relatively homogeneous cell morphology and if high-throughput is required.

Isolation of cells with single cell specificity from morphologically complex tissues is time consuming due to the limited speed of LCM for single cell dissection. However, dissection time is critical for enrichment of cells from morphologically complex tissues where dissection of thousands of single cells might not be reasonable. Hence, development of new highly sensitive workflows (Figure 37) for processing and analysis of LCM-dissected cells from fresh frozen and FFPE tissue was performed. Cells are dissected with single cell specificity using LCM and directly captured on a chip for processing, which can include protein extraction, antigen retrieval and digestion. The resulting tryptic peptides can be analyzed by MALDI FT-ICR MS which can provide cell type specific profiles for the enriched cell population. Excellent reproducibility for routine analysis from as few as 100 cells could be demonstrated and detection of proteins from fewer than 20 cells is feasible. The ability to enrich cells prior to analysis increases the sensitivity of the method. More than 3,000 peaks could be detected which compared favorability to *in situ* digestion where detection of up to 1,000 peaks has been reported.[153] Importantly, the new workflows can provide single cell population specificity. The throughput of the LCM-based workflow is lower compared with MALDI IMS. However, it is expected that progress in LCM technology could soon overcome this limitation.

Applications of the new workflows for discovery of differentially expressed proteins in prostate cancer and in rat neurons are presented in chapter V. The prostate cancer study revealed several differentially expressed peaks between tumor cells and normal epithelial cells. The profiling of neurons in rat demonstrated that proteins from distinct neuron populations can be profiled with single cell population specificity. This provides new possibilities to study molecular processes in neural signaling.
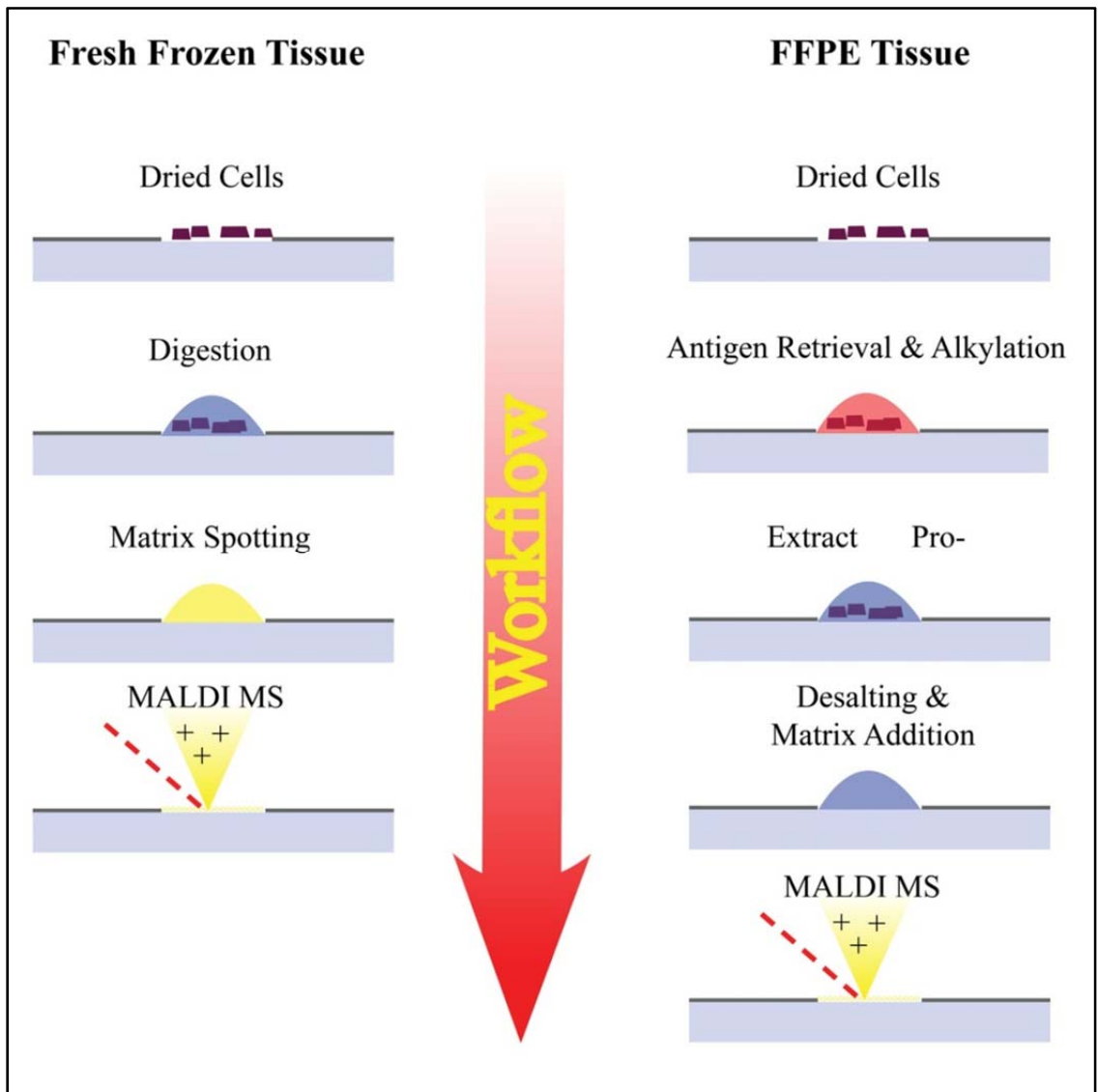
Figure 37: Summary of the new workflows for on-chip processing of LCM-dissected cells.

Perspectives

The promise of protein analysis in tissues is that the discovery of proteins is facilitated by studying them at the site of pathology.[170] Mass spectrometry is a powerful tool for molecular discovery in tissues as it can provide molecular specificity and high sensitivity. Emerging techniques for mapping proteins in tissue are MALDI IMS and LCM assisted profiling of cells with MALDI MS. Sample preparation is one of the most critical steps in MALDI IMS as it can limit spatial resolution and sensitivity. Reliable matrix deposition is critical to obtain reproducible IMS results. In this study, we developed new robotic strategies for matrix deposition allowing reproducible matrix deposition and high spatial resolution. Importantly, the platforms are completely automated, providing an opportunity for standardized matrix application and improved reproducibility within and between laboratories. This will be critical for the integration of MALDI IMS for applications in diagnostics especially molecular pathology.

Although direct analysis of proteins with IMS shows great promise it remains limited for the analysis at the single cell level. This study focused on the development of new strategies that can overcome this challenge by enriching specific cell populations prior to MALDI MS analysis. The use of LCM for MALDI MS profiling of cells from fresh frozen tissue has been described prior to this work. However, the integration of contact-free cell transfer with laser pressure catapulting enables rapid enrichment of large numbers of cells. Concentrating and manipulating the cells on a chip allows higher sensitivity for the analysis of tissues such as FFPE which are clinically relevant. Importantly, several samples can be captured on a single chip and analyzed in parallel. By combining LCM, on-chip processing and MALDI FT-ICR, the discovery of large

numbers of proteins can be accomplished by working with as few as 20 cells. Even higher sensitivities[105] have been described for LCM-based protein profiling, but in this case intact proteins were analyzed which requires subsequent identification with time- and sample-consuming fractionation approaches. The new chip based strategy eliminates these steps as identification of proteins directly from the chip can be performed.

While the scope of this work is limited in terms of applications of the technology, it clearly demonstrates the potential for analysis of single cell populations in morphologically complex tissues. Aside from applications in fresh frozen and FFPE tissues, this method may also prove useful in cytology where the availability of cells is often limiting.

The sensitivity and capabilities of this workflow may be even further enhanced in the future. As discussed in chapter IV, initial results indicate that reduction of the size of the hydrophilic anchors on the capture chip could further improve sensitivity. Analyte density is critical for sensitivity in MALDI MS and smaller wells are expected to significantly improve performance.[41] In theory, the sensitivity of the peptide workflow is expected to improve over 1,100-fold if the well size was reduced from a diameter of 2 mm to 60 μm. This may open opportunities for protein profiling at high resolution with sensitivities for single cell or subcellular proteomic analysis.

Future Work

Selective Chemistry for On-Chip Enrichment

On-chip processing provides unique new opportunities for chemical and physical approaches than can be applied to increase the dynamic range of the experiment. For example, the capture chip could be coated with analyte-selective surfaces that would enable enrichment of proteins or peptides. One way to achieve this would be the use of functionalized surfaces, e.g. a strong anion exchanger, which may provide the possibility of enriching phosphorylated peptides. Alternative methods for on-chip enrichment and separation of specific proteins classes could be explored e.g. using antibodies or activity based probes.[171] This is expected to significantly reduce the complexity of the sample thereby increasing dynamic range.

Higher Peak Capacity and Sensitivity for MALDI FT-ICR MS

The ability to detect low abundance peptides in complex mixtures without separation requires methods that can provide high peak capacity. As shown in this work, FT-ICR MS allowed the detection of 3,000 peaks in a single analysis. The number of detected peaks could be increased by improving the resolution and sensitivity of the FT-ICR instrument. Initial experiments with narrow-band[172] detection demonstrated a resolving power exceeding 1 million for the triply charged peptide angiotensin II. However, narrowband detection limits the useable mass range for each scan event. Therefore, an algorithm is needed post-acquisition that combines several narrowband scan windows into a spectrum that covers the entire mass range for peptides. This approach could be especially useful if combined with methods that improve sensitivity.

CASI (Continuous Accumulation of Selected Ions), is a new method for ion accumulation in the external hexapole prior to mass analysis in the FT-ICR cell.[173] Significant improvements for detection of low abundance peaks for lipids and small molecules using MALDI ionization have been demonstrated in our laboratory, and we anticipate that this approach will be useful for detection of lower abundance peptides from on-chip digested cells. CASI would be especially useful if combined with narrowband detection. The availability of sufficient MALDI sample is critical for this approach as it requires a large number of laser shots for ion accumulation. Calculations indicate that currently less than 1 % of the available matrix spot is consumed (assuming a 130 μm laser spot diameter and random sampling of 20 positions on a matrix spot with 2 mm diameter). Thus there is significant potential for this method to increase sensitivity.

Imaging

On-chip processing provides unique advantages, namely the ability to extract and process proteins prior to analysis. As the sensitivity of the method is further increased, the complete analysis of all cells in a tissue with single cell specificity could be envisioned. If the isolated cells are correlated with the corresponding location in the original tissue, molecular images could be generated that combine the advantages of MALDI IMS and on-chip processing. Automated parallel dissection of cells would be desirable for such an approach to provide high-throughput. Several possibilities for improved laser dissection could be envisioned. First, a micro lens array, proposed for high-throughput laser fabrication, could be adapted for parallel LCM.[174] Second, dynamic laser beam patterning using a next generation digital micromirror device[175] could be developed. Dissected cells could be captured on a stretchable membrane that is placed in

direct contact with the tissue, preventing the spread of the dissected material during laser catapulting (chapter IV). Once the tissue is dissected, membrane stretching could be performed[176] which would create an array of isolated cells on the membrane accessible for on-chip chemistry and MALDI MS.

Quantitative Proteomics

One focus of current proteomic developments is the reliable and reproducible quantitation of proteins.[14] Development and validation of methods for protein quantitation remains difficult and time consuming which can be limiting for antibody based quantitation e.g. with ELISA. A limitation of ELISA is the requirement of specific antibody probes for protein capturing and quantitation of proteins with post-translational modifications. Therefore, there is an increasing trend to use mass spectrometry, specifically LC-MS with MRM, for protein quantitation. These assays can rapidly map multiple relevant peptides for each protein in a complex mixture while providing relatively high sample throughput (3-10 min/sample).[177]

On-chip quantitation of proteins using MALDI could provide a useful strategy for rapid targeted quantitation of a large number of samples. MALDI MS is powerful for high-throughput analysis because sample processing times are in the range of seconds or faster depending on the instrument used. Indeed, MALDI MS has been successfully used for protein quantitation.[178] Sensitivity of the method could be modified by varying the number of cells enriched. Stable isotope labeled peptides or proteins[179, 180] are available and can be added to the chip prior to processing and analysis. By using a chemically identical protein or peptide as a standard for quantitation, issues with ionization and sample loss during processing can be addressed. Quantitation is then carried out by

monitoring peptide specific ions or fragment ions for the labeled and unlabeled peptide. The intensity ratio between these ions can then be used for absolute quantitation. Alternatively, chemical labeling of peptides on the chip, which could be combined with on-chip enrichment, could be performed. Potential chemistries are isotope-coded affinity tags[181] (ICAT) which reduce the complexity of the sample since labeled peptides could be enriched from the chip. With this approach and using a pooled sample internal standard, relative quantitation of peptides would be feasible. Such quantification strategies are successfully used in proteomics (e.g. two-dimensional difference gel electrophoresis, 2-D DIGE).[182]

Conclusions

On-chip based proteomics of selected cell populations enables highly sensitive protein analysis with single cell population specificity. The versatility and sensitivity of the new workflows has been demonstrated providing new possibilities for tissue proteomics. Undoubtedly, cell type specific profiling has great potential and will enable novel insights into the complex interplay of cells in tissues, yet it provides exciting opportunities for biological discovery and diagnostics. This research will continue to advance, driven by the need to map proteins in cells at ever higher sensitivity and resolution and it will be critical for the development of the next generation tools for individualized medicine.

APPENDIX

Contents

Appendix A

Protein Method for ImagePrep

Method Name	SA10gl-9t
Matrix	10 mg/ml sinapinic acid in 1:1 mix of 50 % ACN 0.2 % TFA
Application	Protein imaging, washed tissue, 12 μm
Global spray power adjustment	0

Spray error handling			
	Start detecting after	2.5	s
	Minimal slope	0.5	V/s
	Spray power boost	10	%

Phase # **1: 0.3 V Initialization**

Thickness

Fixed number of cycles	No	1		
Sensor Control	Yes			
Final Voltage Difference	0.3	±	0	V
Within	2	AND	90	Cycles

Nebulize

Spray Power	15			%
Modulation	12			%
Spray Time: Fixed Time	-			s
Spray Time: Sensor control	0.03			V
Duty sequence	20			s
Wait before Start	5			s
Sequence, Curr. Spray Time	20			s
Break Time	0.1			s

Incubation

Incubation Time	3	±	0	s

Dry

Fixed Dry Time	-			s
Sensor control	Yes			
Residual Wetness Grade	0	±		%
Complete drying ever….. Cycle	5			Cycle
Safe Dry	4			s

Protein Method for ImagePrep (cont.)

Phase #	2: 60 s drying			
Thickness				
Fixed number of cycles	Yes	1		
Sensor Control	No			
Final Voltage Difference		±		V
Within		AND		Cycles
Nebulize				
Spray Power	1			%
Modulation	0			%
Spray Time: Fixed Time	0.01			s
Spray Time: Sensor control	No			V
Duty sequence	20			s
Wait before Start	3			s
Sequence, Curr. Spray Time	20			s
Break Time	0.1			s
Incubation				
Incubation Time	0	±	0	s
Dry				
Fixed Dry Time	60			s
Sensor control	No			
Residual Wetness Grade		±		%
Complete drying ever….. Cycle				Cycle
Safe Dry				s

Protein Method for ImagePrep (cont.)

Phase #   **3:0.2 V Coating**

Thickness

Fixed number of cycles	No	1		
Sensor Control	Yes			
Final Voltage Difference	0.2	±	0	V
Within	6	AND	95	Cycles

Nebulize

Spray Power	14			%
Modulation	20			%
Spray Time: Fixed Time	No			s
Spray Time: Sensor control	0.05			V
Duty sequence	20			s
Wait before Start	0			s
Sequence, Curr. Spray Time	20			s
Break Time	0.1			s

Incubation

Incubation Time	15	±	30	s

Dry

Fixed Dry Time	No			s
Sensor control	Yes			
Residual Wetness Grade	20	±	0	%
Complete drying ever….. Cycle	3			Cycle
Safe Dry	20			s

Phase #   **4: 0.2 V coating**

Thickness

Fixed number of cycles	No	1		
Sensor Control	Yes			
Final Voltage Difference	0.2	±	0	V
Within	6	AND	138	Cycles

Protein Method for ImagePrep

Nebulize

Spray Power	14			%
Modulation	20			%
Spray Time: Fixed Time	No			s
Spray Time: Sensor control	0.15			V
Duty sequence	20			s
Wait before Start	1			s
Sequence, Curr. Spray Time	20			s
Break Time	0.1			s

Incubation

Incubation Time	15	±	15	s

Dry

Fixed Dry Time	No			s
Sensor control	Yes			
Residual Wetness Grade	30	±	10	%
Complete drying ever….. Cycle	5			Cycle
Safe Dry	30			s

Phase #	**5: 0.2V coating**

Thickness

Fixed number of cycles	No	1		
Sensor Control	Yes			
Final Voltage Difference	0.2	±	0.2	V
Within	8	AND	95	Cycles

Nebulize

Spray Power	30			%
Modulation	25			%
Spray Time: Fixed Time	No			s
Spray Time: Sensor control	0.3			V
Duty sequence	20			s
Wait before Start	1			s
Sequence, Curr. Spray Time	20			s
Break Time	0.1			s

Protein Method for ImagePrep

Incubation

Incubation Time	25	±	3 0	s

Dry

Fixed Dry Time	No			s
Sensor control	Yes			
Residual Wetness Grade	50	±	1 0	%
Complete drying ever….. Cycle	6			Cy cle
Safe Dry	45			s

Phase #	**6: 0.2V coating**			

Thickness

Fixed number of cycles	No	1		
Sensor Control	Yes			
Final Voltage Difference	0.2	±	0 . 4	V
Within	5	A N D	3 0	Cy cles

Nebulize

Spray Power	34			%
Modulation	27			%
Spray Time: Fixed Time	No			s
Spray Time: Sensor control	0.6			V
Duty sequence	20			s
Wait before Start	1			s
Sequence, Curr. Spray Time	20			s
Break Time	0.1			s

Incubation

Incubation Time	35	±	3 0	s

Protein Method for ImagePrep

Dry

Fixed Dry Time	No			s
Sensor control	Yes			
Residual Wetness Grade	70	±	1 0	%
Complete drying ever….. Cycle	6			Cy cle
Safe Dry	40			s

Phase #	7: 0.4V coating			

Thickness

Fixed number of cycles	No	1		
Sensor Control	Yes			
Final Voltage Difference	0.4	±	0 . 4	V
Within	5	A N D	1 5	Cy cles

Nebulize

Spray Power	25			%
Modulation	21			%
Spray Time: Fixed Time	No			s
Spray Time: Sensor control	0.85			V
Duty sequence	20			s
Wait before Start	1			s
Sequence, Curr. Spray Time	20			s
Break Time	0.1			s

Incubation

Incubation Time	40	±	3 0	s

Dry

Fixed Dry Time	No			s
Sensor control	Yes			
Residual Wetness Grade	90	±	1 0	%
Complete drying every Cycle	8			Cy cle
Safe Dry	45			s

Appendix B

Matching fragment ions from the fragmentation of $[M+12H]^{12+} = 1029.4$ for the protein MIF (Swiss-Prot P14174).

Ion	Observed Mass (Da)	Theoretical Mass (Da)	Mass Error (Da)	Mass Error (PPM)
B14	1526.81	1526.815	-0.005	-3.4
B17	1795.91	1795.916	-0.006	-3.5
B18	1942.98	1942.985	-0.005	-2.4
B19	2056.06	2056.069	-0.009	-4.3
B21	2272.14	2272.143	-0.003	-1.5
B41	4416.3	4416.318	-0.018	-4
B42	4515.37	4515.386	-0.016	-3.5
B46	4968.6	4968.608	-0.008	-1.7
Y8	896.389	896.392	-0.003	-3.3
Y61	6732.28	6732.327	-0.047	-7
Y64	6964.4	6964.42	-0.02	-2.9
Y67	7238.48	7238.539	-0.059	-8.2

Appendix C

Parameters for database searching with Myrimatch and IdPicker software.

Identification	
Parameter	Value
Software name	MyriMatch
Software version	1.2.9
AdjustPrecursorMass	1
CalculateRelativeScores	0
ClassSizeMultiplier	2
CleavageRules	[|[M|K|R . .]
ComplementMzTolerance	0.5
DeisotopingMode	0
DuplicateSpectra	1
DynamicMods	M * 15.994915 (Q! % -17.026549
EndProteinIndex	-1
EndSpectraScanNum	-1
FragmentMzTolerance	0.5
IsotopeMzTolerance	0.25
MakeScoreHistograms	0
MakeSpectrumGraphs	0
MaxDynamicMods	2
MaxFragmentChargeState	1
MaxPrecursorAdjustment	1.008665
MaxResults	5
MaxScoreHistogramValues	100
MaxSequenceMass	10000
MinCandidateLength	5
MinPrecursorAdjustment	-1.008665
MinResultScore	0
MinSequenceMass	0
NumBatches	50
NumChargeStates	3
NumIntensityClasses	3
NumMaxMissedCleavages	-1
NumMinTerminiCleavages	1
NumMzFidelityClasses	3
NumScoreHistogramBins	100

Parameters for database searching with Myrimatch and IdPicker software (cont.)

Parameter	Value
NumSearchBestAdjustments	3
OutputSuffix	
PeakCounts: 1stQuartile: Filtered	116
PeakCounts: 1stQuartile: Original	137
PeakCounts: 2ndQuartile: Filtered	137
PeakCounts: 2ndQuartile: Original	159
PeakCounts: 3rdQuartile: Filtered	154
PeakCounts: 3rdQuartile: Original	176
PeakCounts: Mean: Filtered	132
PeakCounts: Mean: Original	153
PeakCounts: Min/Max: Filtered	17 / 183
PeakCounts: Min/Max: Original	32 / 200
PrecursorAdjustmentStep	1.008665
PrecursorMzTolerance	0.5
PreferIntenseComplements	1
ProteinDatabase	/hactar/fasta/20080430-IPIMouse342-Cntms-reverse.fasta
ProteinSampleSize	100
ScoreHistogramHeight	600
ScoreHistogramWidth	800
SearchStats: Nodes	32
SearchStats: Overall	188776 proteins; 787196833 candidates; 317543051 queries; 559060514 comparisons
SearchTime: Duration	141.7816 seconds
StartProteinIndex	0
StartSpectraScanNum	0
StaticMods	C 57.021464
StatusUpdateFrequency	5
ThreadCountMultiplier	10
TicCutoffPercentage	0.95
UseAvgMassOfSequences	0
UseChargeStateFromMS	1
UseMultipleProcessors	1

Parameters for database searching with Myrimatch and IdPicker software (cont.)

UseSmartPlusThreeModel	1
WorkingDirectory	/hactar/data/unorganized/20080717-Aerni-Mouse-Liver
Validation	
Parameter	Value
Software name	idpQonvert
Software version	2.1.4
DecoyPrefix	rev_
HasDecoyDatabase	1
MaxFDR	0.05
MaxResultRank	1
NormalizeSearchScores	0
NumChargeStates	3
OptimizeScorePermutations	200
OptimizeScoreWeights	0
OutputSuffix	
PreserveInputHierarchy	0
ProteinDatabase	c:Êliburdatabase 80430-IPIMouse342-Cntms-reverse.fasta
SearchScoreWeights	mvh 1 xcorr 1 expect -1 ionscore 1
StatusUpdateFrequency	5
WorkingDirectory	
WriteQonversionDetails	0
Presentation/filtration	
Parameter	Value
Software name	idpReport
Software version	2.1.1 (4/8/2008)
MinAdditionalPeptides	1
GenerateBipartiteGraphs	FALSE
ModsAreDistinctByDefault	TRUE
DistinctModsOverride	
IndistinctModsOverride	
RawSourceHostURL	http://localhost/
RawSourceExtension	.*
RawSourcePath	
MaxFDR	0.05
MaxResultRank	1
MinPeptideLength	5

Parameters for database searching with Myrimatch and IdPicker software (cont.)

MinDistinctPeptides	1
MaxAmbiguousIds	2
AllowSharedSourceNames	TRUE

Appendix D

IdPicker report showing the results from a LC MALDI run from mouse liver.

Peptide	Decoy	Mass of unmodified peptide	Protein
AFAISGPFNVQFLVK	No	1636.887	IPI00111908.8
EIEYEVVR	No	1035.524	IPI00111908.8
FLEEATR	No	864.4341	IPI00111908.8
FLGVAEQLHNEGFK	No	1587.794	IPI00111908.8
FVHDNYVIR	No	1161.593	IPI00111908.8
GILIGIQQSFR	No	1230.708	IPI00111908.8
GILIGIQQSFRPR	No	1483.862	IPI00111908.8
GQNQPVLNITNR	No	1352.716	IPI00111908.8
GYSFGHPSSVAGEVVFNTGLGG YPEALTDPAYK	No	3386.598	IPI00111908.8
IAPSFAVESM(15.9949)EDALK	No	1606.78	IPI00111908.8
QADAVYFLPITPQFVTEVIK	No	2278.214	IPI00111908.8
Q(-17.0265)ADAVYFLPITPQFVTEVI K	No	2278.214	IPI00111908.8
RLPTLEQPIIPSDYVAIK	No	2052.151	IPI00111908.8
SIFSAVLDELK	No	1220.654	IPI00111908.8
SLFHYR	No	821.4184	IPI00111908.8
VPAIYGVDTR	No	1089.582	IPI00111908.8
DFTPAAQAAFQK	No	1293.624	IPI00762198.2/I PI00553333.2
LHVDPENFR	No	1125.557	IPI00762198.2/I PI00553333.2
LLGNM(15.9949)IVIVLGHHLGK	No	1713.002	IPI00762198.2/I PI00553333.2
LLVVYPWTQR	No	1273.718	IPI00762198.2/I PI00553333.2
VITAFNDGLNHLDSLK	No	1755.905	IPI00762198.2/I PI00553333.2
YFDSFGDLSSASAIM(15.9949)GN AK	No	1979.882	IPI00762198.2/I PI00553333.2
VNADEVGGEALGR	No	1285.626	IPI00762198.2
VNSDEVGGEALGR	No	1301.621	IPI00553333.2

AGFAGDDAPR	No	975.4409	IPI00110850.1
AVFPSIVGR	No	944.5444	IPI00110850.1
AVFPSIVGRPR	No	1197.698	IPI00110850.1
GYSFTTTAER	No	1131.52	IPI00110850.1
QEYDESGPSIVHR	No	1515.695	IPI00110850.1
Q(-17.0265)EYDESGPSIVHR	No	1515.695	IPI00110850.1
SYELPDGQVITIGNER	No	1789.885	IPI00110850.1
VAPEEHPVLLTEAPLNPK	No	1953.046	IPI00110850.1
FNSANEDNVTQVR	No	1492.69	IPI00231742.5
FSTVAGESGSADTVRDPR	No	1850.876	IPI00231742.5
GAGAFGYFEVTHDITR	No	1739.827	IPI00231742.5
GPLLVQDVVFTDEM(15.9949)AHFDR	No	2188.062	IPI00231742.5
LAQEDPDYGLR	No	1275.609	IPI00231742.5
LFAYPDTHR	No	1118.551	IPI00231742.5
NFTDVHPDYGAR	No	1390.626	IPI00231742.5
GIYETPAGTILYHAHLDIEAFTM(15.9949)DR	No	2833.374	IPI00134746.5
GQVYILGR	No	904.5131	IPI00134746.5
MPEFYNR	No	955.4222	IPI00134746.5
NQAPPGLYTK	No	1087.555	IPI00134746.5
Q(-17.0265)HGIPIPVTPK	No	1185.676	IPI00134746.5
RQVEIAQR	No	998.5622	IPI00134746.5
AHGGYSVFAGVGER	No	1405.674	IPI00468481.2
AIAELGIYPAVDPLDSTSR	No	1987.026	IPI00468481.2
DQEGQDVLLFIDNIFR	No	1920.958	IPI00468481.2
IM(15.9949)DPNIVGNEHYDVAR	No	1841.873	IPI00468481.2
LVLEVAQHLGESTVR	No	1649.91	IPI00468481.2
VALTGLTVAEYFR	No	1438.782	IPI00468481.2
DGFNPAHVEAGLYGSR	No	1688.791	IPI00623845.3
LAGQIFLGGSIVR	No	1329.777	IPI00623845.3
LNPNFLVDFGKEPLGPALAHELR	No	2546.354	IPI00623845.3
Q(-17.0265)YDISNPQKPR	No	1344.668	IPI00623845.3
SPQYSQVIHR	No	1213.62	IPI00623845.3
APQVSTPTLVEAAR	No	1438.778	IPI00131695.3
DVFLGTFLYEYSR	No	1608.782	IPI00131695.3
GLVLIAFSQYLQK	No	1478.839	IPI00131695.3
LGEYGFQNAILVR	No	1478.788	IPI00131695.3
RHPDYSVSLLLR	No	1454.799	IPI00131695.3

NQTAEKEEFEHQQK	No	1744.78	IPI00208205.1
QTQTFTTYSDNQPGVLIQVYEGER	No	2773.319	IPI00208205.1
SQIHDIVLVGGSTR	No	1480.8	IPI00208205.1
STAGDTHLGGEDFDNR	No	1690.718	IPI00208205.1
TVTNAVVTVPAYFNDSQR	No	1980.99	IPI00208205.1
DLGEAALNEYLR	No	1362.678	IPI00153317.3
DTNHGPQNHEAHLR	No	1624.745	IPI00153317.3
HGSIIYHPSLLPR	No	1488.82	IPI00153317.3
PGFFFQPTVFTDVEDHM(15.9949)YIAK	No	2488.166	IPI00153317.3
RPQPEEGATYEGIQK	No	1701.821	IPI00153317.3
AGPWTPEAAVEHPEAVR	No	1815.89	IPI00130950.1
EATTEQQLR	No	1074.531	IPI00130950.1
EAYNLGVR	No	920.4716	IPI00130950.1
QGFIDLPEFPFGLEPR	No	1860.941	IPI00130950.1
DIVYIGLR	No	947.544	IPI00117914.3
LKETEYDVR	No	1151.571	IPI00117914.3
VM(15.9949)EETFSYLLGR	No	1443.707	IPI00117914.3
VSVVLGGDHSLAVGSISGHAR	No	2017.07	IPI00117914.3
IGGHGAEYGAEALER	No	1528.727	IPI00110658.1
LRVDPVNFK	No	1086.608	IPI00110658.1
M(15.9949)FASFPTTK	No	1028.489	IPI00110658.1
TYFPHFDVSHGSAQVK	No	1818.858	IPI00110658.1
FPGQLNADLR	No	1129.588	IPI00109061.1
GHYTEGAELVDSVLDVVR	No	1957.974	IPI00109061.1
IREEYPDR	No	1076.525	IPI00109061.1
EQAGGDATENFEDVGHSTDAR	No	2204.92	IPI00230113.5
FLEEHPGGEEVLR	No	1510.742	IPI00230113.5
TYIIGELHPDDR	No	1427.704	IPI00230113.5
DVLFPGYTHLQR	No	1444.746	IPI00314788.5
INVLPLGSGAIAGNPLGVDR	No	1932.079	IPI00314788.5
LHPNDEDIHTANER	No	1659.76	IPI00314788.5
TEQGPQVDETQFK	No	1505.689	IPI00197770.1
TFVQEDVYDEFVER	No	1774.805	IPI00197770.1
VVGNPFDSR	No	989.493	IPI00197770.1
HNFTPLAR	No	954.5036	IPI00201413.1
ITAHLVHELR	No	1187.677	IPI00201413.1
YALQSQQR	No	992.504	IPI00201413.1

HGGTIPVVPTAEFQDR	No	1722.869	IPI00114209.1
IIAEGANGPTTPEADKIFLER	No	2241.153	IPI00114209.1
NLNHVSYGR	No	1058.526	IPI00114209.1
DNIQGITKPAIR	No	1324.735	IPI00231340.8
VFLENVIR	No	988.5706	IPI00231340.8
EAYPGDVFYLHSR	No	1552.731	IPI00130280.1
TGAIVDVPVGEELLGR	No	1623.883	IPI00130280.1
FAVELEGEQPISVPPSTNHTVYR	No	2569.281	IPI00405699.2
STGSVVGQQPFGGAR	No	1446.722	IPI00405699.2
EKIEDNGNFR	No	1220.568	IPI00466399.1
LFLEQIHVLENSLVLK	No	1894.082	IPI00466399.1
EGHPVTSEPSRPEPAVFK	No	1962.969	IPI00223216.5
YLGTQPEPDIVGLDSGHIR	No	2066.043	IPI00223216.5
DSQGNLFR	No	935.4461	IPI00127206.6
ELSEIAQR	No	944.4929	IPI00127206.6
AEELGLPILGVLR	No	1378.818	IPI00121833.3
IAQFLSGIPETVPLSTVNR	No	2041.121	IPI00121833.3
AAYQVAALPR	No	1058.587	IPI00130640.5
APAAIGPYSQAVQVDR	No	1641.847	IPI00130640.5
DILQDVLDADLSNEAFPFSTHQL VR	No	2842.413	IPI00136213.5
FHHSLTDHTR	No	1249.595	IPI00136213.5
AHPLFTFLR	No	1100.613	IPI00192301.2
YVRPGGGFEPNFTLFEK	No	1956.962	IPI00192301.2
FEDGDLTLYQSNAILR	No	1853.916	IPI00231229.9
PPYTIVYFPVR	No	1350.733	IPI00231229.9
HHLDGETEEER	No	1350.58	IPI00230212.5
KHHLDGETEEER	No	1478.664	IPI00230212.5
GKPDVVVKEDEEYKR	No	1789.888	IPI00154054.1
Q(-17.0265)EQDTYALSSYTR	No	1560.705	IPI00154054.1
HIDGAYVYHNEHEVGEAIR	No	2208.035	IPI00122657.1
SLGVSNFNR	No	992.504	IPI00122657.1
LISWYDNEYGYSNR	No	1778.79	IPI00554039.1
LVNNGKPITIFQER	No	1627.894	IPI00554039.1
KFLQPGSQR	No	1059.572	IPI00116055.6
SHGQDYLVGNR	No	1244.59	IPI00116055.6
FYGPEGPYGVFAGR	No	1515.714	IPI00319973.3
KFYGPEGPYGVFAGR	No	1643.799	IPI00319973.3
FHHTIGGSR	No	1010.505	IPI00231445.5

GATYGKPVHHGVNQLK	No	1704.884	IPI00231445.5
GAYPVFFNFTR	No	1317.651	IPI00308328.3
ILEEGSFLLEVLR	No	1516.85	IPI00308328.3
GGPLSGPYR	No	902.461	IPI00221890.6
VVFDDTYDR	No	1128.509	IPI00221890.6
GFFVQPTVFSNVTDEM(15.9949)R	No	1972.935	IPI00626662.3
IHGQTIPSDGDIFTYTR	No	1919.938	IPI00626662.3
FAFQAEVNR	No	1080.535	IPI00129526.1
KPEEVDDEVFYSPR	No	1708.783	IPI00116603.1
NAVTQEFGPVPDTAR	No	1600.784	IPI00116074.1
QASGGPVDIGPEYQQDLDR	No	2043.95	IPI00125460.1
HAYGDQYR	No	1008.441	IPI00135231.2
GFVVQGSTGEFPFLTSLER	No	2070.042	IPI00560967.1
HEYQANGPEDLNR	No	1541.686	IPI00127942.4
HGRPGIGATHSSR	No	1331.681	IPI00231692.5
AAATFNPELITHILDGSPENTR	No	2366.186	IPI00409360.3
GENLSLVVHGPGDIR	No	1561.821	IPI00753038.1
FVEGLPINDFSR	No	1392.704	IPI00198717.8
FTPGTFTNQIQAAFR	No	1697.852	IPI00123604.4
GAGVKGPPASTSR	No	1183.62	IPI00387452.1
GAM(15.9949)KGLGTDEDTLIEIL TTR	No	2133.088	IPI00230395.5
ADHGEPIGR	No	950.457	IPI00229080.7
IQTQPGYANTLR	No	1360.71	IPI00124771.1
INEAFDLLR	No	1089.582	IPI00221400.5
IYHTIAYLTPLPQPNR	No	1896.026	IPI00230889.5
AGLQFPVGR	No	943.524	IPI00153400.2
KANGTVVDSGFDPQSRQLNLPTP IAPK	Yes	2849.481	IPI:IPI00664248. 3
IISQEILNLIELR	No	1552.919	IPI00323496.5
HQGSLYSLFPDHSVK	No	1713.836	IPI00133456.1
HGVYNPNK	No	927.4453	IPI00197696.2
HYNGEAYEDDEHHPR	No	1867.75	IPI00132208.1
IGHHSTSDDSSAYR	No	1531.665	IPI00331555.2
IFFYDAENPPGSEVLR	No	1852.899	IPI00317356.10
FALDGFFSTIR	No	1272.65	IPI00115599.6
ALLELQLEPEELYQTFQR	No	2219.148	IPI00203214.6
ALHGEQYLELYKPLPR	No	1926.025	IPI00331628.5
APLVLEQGLR	No	1094.645	IPI00210444.5

IdPicker report showing the results from a LC MALDI run from mouse liver (cont.)

AQFGQPEILLGTIPGAGGTQR	No	2110.117	IPI00207217.1
AQELAQRLKQEQR	No	1596.859	IPI00468895.2
ALETASQDFSLDLR	No	1564.773	IPI00108982.1
AGVPPGVINIVFGTGPR	No	1649.925	IPI00267407.1
AFEEEQALR	No	1091.525	IPI00211507.3
AHHDLGYFYGSSYVAAPDGSR	No	2269.018	IPI00121639.1
ALESPERPFLAILGGAK	No	1767.978	IPI00231426.6
AISFVGSNQAGEYIFER	No	1886.916	IPI00205018.2
ELNDFISYLQR	No	1396.699	IPI00230108.6
EADNPGILHPFGSVPFGYGVR	No	2228.101	IPI00119685.1
EVSVFGAVSELFTR	No	1539.793	IPI00127625.1
FAGPYDKGEYSPSVQK	No	1771.82	IPI00223367.5
AEAVQSFLAFIQHLR	No	1728.931	IPI00212316.1
DVNQQEFVR	No	1133.546	IPI00113241.7
AVIGDHGDEIFSVFGSPFLK	No	2134.062	IPI00387289.3
ASGGGVPTDEEQATGLER	No	1772.818	IPI00116154.2
DFIDYFLIQR	No	1328.676	IPI00114781.1
DLGTQLAPIIQEFFHSEQYR	No	2391.186	IPI00339188.2
DFVENVTSGNAVDFFPVLR	No	2125.048	IPI00128287.1
KSSLSLDSLKR	Yes	1232.687	IPI00368909.3
TSYAQHQQVR	No	1216.595	IPI00231693.5
TLIEFLLR	No	1003.607	IPI00331436.4
TTPDVIFVFGFR	No	1397.734	IPI00214654.1
VAAFDLDGVLALPSIAGAFR	No	2002.089	IPI00321617.1
TVLGVPEVLLGILPGAGGTQR	No	2046.184	IPI00212622.2
TATPQQAQEVHEK	No	1465.705	IPI00231767.5
SLRPGVAIADFVIFPPR	No	1854.051	IPI00114330.3
SGYQQAASEHGLVVIAPDTSPR	No	2282.129	IPI00109142.4
SSGSPYGGGYGSGGGSGGYGSR	No	1909.783	IPI00269661.1
SSQQEHKR	Yes	998.4786	IPI00206433.3
SSPKKPR	No	798.4494	IPI00226378.1
VAGHPDVVINNAAGNFISPSER	No	2263.134	IPI00213659.3
DFDPAINEYIQR/DFDPAINEYLQR	No	1479.699	IPI00228630.5
YYVTIIDAPGHR	No	1403.72	IPI00195372.1
IQDKEGIPPDQQR/IQDKEGLPPDQQR	No	1522.763	IPI00138892.2
YTDQSGEEEEDYESEEQIQHR/YTDQSGEEEEDYESEEQLQHR	No	2600.042	IPI00169862.1

IdPicker report showing the results from a LC MALDI run from mouse liver (cont.)

SLGVAAEGIPDQYADGEAAR/SL GVAAEGLPDQYADGEAAR	No	1988.944	IPI00231648.5
YTPPPHHSGR	No	1147.552	IPI00117300.3
VIHDNFGIVKGLM(15.9949)TTVH AITATQK	No	2593.384	IPI00462605.5
VDATEESDLAQQYGVR	No	1779.827	IPI00122815.3
VTHAVVTVPAYFNDAQR	No	1886.964	IPI00206624.1
YQLQSQENFEPFM(15.9949)K	No	1787.808	IPI00120451.1
YLDEDTVYHLQPSGR	No	1791.843	IPI00128518.1
SEDYAFPTYADR	No	1433.61	IPI00117978.1
LPIFIADAFTATAFR	No	1652.893	IPI00110528.1
LLYDLADQLHAAVGASR	No	1811.953	IPI00116753.4
LVQAFQFTDK	No	1195.613	IPI00121788.1
MAELNSAASEMPFNLR	No	1779.828	IPI00127317.1
LVQDVANNTNEEAGDGTTTATV LAR	No	2559.241	IPI00308885.6
LLVPYLIEAVR	No	1284.781	IPI00121105.2
LFDHPEVPTPPESASVSR	No	1963.964	IPI00113223.2
KTDGVYDPVEYEKYPER	No	2086.963	IPI00387491.1
LISQIVSSITASLR	No	1486.872	IPI00117348.4
LLGQFTLIGIPPAPR	No	1591.945	IPI00133903.1
LKQEYFVVAATLQDVIR	No	1992.094	IPI00190179.3
M(15.9949)VNVFLGIPFAQAPLGP LR	No	2039.139	IPI00381178.3
QQKWLLFAC(57.0215)ETALGR	Yes	1819.93	IPI00849514.1
QLLPM(15.9949)QVTQHAK	No	1392.744	IPI00370138.4
RDLPVDPR	No	966.5246	IPI00763061.1
RLAVSVLREIR	No	1310.815	IPI00222072.1
RGDGTMGPGR	Yes	1002.466	IPI00650051.1
Q(- 17.0265)ATVGDVNTDRPGLLDLK	No	1910.995	IPI00222430.5
NIIVFYGSQTGTAEEFANR	No	2116.022	IPI00231200.5
NFLASQVPFPSR	No	1361.709	IPI00231253.5
NKPEDYQGGR	No	1162.526	IPI00222496.3
PGGLLLGDEAPNFEANTTIGR	No	2141.075	IPI00555059.2
NVVGDHADDVYSVFGAPILR	No	2143.07	IPI00128399.3

REFERENCES

1. Hood, L., A Personal Journey of Discovery: Developing Technology and Changing Biology. *Annu. Rev. Anal. Chem.* **2008,** *1*, 1-43.

2. Hanash, S., Integrated global profiling of cancer. *Nat Rev Cancer* **2004,** *4* (8), 638-644.

3. Phizicky, E.; Bastiaens, P. I. H.; Zhu, H.; Snyder, M.; Fields, S., Protein analysis on a proteomic scale. *Nature* **2003,** *422* (6928), 208-215.

4. Legrain, P.; Aebersold, R.; Archakov, A.; Bairoch, A.; Bala, K.; Beretta, L.; Bergeron, J.; Borchers, C.; Corthals, G. L.; Costello, C. E.; Deutsch, E. W.; Domon, B.; Hancock, W.; He, F.; Hochstrasser, D.; Marko-Varga, G.; Salekdeh, G. H.; Sechi, S.; Snyder, M.; Srivastava, S.; Uhlen, M.; Hu, C. H.; Yamamoto, T.; Paik, Y.-K.; Omenn, G. S., The human proteome project: Current state and future direction. *Mol. Cell. Proteomics* **2011**.

5. Ghaemmaghami, S.; Huh, W. K.; Bower, K.; Howson, R. W.; Belle, A.; Dephoure, N.; O'Shea, E. K.; Weissman, J. S., Global analysis of protein expression in yeast. *Nature* **2003,** *425* (6959), 737-41.

6. Hortin, G. L.; Sviridov, D.; Anderson, N. L., High-Abundance Polypeptides of the Human Plasma Proteome Comprising the Top 4 Logs of Polypeptide Abundance. *Clin. Chem.* **2008**, clinchem.2008.108175.

7. Vestal, M. L., The Future of Biological Mass Spectrometry. *J. Am. Soc. Mass. Spectrom.* **2011,** *22* (6), 953-959.

8. Qian, W. J.; Jacobs, J. M.; Liu, T.; Camp, D. G., 2nd; Smith, R. D., Advances and challenges in liquid chromatography-mass spectrometry based proteomic profiling for clinical applications. *Mol. Cell. Proteomics* **2006**.

9. Macher, B. A.; Yen, T. Y., Proteins at membrane surfaces-a review of approaches. *Molecular BioSystems* **2007,** *3* (10), 705-13.

10. Mann, M.; Jensen, O. N., Proteomic analysis of post-translational modifications. *Nat. Biotechnol.* **2003,** *21* (3), 255-61.

11. Chautard, E.; Thierry-Mieg, N.; Ricard-Blum, S., Interaction networks: from protein functions to drug discovery. A review. *Pathologie-biologie* **2009,** *57* (4), 324-33.

12. Rifai, N.; Gillette, M. A.; Carr, S. A., Protein biomarker discovery and validation: the long and uncertain path to clinical utility. *Nat. Biotechnol.* **2006,** *24* (8), 971-83.

13. Sung-Min Ahn, R. J. S., Body fluid proteomics: Prospects for biomarker discovery. *Proteomics: Clinical Applications* **2007,** *1* (9), 1004-1015.

14. Hoofnagle, A. N.; Aebersold, R.; Anderson, N. L.; Felsenfeld, A.; Liebler, D. C., Painting a Moving Picture: Large-Scale Proteomics Efforts and Their Potential for Changing Patient Care. *Clin. Chem.* **2011,** *Epub ahead of print*, clinchem.2010.158311.

15. Delahunty, C.; Yates, J. R., 3rd, Protein identification using 2D-LC-MS/MS. *Methods* **2005,** *35* (3), 248-55.

16. Tanaka, K.; Waki, H.; Ido, Y.; Akita, S.; Yoshida, Y.; Yoshida, T., Protein and Polymer Analyses up to m/z 100 000 by Laser Ionization Time-of-flight Mass Spectrometry. *Rapid Commun. Mass Spectrom.* **1988,** *2* (8), 151-153.

17. Karas, M.; Hillenkamp, F., Laser desorption ionization of proteins with molecular masses exceeding 10,000 daltons. *Anal. Chem.* **1988,** *60* (20), 2299-2301.

18. Zhang, N.; Doucette, A.; Li, L., Two-Layer Sample Preparation Method for MALDI Mass Spectrometric Analysis of Protein and Peptide Samples Containing Sodium Dodecyl Sulfate. *Anal. Chem.* **2001,** *73*, 2968-2975.

19. Reyzer, M. L.; Hsieh, Y.; Ng, K.; Korfmacher, W. A.; Caprioli, R. M., Direct analysis of drug candidates in tissue by matrix-assisted laser desorption/ionization mass spectrometry. *J. Mass Spectrom.* **2003,** *38* (10), 1081-92.

20. Wang, H.-Y.; Chu, X.; Zhao, Z.-X.; He, X.-S.; Guo, Y.-L., Analysis of low molecular weight compounds by MALDI-FTICR-MS. *J. Chromatogr. B* **2011,** *879* (17-18), 1166-79.

21.	Murphy, R. C.; Hankin, J. A.; Barkley, R. M.; Berry, K. A. Z., MALDI Imaging of Lipids after Matrix Sublimation/Deposition. *Biochim. Biophys. Acta* **2011,** *In Press, Accepted Manuscript*.

22.	Harvey, D. J., Matrix-assisted laser desorption/ionization mass spectrometry of carbohydrates and glycoconjugates. *Int. J. Mass spectrom.* **2003,** *226*, 1-35.

23.	Meng, Z.; Simmons-Willis, T. A.; Limbach, P. A., The use of mass spectrometry in genomics. *Biomol. Eng* **2004,** *21*, 1-13.

24.	Li, L., *MALDI-MS for Polymer Characterization*. Wiley-VCH Verlag GmbH & Co. KGaA: 2007; p 245-297.

25.	Hillenkamp, F.; Peter-Katalini, J., *MALDI MS: A Practical Guide to Instrumentation, Methods and Applications*. Wiley-VCH Verlag GmbH & Co. KGaA: Weinheim, 2007; p 41.

26.	Sauer, S.; Kliem, M., Mass spectrometry tools for the classification and identification of bacteria. *Nat Rev Micro* **2010,** *8* (1), 74-82.

27.	Schwamborn, K.; Caprioli, R. M., Molecular imaging by mass spectrometry - looking beyond classical histology. *Nat Rev Cancer* **2010,** *10* (9), 639-46.

28.	Seeley, E. H.; Caprioli, R. M., MALDI imaging mass spectrometry of human tissue: method challenges and clinical perspectives. *Trends Biotechnol.* **2011,** *29* (3), 136-143.

29.	Hillenkamp, F.; Tsarbopoulos, A.; Gross, M. L., Focus on desorption ionization and macromolecular mass spectrometry. *J. Am. Soc. Mass Spectrom.* **2008,** *19* (8), 1041-4.

30.	Meier, M. A. R.; Adams, N.; Schubert, U. S., Statistical Approach To Understand MALDI-TOFMS Matrices: Discovery and Evaluation of New MALDI Matrices. *Anal. Chem.* **2007,** *79* (3), 863-9.

31.	Strupat, K.; Karas, M.; Hillenkamp, F., 2,5-Dihydroxybenzoic Acid - a New Matrix for Laser Desorption Ionization Mass-Spectrometry. *Int. J. Mass Spectrom. Ion Processes* **1991,** *111*, 89-102.

32. Beavis, R. C.; Chaudhary, T.; Chait, B. T., a-Cyano-4-hydroxycinnamic acid as a matrix for matrixassisted laser desorption mass spectromtry. *Org. Mass Spectrom.* **1992,** *27* (2), 156-158.

33. Beavis, R. C.; Chait, B. T.; Fales, H. M., Cinnamic acid derivatives as matrices for ultraviolet laser desorption mass spectrometry of proteins. *Rapid Commun. Mass Spectrom.* **1989,** *3* (12), 432-435.

34. Krause, J.; Stoeckli, M.; Schlunegger, U. P., Studies on the Selection of New Matrices for Ultraviolet Matrix-assisted Laser Desorption/Ionization Time-of-flight Mass Spectrometry. *Rapid Commun. Mass Spectrom.* **1996,** *10* (15), 1927-1933.

35. Burnum, K. E.; Cornett, D. S.; Puolitaival, S. M.; Milne, S. B.; Myers, D. S.; Tranguch, S.; Brown, H. A.; Dey, S. K.; Caprioli, R. M., Spatial and temporal alterations of phospholipids determined by mass spectrometry during mouse embryo implantation. *J. Lipid Res.* **2009**.

36. Rohlfing, A.; Leisner, A.; Hillenkamp, F.; Dreisewerd, K., Investigation of the Desorption Process in UV Matrix-Assisted Laser Desorption/Ionization with a Liquid 3-Nitrobenzyl Alcohol Matrix by Photoacoustic Analysis, Fast-Flash Imaging, and UV-Laser Postionization. *The Journal of Physical Chemistry C* **2010,** *114* (12), 5367-5381.

37. Knochenmuss, R., Ion formation mechanisms in UV-MALDI. *Analyst* **2006,** *131* (9), 966-86.

38. Dreisewerd, K., The desorption process in MALDI. *Chem. Rev.* **2003,** *103* (2), 395-426.

39. Jaskolla, T.; Karas, M., Compelling Evidence for Lucky Survivor and Gas Phase Protonation: The Unified MALDI Analyte Protonation Mechanism. *J. Am. Soc. Mass. Spectrom.* **2011,** *22* (6), 976-988.

40. Wenzel, R. J.; Matter, U.; Schultheis, L.; Zenobi, R., Analysis of megadalton ions using cryodetection MALDI time-of-flight mass spectrometry. *Anal. Chem.* **2005,** *77* (14), 4329-37.

41. Keller, B. O.; Li, L., Detection of 25,000 Molecules of Substance P by MALDI-TOF Mass Spectrometry and Investigations into the Fundamental Limits of Detection in MALDI. *J. Am. Soc. Mass Spectrom.* **2001,** *12*, 1055-1063.

42. Mock, K. K.; Sutton, C. W.; Cottrell, J. S., Sample Immobilization Protocols for Matrix-assisted laser-desorption Mass Spectrometry. *Rapid Commun. Mass Spectrom.* **1992,** *6*, 233-238.

43. Caprioli, R. M.; Farmer, T. B.; Gile, J., Molecular Imaging of Biological Samples: Localization of Pepdides and Proteins Using MALDI-TOF MS. *Anal. Chem.* **1997,** *69*, 4751-4760.

44. Prideaux, B.; Dartois, V. r.; Staab, D.; Weiner, D. M.; Goh, A.; Via, L. E.; Barry Iii, C. E.; Stoeckli, M., High-Sensitivity MALDI-MRM-MS Imaging of Moxifloxacin Distribution in Tuberculosis-Infected Rabbit Lungs and Granulomatous Lesions. *Anal. Chem.* **2011,** *83* (6), 2112-2118.

45. Reyzer, M. L.; Caprioli, R. M., MALDI-MS-based imaging of small molecules and proteins in tissues. *Curr. Opin. Chem. Biol.* **2007,** *11*, 1-7.

46. Yunsheng Hsieh, R. C. E. F. J. C. I. K. J. W. R. M. W. K., Matrix-assisted laser desorption/ionization imaging mass spectrometry for direct measurement of clozapine in rat brain tissue. *Rapid Commun. Mass Spectrom.* **2006,** *20* (6), 965-972.

47. Khatib-Shahidi, S.; Andersson, M.; Herman, J. L.; Gillespie, T. A.; Caprioli, R. M., Direct Molecular Analysis of Whole-Body Animal Tissue Sections by Imaging MALDI Mass Spectrometry. *Anal. Chem.* **2006,** *78* (18), 6448-6456.

48. Hsieh, Y.; Chen, J.; Korfmacher, W. A., Mapping pharmaceuticals in tissues using MALDI imaging mass spectrometry. *J. Pharmacol. Toxicol. Methods* **2006**.

49. McDonnell, L. A.; van Remoortere, A.; de Velde, N.; van Zeijl, R. J. M.; Deelder, A. M., Imaging Mass Spectrometry Data Reduction: Automated Feature Identification and Extraction. *J. Am. Soc. Mass. Spectrom.* **2010,** *21* (12), 1969-1978.

50. Urban, P. L.; Chang, C.-H.; Wu, J.-T.; Chen, Y.-C., Microscale MALDI Imaging of Outer-Layer Lipids in Intact Egg Chambers from Drosophila melanogaster. *Anal. Chem.* **2011**, null-null.

51. Spraggins, J.; Caprioli, R., High-Speed MALDI-TOF Imaging Mass Spectrometry: Rapid Ion Image Acquisition and Considerations for Next Generation Instrumentation. *J. Am. Soc. Mass. Spectrom.* **2011**, 1-10.

52. McLean, J. A.; Ridenour, W. B.; Caprioli, R. M., Profiling and imaging of tissues by imaging ion mobility-mass spectrometry. *J. Mass Spectrom.* **2007,** *42* (8), 1099-1105.

53. Miyamura, N.; Nakamura, T.; Goto-Inoue, N.; Zaima, N.; Hayasaka, T.; Yamasaki, T.; Terai, S.; Sakaida, I.; Setou, M.; Nishina, H., Imaging mass spectrometry reveals characteristic changes in triglyceride and phospholipid species in regenerating mouse liver. *Biochem. Biophys. Res. Commun. In Press, Accepted Manuscript*.

54. Hardesty, W. M.; Kelley, M. C.; Mi, D.; Low, R. L.; Caprioli, R. M., Protein signatures for survival and recurrence in metastatic melanoma. *Journal of Proteomics* **2011,** *74* (7), 1002-14.

55. Willems, S. M.; van Remoortere, A.; van Zeijl, R.; Deelder, A. M.; McDonnell, L. A.; Hogendoorn, P. C. W., Imaging mass spectrometry of myxoid sarcomas identifies proteins and lipids specific to tumour type and grade, and reveals biochemical intratumour heterogeneity. *The Journal of Pathology* **2010,** *222* (4), 400-409.

56. Lagarrigue, M.; Becker, M.; Lavigne, R.; Deininger, S.-O.; Walch, A.; Aubry, F.; Suckau, D.; Pineau, C., Revisiting rat spermatogenesis with MALDI imaging at 20 μm resolution. *Mol. Cell. Proteomics* **2011,** *10* (3), M110.005991.

57. Fournier, I.; Wisztorski, M.; Salzet, M., Tissue imaging using MALDI-MS: a new frontier of histopathology proteomics. *Expert Rev Proteomics* **2008,** *5* (3), 413-24.

58. Grey, A.; Chaurand, P.; Caprioli, R.; Schey, K., MALDI Imaging Mass Spectrometry of Integral Membrane Proteins from Ocular Lens and Retinal Tissue. *Journal of Proteome Research* **2009,** *8* (7), 3278-83.

59. Guenther, S.; Römpp, A.; Kummer, W.; Spengler, B., AP-MALDI imaging of neuropeptides in mouse pituitary gland with 5 μm spatial resolution and high mass accuracy *Int. J. Mass spectrom.* **2011,** *In Press, Accepted Manuscript*.

60. Verhaert, P. D.; Conaway, M. C. P.; Pekar, T. M.; Miller, K., Neuropeptide imaging on an LTQ with vMALDI source: The complete `all-in-one' peptidome analysis. *Int. J. Mass spectrom.* **2007,** *260* (2-3), 177.

61. Norris, J. L.; Cornett, D. S.; Mobley, J. A.; Andersson, M.; Seeley, E. H.; Chaurand, P.; Caprioli, R. M., Processing MALDI Mass Spectra to Improve Mass Spectral Direct Tissue Analysis. *Int J Mass Spectrom* **2007,** *260* (2-3), 212-221.

62. Crecelius, A. C.; Cornett, D. S.; Caprioli, R. M.; Williams, B.; Dawant, B. M.; Bodenheimer, B., Three-Dimensional Visualization of Protein Expression in Mouse Brain Structures Using Imaging Mass Spectrometry. *J. Am. Soc. Mass Spectrom.* **2005**.

63. Andersson, M.; Groseclose, M. R.; Deutch, A. Y.; Caprioli, R. M., Imaging mass spectrometry of proteins and peptides: 3D volume reconstruction. *Nat Methods* **2008,** *5* (1), 101-108.

64. Sinha, T. K.; Khatib-Shahidi, S.; Yankeelov, T. E.; Mapara, K.; Ehtesham, M.; Cornett, D. S.; Dawant, B. M.; Caprioli, R. M.; Gore, J. C., Integrating spatially resolved three-dimensional MALDI IMS with in vivo magnetic resonance imaging. *Nat Methods* **2008,** *5* (1), 57-9.

65. Schwamborn, K.; Caprioli, R. M., MALDI Imaging Mass Spectrometry - Painting Molecular Pictures. *Molecular Oncology* **2010,** *4* (6), 529-538.

66. Palkovits, M., Isolated removal of hypothalamic or other brain nuclei of the rat. *Brain Res.* **1973,** *59*, 449-50.

67. Going, J. J.; Lamb, R. F., Practical histological microdissection for PCR analysis. *J. Pathol.* **1996,** *179* (1), 121-4.

68. EmmertBuck, M. R.; Bonner, R. F.; Smith, P. D.; Chuaqui, R. F.; Zhuang, Z. P.; Goldstein, S. R.; Weiss, R. A.; Liotta, L. A., Laser capture microdissection. *Science* **1996,** *274* (5289), 998-1001.

69. Bohm, M.; Wieland, I.; Schutze, K.; Rubben, H., Microbeam MOMeNT: non-contact laser microdissection of membrane-mounted native tissue. *Am. J. Pathol.* **1997,** *151* (1), 63-7.

70. Schutze, K.; Lahr, G., Identification of expressed genes by laser-mediated manipulation of single cells. *Nat. Biotechnol.* **1998,** *16* (8), 737-42.

71.   Murray, G. I., An overview of laser microdissection technologies. *Acta Histochem.* **2007,** *109* (3), 171-6.

72.   Blow, N., Tissue preparation: Tissue issues. *Nature* **2007,** *448* (7156), 959.

73.   Vogel, A.; Lorenz, K.; Horneffer, V.; Huttmann, G.; von Smolinski, D.; Gebert, A., Mechanisms of laser-induced dissection and transport of histologic specimens. *Biophys. J.* **2007,** *93* (12), 4481-500.

74.   Elvers, D.; Remer, L.; Arnold, N.; Bauerle, D., Laser microdissection of biological tissues: process optimization. *Applied Physics a-Materials Science & Processing* **2005,** *80* (1), 55-59.

75.   Colombelli, J.; Reynaud, E. G.; Rietdorf, J.; Pepperkok, R.; Stelzer, E. H., In vivo selective cytoskeleton dynamics quantification in interphase cells induced by pulsed ultraviolet laser nanosurgery. *Traffic* **2005,** *6* (12), 1093-102.

76.   Horneffer, V.; Linz, N.; Vogel, A., Principles of laser-induced separation and transport of living cells. *J Biomed Opt* **2007,** *12* (5), 054016.

77.   Wiley, W. C.; McLaren, I. H., Time-of-Flight Mass Spectrometer with Improved Resolution. *Rev. Sci. Instrum.* **1955,** *26* (12), 1150-1157.

78.   Mamyrin, B. A., Laser-Assisted Reflectron Time-of-Flight Mass-Spectrometry. *Int. J. Mass Spectrom. Ion Processes* **1994,** *131*, 1-19.

79.   Stahl-Zeng, J.; HILLENKAMP, F., Metastable fragment-ion analysis in a reflectron instrument with a gridless ion mirror. *Eur. Mass. Spectrom.* **1996,** *2*, 23-32.

80.   Medzihradszky, K.; Campbell, J.; Baldwin, M.; Falick, A.; Juhasz, P.; Vestal, M.; Burlingame, A., The characteristics of peptide collision-induced dissociation using a high-performance MALDI-TOF/TOF tandem mass spectrometer. *Anal. Chem.* **2000,** *72* (3), 552-558.

81.   Suckau, D.; Resemann, A.; Schuerenberg, M.; Hufnagel, P.; Franzen, J.; Holle, A., A novel MALDI LIFT-TOF/TOF mass spectrometer for proteomics. *Anal Bioanal Chem* **2003,** *376* (7), 952-65.

82. Vestal, M.; Juhasz, P., Resolution and mass accuracy in matrix-assisted laser desorption ionization time-of-flight. *J. Am. Soc. Mass. Spectrom.* **1998,** *9* (9), 892-911.

83. Chaurand, P.; Schriver, K. E.; Caprioli, R. M., Instrument design and characterization for high resolution MALDI-MS imaging of tissue sections. *J. Mass Spectrom.* **2007,** *42* (4), 476-489.

84. Spengler, B.; Hubert, M., Scanning Microprobe Matrix-Assisted Laser Desorption Ionization (SMALDI) Mass Spectrometry: Instrumentation for Sub-Micrometer Resolved LDI and MALDI Surface Analysis. *J. Am. Soc. Mass Spectrom.* **2002,** *13*, 735–748.

85. Hui Qiao, V. S. W. E., The effect of laser profile, fluence, and spot size on sensitivity in orthogonal-injection matrix-assisted laser desorption/ionization time-of-flight mass spectrometry. *Rapid Commun. Mass Spectrom.* **2008,** *22* (18), 2779-2790.

86. Holle, A.; Haase, A.; Kayser, M.; Hohndorf, J., Optimizing UV laser focus profiles for improved MALDI performance. *J. Mass Spectrom.* **2006,** *41* (6), 705-716.

87. Aerni, H.-R.; Cornett, D. S.; Caprioli, R. M., High-Throughput Profiling of Formalin-Fixed Paraffin-Embedded Tissue Using Parallel Electrophoresis and Matrix-Assisted Laser Desorption Ionization Mass Spectrometry. *Anal. Chem.* **2009,** *81* (17), 7490-7495.

88. Strupat, K.; Kovtoun, V.; Bui, H.; Viner, R.; Stafford, G.; Horning, S., MALDI Produced Ions Inspected with a Linear Ion Trap-Orbitrap Hybrid Mass Analyzer. *J. Am. Soc. Mass. Spectrom.* **2009,** *20* (8), 1451-1463.

89. Paul W.; H., S., Ein neues Massenspektrometer ohne Magnetfeld. *Zeitschrift für Naturforschung A* **1953,** *8* (7), 448-450.

90. Gross, J. H., *"Mass Spectrometry - A Textbook"*. Springer: 2004.

91. Schwartz, J. C.; Senko, M. W.; Syka, J. E., A two-dimensional quadrupole ion trap mass spectrometer. *J. Am. Soc. Mass Spectrom.* **2002,** *13* (6), 659-69.

92. Mayrhofer, C.; Krieger, S.; Raptakis, E.; Allmaier, G., Comparison of vacuum matrix-assisted laser desorption/ionization (MALDI) and atmospheric pressure MALDI (AP-MALDI) tandem mass spectrometry of 2-dimensional separated and trypsin-digested glomerular proteins for database search derived identification. *J Proteome Res* **2006,** *5* (8), 1967-78.

93. Garrett, T. J.; Prieto-Conaway, M. C.; Kovtoun, V.; Bui, H.; Izgarian, N.; Stafford, G.; Yost, R. A., Imaging of small molecules in tissue sections with a new intermediate-pressure MALDI linear ion trap mass spectrometer. *Int. J. Mass spectrom.* **2006,** *260* (2-3), 166-176.

94. Yates, J. R., Mass Spectrometry and the Age of the Proteome. *J. Mass Spectrom.* **1998,** *33*, 1-19.

95. Loboda, A. V.; Krutchinsky, A. N.; Bromirski, M.; Ens, W.; Standing, K. G., A tandem quadrupole/time-of-flight mass spectrometer with a matrix-assisted laser desorption/ionization source: design and performance. *Rapid Commun. Mass Spectrom.* **2000,** *14* (12), 1047-1057.

96. Chernushevich, I. V.; Loboda, A. V.; Thomson, B. A., An introduction to quadrupole-time-of-flight mass spectrometry. *J. Mass Spectrom.* **2001,** *36*, 849-865.

97. Hopfgartner, G.; Varesio, E.; Tschappat, V.; Grivet, C.; Bourgogne, E.; Leuthold, L. A., Triple quadrupole linear ion trap mass spectrometer for the analysis of small molecules and macromolecules. *J. Mass Spectrom.* **2004,** *39* (8), 845-55.

98. Hu, Q.; Noll, R.; Li, H.; Makarov, A.; Hardman, M.; Cooks, R., The Orbitrap: a new mass spectrometer. *J. Mass Spectrom.* **2005,** *40* (4), 430-443.

99. Marshall, A. G.; Hendrickson, C. L., High-resolution mass spectrometers. *Annu. Rev. Anal. Chem.* **2008,** *1*, 579-99.

100. Perry, R. H.; Cooks, R. G.; Noll, R. J., Orbitrap mass spectrometry: Instrumentation, ion motion and applications. *Mass Spectrom. Rev.* **2008,** *27* (6), 661-699.

101. Marshall, A. G.; Hendrickson, C. L.; Jackson, G. S., Fourier transform ion cyclotron resonance mass spectrometry: A primer. *Mass Spectrom. Rev.* **1998,** *17* (1), 1-35.

102. Schwartz, S. A.; Reyzer, M. L.; Caprioli, R. M., Direct tissue analysis using matrix-assisted laser desorption/ionization mass spectrometry: practical aspects of sample preparation. *J. Mass Spectrom.* **2003,** *38*, 699-708.

103. Terracio, L.; Schwabe, K. G., Freezing and drying of biological tissues for electron microscopy. *J. Histochem. Cytochem.* **1981,** *29* (9), 1021-8.

104. Seeley, E. H.; Oppenheimer, S. R.; Mi, D.; Chaurand, P.; Caprioli, R. M., Enhancement of Protein Sensitivity for MALDI Imaging Mass Spectrometry after Chemical Treatment of Tissue Sections. *J. Am. Soc. Mass. Spectrom.* **2008,** *19* (8), 1069-1077.

105. Xu, B. J.; Caprioli, R. M.; Sanders, M. E.; Jensen, R. A., Direct analysis of laser capture microdissected cells by MALDI mass spectrometry. *J. Am. Soc. Mass Spectrom.* **2002,** *13* (11), 1292-1297.

106. Chaurand, P.; Schwartz, S. A.; Billheimer, D.; Xu, B. G. J.; Crecelius, A.; Caprioli, R. M., Integrating histology and imaging mass spectrometry. *Anal. Chem.* **2004,** *76* (4), 1145-1155.

107. Stoeckli, M.; Staab, D.; Staufenbiel, M.; Wiederhold, K.-H.; Signor, L., Molecular imaging of amyloid ß peptides in mouse brain sections using mass spectrometry. *Anal. Biochem.* **2002,** *311*, 33-39.

108. Sugiura, Y.; Shimma, S.; Setou, M., Thin Sectioning Improves the Peak Intensity and Signal-to-Noise Ratio in Direct Tissue Mass Spectrometry. *J. Mass Spectrom. Soc. Jpn.* **2006,** *54* (2), 45-48.

109. Ketterlinus, R.; Aerni, H. R.; Schürenberg, M.; Deininger, S.; Suckau, D., Lokalisierung von Biomarkern in Gewebeschnitten: Praktische Anwendungen. *Biospektrum* **2007,** (05), 512-513.

110. Allmaier, G., Picoliter to nanoliter deposition of peptide and protein solutions for matrix-assisted laser desorption/ionization mass spectrometry. *Rapid Commun. Mass Spectrom.* **1997,** *11*, 1567-1569.

111. Baluya, D. L.; Garrett, T. J.; Yost, R. A., Automated MALDI Matrix Deposition Method with Inkjet Printing for Imaging Mass Spectrometry. *Anal. Chem.* **2007,** *79* (17), 6862-7.

112. Sloane, A. J.; Duff, J. L.; Wilson, N. L.; Gandhi, P. S.; Hill, C. J.; Hopwood, F. G.; Smith, P. E.; Thomas, M. L.; Cole, R. A.; Packer, N. H.; Breen, E. J.; Cooley, P. W.; Wallace, D. B.; Williams, n. L.; Gooley, A. A., High Throughput Peptide Mass Fingerprinting and Protein Macroarray Analysis Using Chemical Printing Strategies. *Mol. Cell. Proteomics* **2002,** *1* (7), 490-9.

113. Aerni, H. R.; Cornett, D. S.; Caprioli, R. M., Automated Acoustic Matrix Deposition for MALDI Sample Preparation. *Anal. Chem.* **2006,** *78*, 827-834.

114. Liu, Z.; Schey, K. L., Optimization of a MALDI TOF-TOF Mass Spectrometer for Intact Protein Analysis. *J. Am. Soc. Mass Spectrom.* **2005,** *16* (4), 482-490.

115. Lam, Y. W.; Mobley, J. A.; Evans, J. E.; Carmody, J. F.; Ho, S. M., Mass profiling-directed isolation and identification of a stage-specific serologic protein biomarker of advanced prostate cancer. *Proteomics* **2005,** *5* (11), 2927-38.

116. Burnum, K. E.; Tranguch, S.; Mi, D.; Daikoku, T.; Dey, S. K.; Caprioli, R. M., Imaging mass spectrometry reveals unique protein profiles during embryo implantation. *Endocrinology* **2008,** *149* (7), 3274-8.

117. Aerni, H. R.; Cornett, D. S.; Caprioli, R. M., Automated acoustic matrix deposition for MALDI sample preparation. *Anal. Chem.* **2006,** *78* (3), 827-834.

118. Suzuki, K.; Yu, X.; Chaurand, P.; Araki, Y.; Lareyre, J. J.; Caprioli, R. M.; Matusik, R. J.; Orgebin-Crist, M. C., Epididymis-specific promoter-driven gene targeting: a transcription factor which regulates epididymis-specific gene expression. *Mol. Cell. Endocrinol.* **2006,** *250* (1-2), 184-9.

119. Chaurand, P.; Fouchécourt, S.; Dague, B. B.; Xu, B. J.; Reyzer, M. L.; Orgebin-Crist, M.-C.; Caprioli, R. M., Profiling and imaging proteins in the mouse epididymis by imaging mass spectrometry. *Proteomics* **2003,** *3*, 2221-2239.

120. Cornett, D. S.; Mobley, J. A.; Dias, E. C.; Andersson, M.; Arteaga, C. L.; Sanders, M. E.; Caprioli, R. M., A novel histology directed strategy for MALDI-MS tissue profiling that improves throughput and cellular specificity in human breast cancer. *Mol. Cell. Proteomics* **2006,** *5* (10), 1975-83.

121. Taylor, G. K.; Kim, Y. B.; Forbes, A. J.; Meng, F.; McCarthy, R.; Kelleher, N. L., Web and database software for identification of intact proteins using "top down" mass spectrometry. *Anal. Chem.* **2003,** *75* (16), 4081-6.

122. Corso, T. N.; Van Pelt, C. K.; Li, J.; Ptak, C.; Huang, X., Ultralow-Volume Fraction Collection from NanoLC Columns for Mass Spectrometric Analysis of Protein Phosphorylation and Glycosylation. *Anal. Chem.* **2006,** *78* (7), 2209-19.

123. Zubarev, R. A., Electron-capture dissociation tandem mass spectrometry. *Curr. Opin. Biotechnol.* **2004,** *15* (1), 12-6.

124. Chaurand, P.; Caprioli, R. M., Direct profiling and imaging of peptides and proteins from mammalian cells and tissue sections by mass spectrometry. *Electrophoresis* **2002,** *23*, 3125-3135.

125. Sompuram, S. R.; Vani, K.; Bogen, S. A., A Molecular Model of Antigen Retrieval Using a Peptide Array. *Am. J. Clin. Pathol.* **2006,** *125* (1), 91-98.

126. Shi, S.-R.; Cote, R. J.; Taylor, C. R., Antigen Retrieval Techniques: Current Perspectives. *J. Histochem. Cytochem.* **2001,** *49* (8), 931-938.

127. Hood, B. L.; Darfler, M. M.; Guiel, T. G.; Furusato, B.; Lucas, D. A.; Ringeisen, B. R.; Sesterhenn, I. A.; Conrads, T. P.; Veenstra, T. D.; Krizman, D. B., Proteomic Analysis of Formalin-fixed Prostate Cancer Tissue. *Mol. Cell. Proteomics* **2005,** *4* (11), 1741-1753.

128. Jiang, X.; Jiang, X.; Feng, S.; Tian, R.; Ye, M.; Zou, H., Development of efficient protein extraction methods for shotgun proteome analysis of formalin-fixed tissues. *J Proteome Res* **2007,** *6* (3), 1038-47.

129. Harkins, J. B. I.; Katz, B. B.; Pastor, S. J.; Osucha, P.; Hafeman, D. G.; Witkowski, C. E., II; Norris, J. L., Parallel electrophoretic depletion, fractionation, concentration, and desalting of 96 complex biological samples for mass spectrometry. *Anal. Chem.* **2008,** *80* (8), 2734-43.

130. Fowler, C. B.; Cunningham, R. E.; O'Leary, T. J.; Mason, J. T., `Tissue surrogates' as a model for archival formalin-fixed paraffin-embedded tissues. *Lab. Invest.* **2007,** *87* (8), 836-846.

131. Alberts, B.; Johnson, A.; Lewis, J.; Raff, M.; Roberts, K.; Walter, P., *Molecular biology of the cell, 4th ed.* Garland Science: New York, 2002; p 1548.

132. Tabb, D. L.; Fernando, C. G.; Chambers, M. C., MyriMatch: Highly Accurate Tandem Mass Spectral Peptide Identification by Multivariate Hypergeometric Analysis. *J Proteome Res* **2007,** *6* (2), 654-661.

133. Zhang, B.; Chambers, M. C.; Tabb, D. L., Proteomic Parsimony through Bipartite Graph Analysis Improves Accuracy and Transparency. *J. Proteome Res.* **2007,** *6* (9).

134. Rahman, S. M.; Gonzalez, A. L.; Li, M.; Seeley, E. H.; Zimmerman, L. J.; Zhang, X. J.; Manier, M. L.; Olson, S. J.; Shah, R. N.; Miller, A. N.; Putnam, J. B.; Miller, Y. E.; Franklin, W. A.; Blot, W. J.; Carbone, D. P.; Shyr, Y.; Caprioli, R. M.; Massion, P. P., Lung cancer diagnosis from proteomic analysis of preinvasive lesions. *Cancer Res.* **2011,** *71* (8), 3009-17.

135. M'Koma, A. E.; Seeley, E. H.; Washington, M. K.; Schwartz, D. A.; Muldoon, R. L.; Herline, A. J.; Wise, P. E.; Caprioli, R. M., Proteomic profiling of mucosal and submucosal colonic tissues yields protein signatures that differentiate the inflammatory colitides. *Inflamm. Bowel Dis.* **2011,** *17* (4), 875-83.

136. Yanagisawa, K.; Shyr, Y.; Xu, B. J.; Massion, P. P.; Larsen, P. H.; White, B. C.; Roberts, J. R.; Edgerton, M.; Gonzalez, A.; Nadaf, S.; Moore, J. H.; Caprioli, R. M.; Carbone, D. P., Proteomic patterns of tumour subsets in non-small-cell lung cancer. *Lancet* **2003,** *362* (9382), 433-439.

137. Chaurand, P.; Sanders, M. E.; Jensen, R. A.; Caprioli, R. M., Proteomics in Diagnostic Pathology: Profiling and Imaging Proteins Directly in Tissue Sections. *Am. J. Pathol.* **2004,** *165*, 1057-1068.

138. Reyzer, M. L.; Caldwell, R. L.; Dugger, T. C.; Forbes, J. T.; Ritter, C. A.; Guix, M.; Arteaga, C. L.; Caprioli, R. M., Early changes in protein expression detected by mass spectrometry predict tumor response to molecular therapeutics. *Cancer Res.* **2004,** *64* (24), 9093-100.

139. Guenther, S.; Koestler, M.; Schulz, O.; Spengler, B., Laser spot size and laser power dependence of ion formation in high resolution MALDI imaging. *Int. J. Mass spectrom* **2010,** *294* (1), 7-15.

140. Espina, V.; Wulfkuhle, J. D.; Calvert, V. S.; VanMeter, A.; Zhou, W.; Coukos, G.; Geho, D. H.; Petricoin, E. F.; Liotta, L. A., Laser-capture microdissection. *Nat. Protocols* **2006,** *1* (2), 586-603.

141. Xu, B. J., Combining laser capture microdissection and proteomics: Methodologies and clinical applications. *Proteomics Clinical Applications* **2010,** *4* (2), 116-123.

142. Luk, V. N.; Mo, G. C. H.; Wheeler, A. R., Pluronic Additives: A Solution to Sticky Problems in Digital Microfluidics. *Langmuir* **2008,** *24* (12), 6382-6389.

143. Patel, D. C.; Luo, R. G., Protein adsorption dissociaton constants in various types of biochromatography. In *Adsorbtion and its Applications in Industry and Environmental Protection Studies in Surface Sciences and Catalysis*, Dabrowski, A., Ed. Elsevier Sciences: 1998; Vol. 120, pp 829-845.

144. Amann, J. M.; Chaurand, P.; Gonzalez, A.; Mobley, J. A.; Massion, P. P.; Carbone, D. P.; Caprioli, R. M., Selective Profiling of Proteins in Lung Cancer Cells from Fine-Needle Aspirates by Matrix-Assisted Laser Desorption Ionization Time-of-Flight Mass Spectrometry. *Clin. Cancer Res.* **2006,** *12* (17), 5142-50.

145. Végvári, Á.; Magnusson, M.; Wallman, L.; Ekström, S.; Bolmsjö, G.; Nilsson, J.; Miliotis, T.; Östling, J.; Kjellström, S.; Ottervald, J.; Franzén, B.; Hultberg, H.; Marko-Varga, G.; Laurell, T., Implementation of a protein profiling platform developed as an academic-pharmaceutical industry collaborative effort. *Electrophoresis* **2008,** *29* (12), 2696-2705.

146. Lee, J.; Soper, S. A.; Murray, K. K., Microfluidics with MALDI analysis for proteomics. A review. *Anal. Chim. Acta* **2009,** *649*, 180-190.

147. Zheng, Z.; Daniel, W. L.; Giam, L. R.; Huo, F.; Senesi, A. J.; Zheng, G.; Mirkin, C. A., Multiplexed Protein Arrays Enabled by Polymer Pen Lithography: Addressing the Inking Challenge. *Angew. Chem. Int. Ed.* **2009,** *48* (41), 7626-9.

148. Chatterjee, D. K.; LaBaer, J., Protein technologies. *Curr. Opin. Biotechnol.* **2006,** *17* (4), 334.

149. Schuerenberg, M.; Luebbert, C.; Eickhoff, H.; Kalkum, M.; Lehrach, H.; Nordhoff, E., Prestructured MALDI-MS Sample Supports. *Anal. Chem.* **2000,** *72*, 3436-3442.

150. Wang, H.; Qian, W. J.; Mottaz, H. M.; Clauss, T. R.; Anderson, D. J.; Moore, R. J.; Camp, D. G., 2nd; Khan, A. H.; Sforza, D. M.; Pallavicini, M.; Smith, D. J.; Smith, R. D., Development and evaluation of a micro- and nanoscale proteomic sample preparation method. *J Proteome Res* **2005,** *4* (6), 2397-403.

151. Fumin Li, C. M. S., Q. C. Ji,, Accelerated tryptic digestion of proteins in plasma for absolute quantitation using a protein internal standard by liquid chromatography/tandem mass spectrometry. *Rapid Commun. Mass Spectrom.* **2009,** *23* (5), 729-732.

152. Hervey, W. J.; Strader, M. B.; Hurst, G. B., Comparison of Digestion Protocols for Microgram Quantities of Enriched Protein Samples. *J. Proteome Res.* **2007,** *6* (8), 3054-61.

153. M. Reid Groseclose, P. P. M. P. C. R. M. C., High-throughput proteomic analysis of formalin-fixed paraffin-embedded tissue microarrays using MALDI imaging mass spectrometry. *Proteomics* **2008,** *8* (18), 3715-3724.

154. Pal, M.; Moffa, A.; Sreekumar, A.; Ethier, S. P.; Barder, T. J.; Chinnaiyan, A.; Lubman, D. M., Differential Phosphoprotein Mapping in Cancer Cells Using Protein Microarrays Produced from 2-D Liquid Fractionation. *Anal. Chem.* **2006,** *78* (3), 702-10.

155. Schwamborn, K.; Caprioli, R. M., Molecular imaging by mass spectrometry--looking beyond classical histology. *Nature reviews. Cancer* **2010,** *10* (9), 639-46.

156. American, C. S. Cancer Facts & Figures 2010.

157. Mearini, E.; Cottini, E.; Cochetti, G.; Antognelli, C.; Talesa, V., Biomarkers of prostate cancer. A review. *Minerva urologica e nefrologica = The Italian journal of urology and nephrology* **2010,** *62* (2), 163-78.

158. Lobo, M. K.; Karsten, S. L.; Gray, M.; Geschwind, D. H.; Yang, X. W., FACS-array profiling of striatal projection neuron subtypes in juvenile and adult mouse brains. *Nat. Neurosci.* **2006,** *9* (3), 443-52.

159. Deutch, A. Y.; Colbran, R. J.; Winder, D. J., Striatal plasticity and medium spiny neuron dendritic remodeling in parkinsonism. *Parkinsonism & Related Disorders* **2007,** *13* (Supplement 3), S251-S258.

160. Bateup, H. S.; Santini, E.; Shen, W.; Birnbaum, S.; Valjent, E.; Surmeier, D. J.; Fisone, G.; Nestler, E. J.; Greengard, P., Distinct subclasses of medium spiny neurons differentially regulate striatal motor behaviors. *Proceedings of the National Academy of Sciences* **2010,** *107* (33), 14845-14850.

161. Jeon, H. G.; Bae, J.; Yi, J.-S.; Hwang, I. S.; Lee, S. E.; Lee, E., Perineural invasion is a prognostic factor for biochemical failure after radical prostatectomy. *Int. J. Urol.* **2009,** *16* (8), 682-686.

162. Liebig, C.; Ayala, G.; Wilks, J. A.; Berger, D. H.; Albo, D., Perineural invasion in cancer: a review of the literature. *Cancer* **2009,** *115* (15), 3379-91.

163. Levavasseur, F.; Zhu, Q.; Julien, J.-P., No requirement of [alpha]-internexin for nervous system development and for radial growth of axons. *Mol. Brain Res.* **1999,** *69* (1), 104-112.

164. Kwak, J. T.; Hewitt, S.; Sinha, S.; Bhargava, R., Multimodal microscopy for automated histologic analysis of prostate cancer. *BMC Cancer* **2011,** *11* (1), 62.

165. Oppenheimer, S. R.; Mi, D.; Sanders, M.; Caprioli, R. M., A Molecular Analysis of Tumor Margins by MALDI Mass Spectrometry in Renal Carcinoma. *Journal of Proteome Research* **2010**.

166. Grey, A. C.; Schey, K. L., Distribution of bovine and rabbit lens alpha-crystallin products by MALDI imaging mass spectrometry. *Mol. Vis.* **2008,** *14*, 171-9.

167. Watrous, J. D.; Alexandrov, T.; Dorrestein, P. C., The evolving field of imaging mass spectrometry and its impact on future biological research. *J. Mass Spectrom.* **2011,** *46* (2), 209-222.

168. Jurchen, J. C.; Rubakhin, S. S.; Sweedler, J. V., MALDI-MS Imaging of Features Smaller than the Size of the Laser Beam. *J. Am. Soc. Mass. Spectrom.* **2005,** *16* (10), 1654-1659.

169. Groseclose, M. R.; Massion, P. R.; Chaurand, P.; Caprioli, R. M., High-throughput proteomic analysis of formalin-fixed paraffin-embedded tissue microarrays using MALDI imaging mass spectrometry. *Proteomics* **2008,** *8* (18), 3715-3724.

170. Sedor, J. R., Tissue proteomics: a new investigative tool for renal biopsy analysis. *Kidney Int.* **2009,** *75* (9), 876-9.

171. Cravatt, B. F.; Wright, A. T.; Kozarich, J. W., Activity-based protein profiling: from enzyme chemistry to proteomic chemistry. *Annu. Rev. Biochem.* **2008,** *77*, 383-414.

172. Amster, I. J., Special Feature: Tutorial Fourier Transform Mass Spectrometry. *J. Mass Spectrom.* **1996,** *31*, 1325-1337.

173. Spraggins, J.; Cornett, S.; Angel, P.; Caprioli, R. M., Direct fragmentation from tissue by combining CASI (Continuous Accumulation of Selected Ions) and SORI-CID: Structural validation of ion images. presente at the 59th ASMS Conference in Denver, 2011.

174. Matsuo, S.; Juodkazis, S.; Misawa, H., Femtosecond laser microfabrication of periodic structures using a microlens array. *Applied Physics A: Materials Science & Processing* **2005,** *80* (4), 683-685.

175. Sherrod, S. D.; Castellana, E. T.; McLean, J. A.; Russell, D. H., Spatially dynamic laser patterning using advanced optics for imaging matrix assisted laser desorption/ionization (MALDI) mass spectrometry. *Int. J. Mass spectrom.* **2007,** *262* (3), 256-262.

176. Tyler A. Zimmerman, E. B. M. J. V. S., Adapting the stretched sample method from tissue profiling to imaging. *Proteomics* **2008,** *8* (18), 3809-3815.

177. Agger, S. A.; Marney, L. C.; Hoofnagle, A. N., Simultaneous Quantification of Apolipoprotein A-I and Apolipoprotein B by Liquid Chromatography-Multiple Reaction Monitoring/Mass Spectrometry. *Clin. Chem.* **2010**, clinchem.2010.152264.

178. Fugmann, T.; Neri, D.; Roesli, C., DeepQuanTR: MALDI-MS-based label-free quantification of proteins in complex biological samples. *Proteomics* **2010,** *10* (14), 2631-2643.

179. Kettenbach, A. N.; Rush, J.; Gerber, S. A., Absolute quantification of protein and post-translational modification abundance with stable isotope-labeled synthetic peptides. *Nat. Protocols* **2011,** *6* (2), 175-186.

180. Pratt, J. M.; Simpson, D. M.; Doherty, M. K.; Rivers, J.; Gaskell, S. J.; Beynon, R. J., Multiplexed absolute quantification for proteomics using concatenated signature peptides encoded by QconCAT genes. *Nat. Protocols* **2006,** *1* (2), 1029-1043.

181. Gygi, S. P.; Rist, B.; Gerber, S. A.; Turecek, F.; Gelb, M. H.; Aebersold, R., Quantitative analysis of complex protein mixtures using isotope-coded affinity tags. *Nat. Biotechnol.* **1999,** *17* (10), 994-9.

182. Friedman, D. B.; Hill, S.; Keller, J. W.; Merchant, N. B.; Levy, S. E.; Coffey, R. J.; Caprioli, R. M., Proteome analysis of human colon cancer by two-dimensional difference gel electrophoresis and mass spectrometry. *Proteomics* **2004,** *4* (3), 793-811.